UNIVERSITÉ PARIS-EST

École Doctorale MSTIC

Laboratoire Images, Signaux et Systèmes Intelligents (LISSI)

THÈSE

Présentée pour l'obtention du grade de DOCTEUR

DE L'UNIVERSITE PARIS-EST

par

ARNEZ PANIAGUA Victor Gustavo

Adaptive control approaches of an actuated ankle foot orthosis for gait assistance

Approches de commande adaptative d'une orthèse actionnée de la cheville pour l'assistance à la marche

---

Spécialité : Robotique

Soutenue le 20/12/2018 devant le jury composé de :

Rapporteur	Prof. Christine CHEVALLEREAU LS2N Directrice de Recherche CNRS, École Centrale de Nantes
Rapporteur	Prof. Philippe FRAISSE Professeur des universités, Université Montpellier
Examinateur	Prof. Stéphane REGNIER Professeur des universités, Université Sorbonne
Directeur de thèse	Prof. Yacine AMIRAT Professeur des universités, Université Paris-Est Créteil
Co-directeur de thèse	Dr. Samer MOHAMMED Maître de conférences, Université Paris-Est Créteil
Co-encadrant de thèse	Dr. Hala RIFAI Maître de conférences, Université Paris-Est Créteil

Thèse effectuée au sein du

Laboratoire Images, Signaux et Systèmes Intelligents

de l'Université Paris-Est Créteil

Domaine Chérioux
122 rue Paul Armangot
94400 Vitry sur Seine
France

Acknowledgements

I would like to acknowledge the support and assistance of my thesis director and co-directors, Prof. Yacine Amirat, Dr. Samer Mohamed and Dr. Hala Rifaï.

I would like to thank the Mexican government through *"Consejo Nacional de Ciencia y Tecnología"* (CONACyT) for the financing of this PhD via a scholarship.

I want to show all my gratitude to my parents and brothers. I wouldn't be who I am without you in my life. You are a continuous source of insipiration and joy. I feel very proud of being your son and brother.

I want to give special thanks to my friend and colleague Dr. Weiguang Huo. Your help was paramount to finish this thesis.

Finally, I dedicate this thesis to the love of my life, Aurélie Labesque. You help me be the best version of myself.

Abstract

Neuro-motor deficiencies following a stroke can lead to a poor control of the ankle joint during walking. One of the major symptoms that illustrate this deficiency is the "foot drop" that appears along the swing phase. In recent years, robotic rehabilitation devices have been the subject of numerous research projects around the world. These devices can enable the patient to achieve the same levels of functional recovery as those achieved with conventional rehabilitation while reducing the workload of physical therapists.

This thesis deals with the problem of the control of an actuated ankle-foot orthosis intended for the walking assistance of paretic patients with motor deficiencies at the ankle level. The originality of our work lies in the consideration of the evolution of the gait cycle in the controlled assistance. The other remark of our work lies in the development of control laws that guarantee the patient safety and a good performance in terms of trajectory tracking accuracy, robustness with respect to parametric uncertainties, variability between subjects and external disturbances.

Three control approaches for reference trajectory tracking are proposed. These approaches have the advantage of not requiring the prior identification of the orthosis-human system parameters. The reference trajectory is generated in real time with an algorithm that exploits the interaction of the feet with the ground to detect the subphases of the gait cycle.

The first approach proposed is a model reference adaptive control that adapts the assistive torque according to the tracking error. This control uses a projection function to limit the values of the adaptive parameters of the control law. A saturation operator is also introduced to limit the assistive torque. The second approach is an adaptive proxy-based sliding mode control that can change the damping effect at the ankle during the transition from the stance phase to the swing phase. The adaptive nature of this controller makes it possible to compensate for changes in system dynamics during the

gait cycle, while the use of the sliding mode makes it possible to guarantee good performance in terms of trajectory tracking. The third approach is an active disturbance rejection control. An extended state observer is used to estimate the disturbances to which the orthotic-human system is subjected in order to compensate for their effects and improve trajectory tracking performance. For each control approach, a Lyapunov stability study is conducted.

The three control approaches have been validated experimentally with the participation of healthy subjects and paretic patients. Regarding the latter, the clinical evaluations were carried out in collaboration with the Department of Physical Medicine and Rehabilitation of the Mondor Hospital.

Keywords: Actuated ankle foot orthosis, adaptive control, sliding mode control, disturbance rejection control, state observer, gait phase detection.

Résumé

Les déficiences neuro-motrices subies à la suite d'un accident vasculaire cérébral, peuvent se traduire par un mauvais contrôle de l'articulation de la cheville lors de la marche du sujet. Un des symptômes majeurs qui illustre cette déficience est celui du "foot drop" ou pied tombant qui apparait le long de la phase d'oscillation. Ces dernières années, les auxiliaires de rééducation robotisés ont fait l'objet de nombreux travaux de recherche à travers le monde. Ces dispositifs peuvent permettre au patient d'atteindre les mêmes niveaux de récupération fonctionnelle que ceux obtenus avec une rééducation conventionnelle tout en réduisant la charge de travail des médecins thérapeutes.

Cette thèse traite du problème de la commande d'une orthèse active de l'articulation de la cheville (AAFO-Actuated Ankle Foot Orthosis) destinée à l'assistance à la marche des patients parétiques présentant des déficiences motrices au niveau de l'articulation de la cheville. L'originalité de nos travaux se situe dans la prise en compte de l'évolution du cycle de marche du sujet dans les commandes orientées assistance. L'autre spécificité de nos travaux réside dans le développement de lois de commande garantissant la sécurité du patient et de bonnes performances à la fois en termes de précision de poursuite de trajectoire, de robustesse vis-à-vis des incertitudes paramétriques, de la variabilité entre sujets et des perturbations externes.

Trois approches de commande pour le suivi d'une trajectoire de référence sont proposées. Ces approches présentent l'intérêt de ne pas nécessiter l'identification préalable des paramètres du système orthèse-humain. La trajectoire de référence est générée en temps réel à partir d'un algorithme exploitant l'interaction du pied avec le sol pour détecter les sous-phases du cycle de marche.

La première approche proposée est une commande adaptative par modèle de référence pour adapter le couple d'assistance en fonction de l'erreur de suivi. Cette commande utilise une fonction de projection pour borner les valeurs des paramètres adaptatifs de

la loi de commande. Un opérateur de saturation est également introduit pour borner le couple d'assistance. La deuxième approche est une commande adaptative par modes glissants basée proxy pour contrôler l'effet d'amortissement au niveau de la cheville lors de la transition de la phase d'appui vers la phase d'oscillation. La nature adaptative de cette commande permet de compenser les modifications de la dynamique du système pendant le cycle de marche tandis que l'utilisation des modes glissants permet de garantir de bonnes performances en termes de suivi de trajectoire. La troisième approche est une commande par rejet actif des perturbations. Un observateur d'état étendu est ainsi utilisé pour estimer les perturbations auxquelles est soumis le système orthèse-humain afin de compenser leurs effets et améliorer les performances de suivi de trajectoire. Pour chaque approche de commande, une étude de stabilité au sens de Lyapunov est menée.

Les trois approches de commande ont été validées expérimentalement avec la participation de sujets sains et de sujets parétiques. Concernant ces derniers, les évaluations cliniques ont été effectuées en collaboration avec le service de médecine physique et de réadaptation du CHU Mondor.

Mots clés: Actuated ankle foot orthosis, commande adaptative, commande par modes glissants, commande par rejet actif des perturbations, observateur d'état, détection des phases de la marche.

List of symbols

AAFO dynamic model

Symbol	Description
θ_s	Angle between the shank and the vertical axis
α	Angle between the foot and the horizontal axis
θ, $\dot{\theta}$, $\ddot{\theta}$	Ankle joint angle, angular velocity and acceleration
$\tilde{\theta}$, $\dot{\tilde{\theta}}$	Ankle joint angle and angular velocity errors
θ_r	Ankle joint angle at the rest position of the foot
J	System's moment of inertia
k_{fs}	System's solid friction coefficient
k_{fv}	System's viscous friction coefficient
k_s	System's stiffness coefficient
k_g	System's gravity torque coefficient
k_r	System's ground reaction torque coefficient
k_a	System's acceleration torque coefficient
a_x, a_y	Longitudinal and vertical linear accelerations
R_1, R_2 , R_3	GRF at the heel, middle and toes levels
x_1, x_2, x_3	Positions of the FSR in $\vec{x}^f$ direction
x_g	Distance of the center of mass from the ankle joint
F_r	Equivalent GRF applied to the center of mass of the foot
τ	Control torque
τ_h	Human muscular torque actuating the ankle joint
τ_f	Solid and viscous friction torques
τ_a	Torque induced by the translational acceleration of the foot
τ_s	System's joint stiffness torque
τ_r	Torque induced by the ground reaction forces
τ_g	Torque exerted by the gravity of the foot at the ankle

Gait phase detection and reference generation

Symbol	Description
j	Region of the foot plant to measure the GRF
i	Gait sub-phase index
r_j	Magnitude range of the measurement from each sensor j
$\vec{F}_{tj}$	Vector that contains the acquired FSR data for a given foot region
N_j	threshold value for each region j
h	Threshold percentage
f_j	Membership function for the foot region j
k_j	gain for each sensor j
μ_i	fuzzy membership value for each gait sub-phase i
a_{shank}	Acceleration in the shank axis

Model reference adaptive control

Symbol	Description
s	MRAC tracking error
λ	Scalar positive gain of the tracking error
κ	Scalar positive gain for the s term in the control law
$\hat{J}$	Estimated torque coefficient for the inertia
$\hat{k}_{fS}$	Estimated torque coefficient for the solid friction
$\hat{k}_{fV}$	Estimated torque coefficient for the viscous friction
$\hat{k}_s$	Estimated torque coefficient for the stiffness
$\hat{k}_a$	Estimated torque coefficient for the acceleration
$\hat{k}_g$	Estimated torque coefficient for the gravity
$\hat{k}_r$	Estimated torque coefficient for the ground reaction
a_n	Positive scalar gains for the adaptive law
n	Index for the adaptive parameters
$\tilde{J}$	Estimation error of the inertia parameter
$\tilde{k}_{fS}$	Estimation error of the solid friction parameter
$\tilde{k}_{fV}$	Estimation error of the viscous friction parameter

Symbol	Description
$\tilde{k}_s$	Estimation error of the stiffness parameter
$\tilde{k}_a$	Estimation error of the acceleration parameter
$\tilde{k}_g$	Estimation error of the gravity parameter
$\tilde{k}_r$	Estimation error of the ground reaction parameter
$W, \hat{W}, \tilde{W}$	Vectors of the system parameters, estimated parameters and estimation error
$Proj(\cdot)$	Projection operator
Γ	Positive definite scaling diagonal matrix
$\alpha_p, \alpha_v, k_p, k_v$	Scalar positive gains for the PD saturation MRAC
N_1, N_2	Bounds of the proportional and derivative actions
$sat_N(\cdot)$	Saturation function

Adaptive proxy-based sliding mode control

Symbol	Description
H, F	Scalar design parameters
θ_p	Proxy angle
K_p, K_i, K_d	Adaptive proportional, integral and differential gains

Active disturbance rejection control

Symbol	Description
$R, \dot{R}$	Parametrization of the system's state θ
R_1, R_2	Estimation of the system's states θ, $\dot{\theta}$
ξ	Perturbation function
e	Estimation error
η_1, η_2	Disturbance estimation and its time derivative
l_3, l_2, l_1, l_0	State observer gain coefficients
P	Solution of the Ricatti equation
$v(\cdot)$	Feedback component of the ADRC

Contents

1 — General Introduction

1.1 Motivation and Challenges

Rates of disability are increasing due to, among other causes, population ageing and chronic health conditions. According to the World Health Organization, a review in 2017 states that around 15% of the world's population lives with some form of disability, and 2-4% of this population experiences significant difficulties in functioning [1]. Some of them show gait pathologies that can threaten their safety and therefore their autonomy. Indeed, every year an augmenting number of people are diagnosed with disabilities that prevent them from performing daily living activities such as walking, stairs ascent/descent, standing up, etc. In the US, more than 795,000 people suffer from a stroke every year[2] and are diagnosed with a disability that prevents them from performing smooth movements. Today stroke is the major reason for disability in adults in western countries [1].

Since different parts of the brain control different bodily functions, if a person survives a stroke, the effects can vary depending on the location of brain damage, severity and duration of the stroke. Broadly, the effects of stroke can be physical, cognitive or emotional in nature. In terms of the physical effects of stroke, the loss of motor abilities of the limbs presents significant challenges for patients, as their mobility and activities of daily living are affected [2]. The upper or lower limbs can experience weakness (paresis) or paralysis (plegia), with the most common type of limb impairment being hemiparesis, which affects eight out of ten stroke survivors [3]. The majority of the stroke survivors suffer from a gait disorder and almost a half of these people cannot walk independently

[1] http://www.who.int/mediacentre/factsheets/fs352/en/, Accessed: 2018-01-10

[2] http://www.cdc.gov/nchs/fastats/stroke.htm, Accessed: 26-10-2016

[3] http://www.stroke.org/we-can-help/survivors/stroke-recovery/post-stroke-conditions/physical/hemiparesis, Accessed: 10-09-2018

without any assistance. Therefore, this urges the researchers to investigate in the area of walking ability recovery or gait rehabilitation.

For stroke patients, rehabilitation is the pathway to regaining or managing their impaired functions [3]. There is no definite end to recovery but the most rapid improvement is within the first six months post stroke. It is theorized that the brain is plastic in nature and that repetitive exercises over long periods can enable the brain to adapt and regain the motor functionality that has been repeatedly stimulated [4]. Depending on the type of impairment, rehabilitation specialists will assess the appropriate therapies needed and set realistic goals for patients to achieve. Evidence suggests that without sufficient ankle rehabilitation: 44% of people will have future problems [5, 6], e.g., ambulation is markedly compromised, re-injury prevalence is high, and approximately 38% of people will have recurrent activity limitations affecting their function [7]. The rehabilitation consist of three phases [8]: 1) mobilization of bedridden patient, 2) gait restoration, and 3) gait improvement. One of the main goals in stroke rehabilitation is the restoration of motor skills, and this involves patients undergoing repetitive, high-intensity, task-specific exercises that enable them to regain their motor and functional abilities [9, 10]. This stimulates the formation of new neuronal interconnections that enable the retransmission of motor signals [11]. Therefore, providing the patients with intense and engaging rehabilitation is paramount for a quick and good recovery of walking functions [12]. However, the traditional rehabilitation process is uneconomical as it is a labor-intensive process as for rehabilitation at least 3 therapists are needed. Furthermore ageing, shortage of healthcare personnel, and the need of higher quality healthcare increases the average cost of rehabilitation [13]. For example, disability-associated health care expenditures accounted for 26.7% of all health care expenditures for adults residing in the United States [14]. Therefore, there is an increasing interest in healthcare technologies with the emergence of new economic and industrial sectors.

A large number of gait rehabilitation robots, together with a variety of control strategies, have been developed and evaluated during the last decade. Initially, control strategies applied to rehabilitation robots were adapted from those applied to traditional industrial robots. However, these strategies cannot optimise effectiveness of gait rehabilitation. As a result, researchers have been investigating control strategies tailored for the needs of rehabilitation based on high repetitions of task-specific exercises [15]. These robotic assistive devices provide consistent and repetitive cycles over long periods and help train the limbs of patients to keep receiving and sending signals from and back to the brain and thereby regain their motor abilities. Such devices are also complex in nature involving interactive automation, sensors and advanced control strategies that allow a

usage without much intervention from physiotherapists [16]. In comparison, for conventional rehabilitation of the lower limbs without assistive devices, it would require at least two physiotherapists to train a patient to walk, and the pace and pattern of walking may not be consistent. It is also physically strenuous for the physiotherapists to sustain the exercise over long periods, thus affecting the rehabilitation progress of the patient. The labor-intensive nature of conventional physiotherapy places great strain on physiotherapists. Coupled with the requirements of stroke patients for medical care and intensive rehabilitation exercises (which frequently entail one-to-one manual interaction with therapists), therapist time and organizational budgets, it is not always possible to provide an optimal rehabilitation program for patients. Therefore, it is hoped that with robotic assistive devices, better rehabilitation progress can be achieved for patients together with alleviation of time and physical demands on physiotherapists [17, 18]. With the assistance of robots, physiotherapists will be able to concentrate more on functional rehabilitation during individual training sessions and supervision of multiple patients simultaneously during robot-assisted therapy sessions. This approach would maximize the expertise and time of physiotherapists, thus improving the effectiveness of the rehabilitation program [19].

Despite the large amount of work done in the field of ankle rehabilitation after stroke [20], there are still many challenges to overcome [21]. For example, developing control startegies able to compensate for the pre-existing gait pathologies produced by the patient is paramount for allowing to undertake long and intense rehabilitation sessions while reducing the risk of falling. Also, since the internal and external forces applied to the ankle joint change significatively during the gait cycle, e.g. muscle torque, friction and stiffness to name a few, it is challenging to assist the ankle joint during the whole gait cycle. In other words, when the foot is in contact with the ground (stance phase), human-muscular torque has to be produced at the ankle joint in order to compensate for the ground reaction forces, which creates a high requirement of assistive torque to change the ankle joint angle. However, when the foot is above the ground (swing phase), a small assistive torque is generally enough to influence the ankle joint angle. This drastic change of the system dynamics makes it challenging to develop a robotic device that is able to provide an appropiate assistive torque throughout the gait cycle. In the following section, the objectives of the thesis will be presented.

1.2 Objectives of the Thesis

The purpose of this work is to improve the state-of-the-art of control strategies for actuated ankle foot orthoses (AAFOs) for the physical assistance of the gait of individuals with limited muscular capabilities. In the following, the list of the detailed objectives of this thesis are identified and described.

1. To develop an adaptive ankle joint reference generation algorithm that is able to produce an ankle joint angle, velocity and acceleration profiles that are adjustable for each subject's walking speed.
2. To develop a control algorithm that adapts the assistive torque to the changes in the system dynamics through the gait cycle.
3. To develop a control algorithm that is able to modify the damping effect at specific gait moments in order to avoid large actuator torque.
4. To develop a control algorithm that estimates and compensates for the disturbances exerted on the ankle-AAFO system through the gait cycle.
5. To evaluate the tracking performance and ankle deficiency compensation of the proposed controllers with healthy subjects and paretic patients.

1.3 Contributions of this work

1. Gait phase detection and adaptive ankle reference generator:
   To generate the desired trajectory for the controllers, a Mamdani fuzzy inference system has been developed to detect the gait sub-phases based on the outputs of force sensitive resistor (FSR) sensors. From the detection of the gait sub-phases, an online adaptive ankle reference generator (AARG) algorithm is developed. The experimental results show that the reference is correctly and consistently being generated in real time.
2. Joint-level reference tracking control:
   To assist individuals with unilateral lower limb muscular weakness in accomplishing a desired movement, three control strategies were developed.

First, a model reference adaptive controller (MRAC) approach with two modifications was used, this controller is robust to the changes in the system dynamics by considering several internal and external torques exerting at the ankle level [4,5]. Furthermore, the projection function to bound the adaptive parameters of the controller[6], and the saturation operator[7] to increase the safety of the system. This control strategy was proven effective in compensating for foot drop and increasing the ankle joit range of motion during the gait for two paretic patients.

Second, an adaptive proxy-based sliding mode controller (APSMC) strategy was evaluated to assist the gait of one paretic patient in a hospital environment while walking on level-ground[8]. This controller implements an adaptation law that improves the system's robustness. Such control allows to variate the damping effect of the controller throught the gait cycle in order to improve the safety of the system and the tracking performance through time.

Finally, an active disturbance rejection control (ADRC) was developed and its tracking performance was evaluated with one healthy subject walking on a treadmill[9]. This control approach allows for estimating the exogenous and endogenous torques of the AAFO-ankle system during walking and compensate for their effects. At the same time, a control Lyapunov function (CLF) was implemented. This controller uses an estimation of the system states by means of a extended state observer (ESO), which allows the controller to compensate for the disturbances exerted on the system and improve the tracking performance without compromising on stability or smoothness of the assistive torque. The experimental results show that the system is able to a track the desired trajectory while correctly estimating the system states with the use of an ESO.

The assistive torque produced by the AAFO for all the controllers was relatively smooth and consistent for every step during the experimental sessions.

[4] **Arnez-Paniagua, V** and Rifai, H and Mohammed, S and Amirat, Y. Adaptive control of an actuated ankle foot orthosis for foot-drop correction. In *International Federation of Automatic Control (IFAC)*, pages 1420–1425. 2017.

[5] **V. Arnez-Paniagua**, H. Rifaï, Y. Amirat, M. Ghedira, J. M. Gracies, S. Mohammed. Adaptive Control of an Actuated Ankle Foot Orthosis for Paretic Patients. *Control Engineering Practice*, p. 16. Elsevier, 2018. *(In revision)*

[6] **Arnez-Paniagua, Victor** and Rifa, Hala and Amirat, Yacine and Mohammed, Samer. Adaptive control of an actuated-ankle-foot-orthosis. In *International Conference on Rehabilitation Robotics (ICORR)*, pages 1584–1589. IEEE, 2017.

[7] **V. Arnez-Paniagua**, H. Rifaï, Y. Amirat, M. Ghedira, J. M. Gracies, S. Mohammed. Modified Adaptive Control of an Actuated Ankle Foot Orthosis to assist Paretic Patients. In *International Conference on Intelligent Robots and Systems (IROS)*, p. 7. IEEE, 2018.

[8] Weiguang Huo, **Victor Arnez-Paniagua**, Guangzheng Ding, Yacine Amirat and Samer Mohammed. Adaptive Proxy-Based Controller of an Active Ankle Foot Orthosis to Assist Lower Limb Movements of Paretic Patients. *Robotica*, p. 27. Cambridge University Press, 2018. *(Minor revision)*

[9] J.F. Guerrero-Castellanos, H. Rifai, **V. Arnez-Paniagua**, J. Linares-Flores, L. Saynes-Torres, S. Mohammed. Robust Active Disturbance Rejection Control via Control Lyapunov Functions: application to Actuated-Ankle-Foot-Orthosis. *Control Engineering Practice*, p. 32. Elsevier, 2018.

1.4 Outline of the Thesis

Chapter 2 presents an overview of actuated ankle foot orthoses for robotic assisted rehabilitation in the literature. A special focus is given to the actuation mechanisms for the AAFOs, the control strategies and the assessment methods.

Chapter 3 describes the AAFO-human system. The ankle joint is described from an anatomical perspective, to arrive to a dynamic model considering the external and internal forces that are exerted on the system during the gait cycle. This is followed by an description of the hardware used in the study.

Chapter 4 describes the gait cycle and the algorithm to detect and measure the gait sub-phases and its proportions, as well as the step duration. This is followed by the description of the AARG algorithm. The performance of this algorithm is evaluated with healthy subjects and the results are presented and discussed.

Chapter 5 introduces two adaptive control approaches proposed in this thesis. Firstly, the basic MRAC approach is presented. Followed by the description of the modified versions of this controller; the projection-based MRAC, and the MRAC with PD saturation. Finally, the APSMC is described. The stability of the adaptive controllers, in terms of Lyapunov stability, is analysed as well.

Chapter 6 presents an ADRC with a CLF that is implemented in the AAFO. A Lyapunov stability analysis is presented.

Chapter 7 presents the experimental evaluation of the proposed controllers' performance. The experimental protocol includes four healthy subjects walking on a treadmill and three paretic patients walking on level ground in a clinical environment.

Chapter 8 draws the conclusions of the thesis and recommends future work.

2 — Overview of actuated ankle foot orthoses

2.1 Introduction

Paretic patients may have different levels of impairment, e.g., some have total loss of strength to initiate a movement, while others are able to move their limbs within a limited range. This reduced mobility affects the quality of the daily life of the patient. The differences in impairment levels require different levels of assistance. Therefore, the required rehabilitation depends on the level of impairment, and it needs to be adjusted as the patient shows strength improvements, coordination and achievement of certain motor tasks. The lack of strength and coordination during a gait cycle derives in pathologies and, oftentimes, the patient adapts the gait movements to circumvent the weaker limb. Such gait pathologies slow down the walking speed and increase the fall risks.

There are several key causes of pathologies that affect the gait, e.g., spasticity [22], co-contraction of plantar flexion muscles, and muscle weaknesses, [23]. Some pathologies of the ankle joint that affect the gait are described in [24] and [25]. For example, defeciencies originated by the dorsiflexor muscle group show show mainly two pathologies: foot drop and foot slap. The former occurs during the swing phase and is due to the lack of sufficient dorsiflexion to ensure toe clearance and results in a steppage-type gait pattern. The latter occurs during the loading response sub-phase, it is caused by the uncontrolled deceleration of the toes shortly after initial contact that generally causes a foot slap [26]. Foot-drop patients are unable to lift their feet and toes properly during walking, affecting thus their movement coordination, their balance and increasing the risk of falling. Dealing clinicaly with foot-drop ranges from conventional rehabilita-

tion, use of passive orthoses, functional electrical stimulation (FES) [27, 28], to the use of wearable robotics based solutions, known also as actuated ankle foot orthosis (AAFO) [29, 30]. For the deficiencies originated by the plantar-flexor muscle group, the main pathologies are in the stance phase of the gait cycle. Limited range ankle plantar-flexors affect the gait stability and reduce the human torque, which is needed for forward progression. Therefore, patients compensate this deficiency by reducing walking speed and shortening contralateral step length.

Conventional rehabilitation include lower limb muscle strengthening exercises, joint stretching to enhance ankle dorsiflexion and plantar-flexion, and ground walking with the assistance of clinical therapists. It is worth noting, however, that such rehabilitation process is difficult and effort demanding to be performed continuously for more than few minutes by both therapists and patients [31, 32].

It is still not clear yet if the robotic rehabilitation is better than the conventional one at the same dose [33, 34, 35, 36, 37, 38]. However, robot-assisted rehabilitation has demonstrated benefits on improving abnormal gaits associated with neuromuscular disorders, and can be used to re-educating the neuro-motor system of stroke patients [39, 40], and spinal cord injured patients [41]. The results show that robotic-assisted physical therapies can provide at least similar benefits compared to the non-robotic-based solutions. It is also becoming clear that an intense and prolonged rehabilitation offers the best outcome in terms of patient recovery for different assessment metrics [12, 42, 43, 44, 45]. Therefore, the inclusion of robotic devices such as AAFOs could potentially increase the dosage and intensity of the rehabilitation while reducing the effort required from the clinical therapists. Thus, the number of wearable robots used in the assistance/rehabilitation of patients with a physical disabilities has been continuously increasing during the last decades [46, 47].

One of the benefits of using robotic-ankle-orthosis is the achievement of smoother, continuous and repeatable movements of the patient's joints compared to manual non-robotic assistance, where the joint motions need to be conducted by external clinical therapists. The smoother the dynamic response and the better the efferent feedback of a control algorithm are, the more easily the central nervous system (CNS) adapts [48, 17]. In this sense, it is clear that there exist a close relationship between AAFO and the control strategies design based on rehabilitation objectives. These benefits are, however, subject to the choice of an appropriate control law. For example, it has been shown by Hidler et al. [49], that for the same motor task, a high-impedance-control strategy was less effective than an equivalent manual assistance performed by a physical therapist.

In this chapter, a basic overview of the existing ankle-foot orthosis, based on a classification of their actuation mechanics, is presented in order to provide a comprehensive understanding of the actuated ankle foot orthosis. Furthermore, an introduction to the control strategies used, in the rehabilitation field, for the lower limb robotic orthoses. Finally, the description of the proposed control strategies in this thesis are explained.

2.2 Actuated Ankle Foot Orthoses - A brief synthesis

Different lower limb orthoses are dedicated to train patients to recover strength and coordination. Recent reviews have presented a comprehensive overview of lower limb robotic orthoses for rehabilitation [16, 47, 50, 51, 52, 53, 54], including those focusing on the ankle joint [12, 20, 26]. Rehabilitation devices can be classified as portable robots worn by the human limbs, or platform based devices. The fromer group assists the patient at specific moments of the gait or during the whole cycle, while the later group assists the patient by moving the ankle joint in the context of in-bed excercises.

An AAFO classification is based on the actuation mechanism of the ankle joint, effectively dividing the devices in passive, semi-active and active orthoses. Indeed, the actuator selection has a direct impact on the usability of the AAFO in a given application. For example, acute stroke survivors, in the early stages of the gait rehabilitation, may need a more direct assistance from the orthotic device, while patients with more voluntary movements could benefit more with a more transparent assistance. For this reason, both active and semi-active orthosis are important in the rehabilitation process. In recent years, several active and semi-active ankle foot orthosis have been developed and different control strategies have been proposed to improve the benefits of active rehabilitation. Semi-active devices normally include an energy-storing element in the mechanical design to re-distribute to the ankle joint the stored energy at appropriate moments of the gait but are not able to introduce new sources of energy to assist the ankle joint. On the contrary, AAFO use direct actuation of the ankle joint.

This section presents a brief review of the actuated ankle foot orthoses for rehabilitation and the classification of the actuation mechanism. The definition, advantages and limitations of the AAFOs are discussed.

2.2.1. Fixed robotic platforms

It has been shown that early initiation of stroke rehabilitation results in improved functional outcomes [55, 56]. A number of robotic ankle rehabilitation devices have been developed in the literature to provide repetitive, task-specific, movement restoration of the impaired limbs. However, people with chronic stroke may have difficulty in actively participating in a rehabilitation process due to their inability to move their impaired limbs. Strengthening exercises of the skeletal muscles acting at the foot level help in maintaining muscular tonus, which results in gait pattern improvement. Dealing with foot drop by stretching the ankle joint along dorsiflexion is important and requires large driven torque from by the clinical therapist. Therefore, robotic devices that could be used in-bed, worn by patients suffering from acute stroke, for improving the ankle range of motion (ROM), and muscle flexibility, have been widely developed in recent studies.

For example, in [57], Ren et al. proposed a wearable robotic device to be used in bed for acute stroke rehabilitation of the ankle joint (Fig. 2.1a). The AAFO consists of a rotating actuator, a leg brace and a foot holder. The device is actuated by a brushless motor with a planetary and a bevel gear set. The bevel-gear mechanism increases the torque output while maintaining the back-drivability through an appropriate control method. The device is equiped with a force sensor between the ankle and the insole to measure the interaction torque between the robot and the wearer's limb. A clinical pilot study was conducted to evaluate the rehabilitation protocol using this robotic device. For this purpose, ten acute patients who suffered a stroke participated in the study. By detecting the joint torque generated by the wearer, the device was able to enhance the movement of the patients by actively involving the wearer in the achievement of the task.

Jamwal et al., present in [58] a parallel robot for the treatments of ankle sprain through physical rehabilitation (Fig. 2.1b). This robot is able to provide assistant along three rotational degrees of freedom of the ankle joint to guarantee important ROM and effective muscle strengthening exercises. The proposed prototype used two parallel platforms; a "U" shaped top platform built-in with a leg support structure and a moving platform at the bottom, designed to accommodate the foot and the ankle of patients. The actuation is done using lightweight but powerful pneumatic muscle actuators (PMA) which mimics the skeletal muscles behaviors. To address nonlinear characteristics of the PMA, a fuzzy-based disturbance observer has been developed. The ankle robot was used by a healthy subject. The robot-human interaction was done in an active-passive scenario while the robot is tracking predefined trajectories commonly adopted by the clinical therapists.

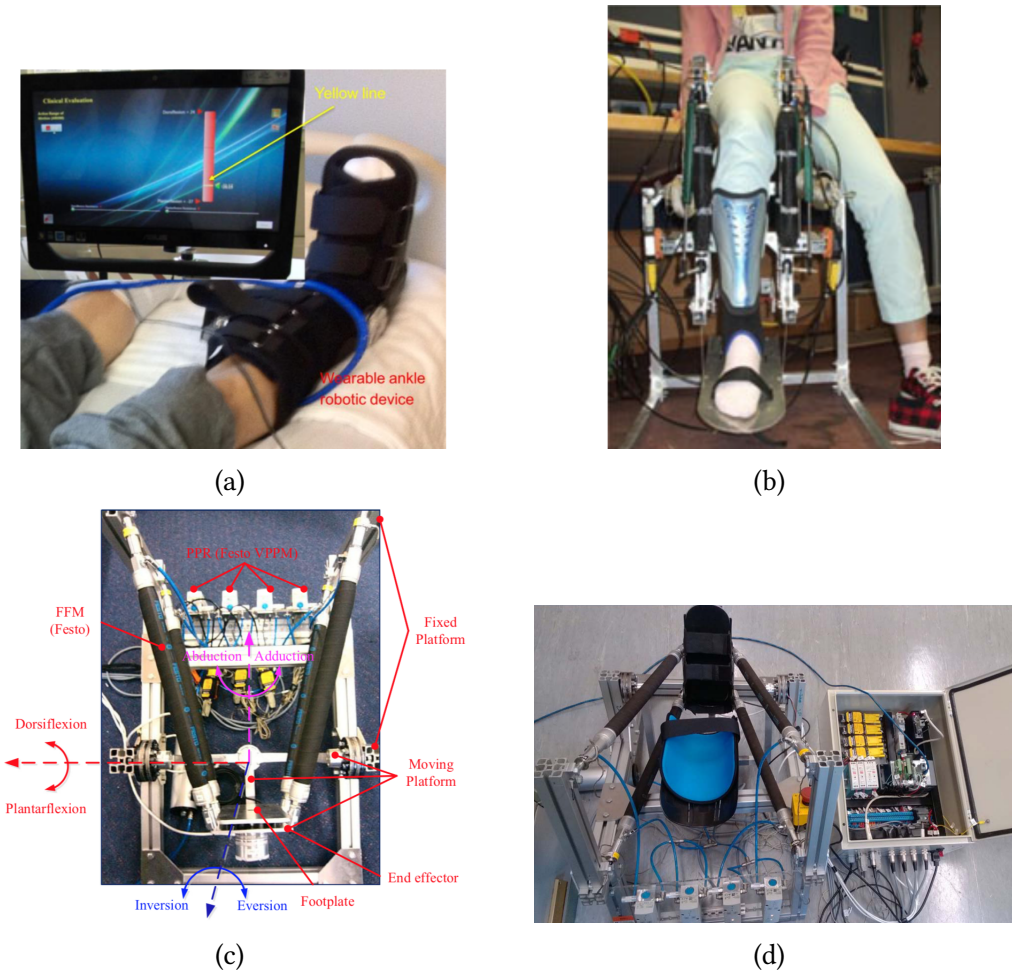

(a) (b) (c) (d)

Figure 2.1 – Non portable AAFOs.

Zhang et al. [59, 60] proposed a compliant ankle rehabilitation robot platform for dealing with foot drop (Fig. 2.1c). The robot has a bio-inspired design by employing four fluidic muscle actuators that mimic the skeletal muscles actuating three rotational degrees of freedom. This non-portable device, as a parallel mechanism, consists of a fixed platform and a moving platform. The moving part is actually a three-link serial manipulator. The third link of the moving platform is also denoted as the end effector that is rigidly connected with the foot plate through a six-axis load cell. A trajectory tracking controller was developed to track the predefined trajectory of the end effector. Preliminary results show that this robot can accurately and reliably stretch the patient's ankle joint towards a desired position.

In [61], Meng et al. proposed a robotic platform that is driven using four pneumatic muscles enabling three rotational movement degrees of freedom (Fig. 2.1d). The end-effector is a three-link serial manipulator with three magnetic encoders embedded to provide

measurements of angular positions of the robot. A healthy participant participated in the experiments while sitting on a chair with his ankle and foot fixed to the end-effector.

2.2.2. Portable AAFOs

Of greatest importance for clinicians and patients are the functional improvements that occur during walking training. As expressed by Ferris et al. [62], the best way to improve performance of a motor task is to execute that specific motor task. Hence, an important number of portable AAFOs that allow walking while wearing the device have been published recently.

In general, the assistance provided by active orthoses during the gait cycle is aimed to correct unnatural movement of the patient. For example, during the swing phase of the gait cycle, the AAFO aims to avoid foot drop by providing sufficient dorsiflexion assistance to ensure appropriate foot clearance with respect to the ground at the moment of heel strike. To deal with foot slap, i.e. the uncontrolled falling of the foot following the heel strike, an assistance to the dorsiflexor muscles should be provided by either: increasing the impedance of the ankle joint or by providing an assitive dorsiflexion torque during the loading response phase. During the mid-stance phase, the plantar flexion muscle group, i.e. the soleus and the gastrocnemius, provides a controlled roll-off of the shank over the foot [63]. Hence, the orthosis assists in the plantar flexion or dorsiflexion direction based on the rate of rotation of the shank over the anlke joint. At the late stance and pre-swing phases, a plantar flexion assistance is provided to contribute to the push-off of the leg into swing.

In the following, a brief synthesis of the AAFO developed in the literature for assisting the ankle joint during the gait cycle are presented based on their actuation system. Note that the robotic devices for the rehabilitation of the ankle joint during in-bed exercises also have different actuation mechanisms. However, since they are not aimed to be portable, they are presented in section 2.2.1.

2.2.2.1. AAFO with hydraulic or pneumatic actuators

In [64, 65], an AAFO was developed to produce plantar and dorsiflexion of the ankle joint with high velocity displacements to test proprioceptive reflexes (Fig. 2.2a). This electrohydraulic orthosis can produce several types of force fields during walking, including constant, position-dependent, and phase-dependent. The device was tested with

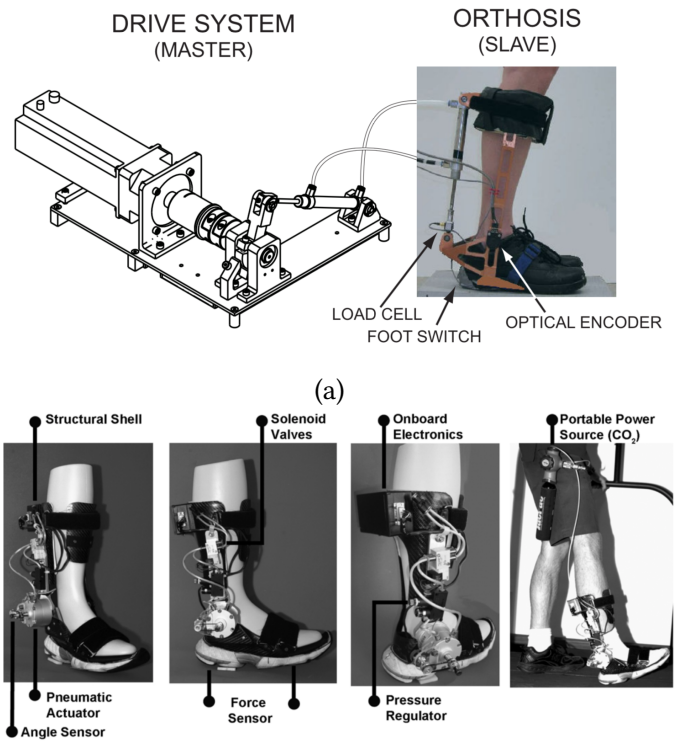

Figure 2.2 – AAFOs with hydraulic and pneumatic actuators.

two groups of healthy subjects (fifteen and twelve, respectively) with no reported history of orthopaedic or neurological disorders. The results presented suggest that, for short duration training with the device, a feedforward modification in muscle torque output occurs during mid-stance but not during push-off. These findings are important for the design of new rehabilitation approaches, as they suggest that the ability to use resistive force fields for training may depend on targeted gait phases.

In [66], Shorter et al. presented an AAFO powered by pneumatic actuators to assist in dorsiflexion and plantar flexion movements of the ankle joint (Fig. 2.2b). A dualvane bidirectional rotary actuator at the ankle joint, fed by a portable compressed liquid carbon dioxide bottle and pressure regulator, was used as the actuation system. The direction of the torque could be switched from dorsiflexor to plantar flexor with two solenoid valves that were controlled based on gait events during the gait cycle, i.e., heel strike, foot landing, heel-off and toe-off. Such events were determined using two force sensors placed beneath the feet, under the heel and metatarsal heads. The system was tested with three healthy subjects and one patient suffering from cauda equina syndrome. The functionality of the device was demonstrated during treadmill walking trials. EMG data

collected from the nondisabled walkers indicated reduced muscle activation during assistance, especially for the tibialis anterior muscle. The patient's assisted walking trials demonstrated that the robotic device was capable of providing functional plantar flexor assistance. However, the kinematics of the ankle joint were minimally affected by the AAFO assistance.

2.2.2.2. AAFO with artificial muscle actuators

Artificial pneumatic muscles are suitable for rehabilitation applications due to their low weight, high output force capability, and inherent compliancy [67]. All of these characteristics are important for designing an efficient AAFO. However, the artificial pneumatic muscles have drawbacks, such as the inherent bandwidth, that constrains the use of such actuators in gait rehabilitation. Therefore, some studies have focused on developing AAFOs with artificial muscle actuators to evaluate the effectiveness of this technology in a rehabilitation context.

Ferris et al. [68, 69, 70, 71] presented an AAFO able to provide actuation of orthosis plantar and dorsiflexion using a electromyography (EMG) based controller (Fig. 2.3a). The orthosis included a carbon fiber and polypropylene shell, a metal hinge joint, and two artificial pneumatic muscles. The study shows that a robotic device that is mechanically coupled to a human could produce substantial alterations in muscle activation signals. In the studies, the AAFO controlled by EMG signals from a biarticular muscle (medial gastrocnemius) or from a uniarticular muscle (soleus) to produce a plantarflexion assistance, and the EMG from tibialis anterior muscle to assist in dorsiflexion. The results show how mechanical energy transfer from a robotic device to the wearer through a neuroelectrical interface can result in primary motor pattern adaptations.

Takahashi et al. [72] proposed an AAFO composed of a custom-fitted carbon fiber shank and foot braces hinged at the ankle joint level, actuated using an artificial pneumatic muscle to provide a plantarflexion torque about the ankle (Fig. 2.3b). The magnitude and timing of the exoskeleton assistance was based on the EMG signal from the subjects'paretic soleus and ground reaction force data from an instrumented treadmill. Five subjects with stroke participated in this study by walking on a treadmill. It was found that the exoskeleton increased the total paretic ankle plantarflexion moment by 16%, which leads to an improved walking. However, there was no statistically significant effects of the exoskeleton on reducing similarly the metabolic cost.

Park et al. [73, 74], developed an actuated ankle foot orthosis (AAFO) using soft ma-

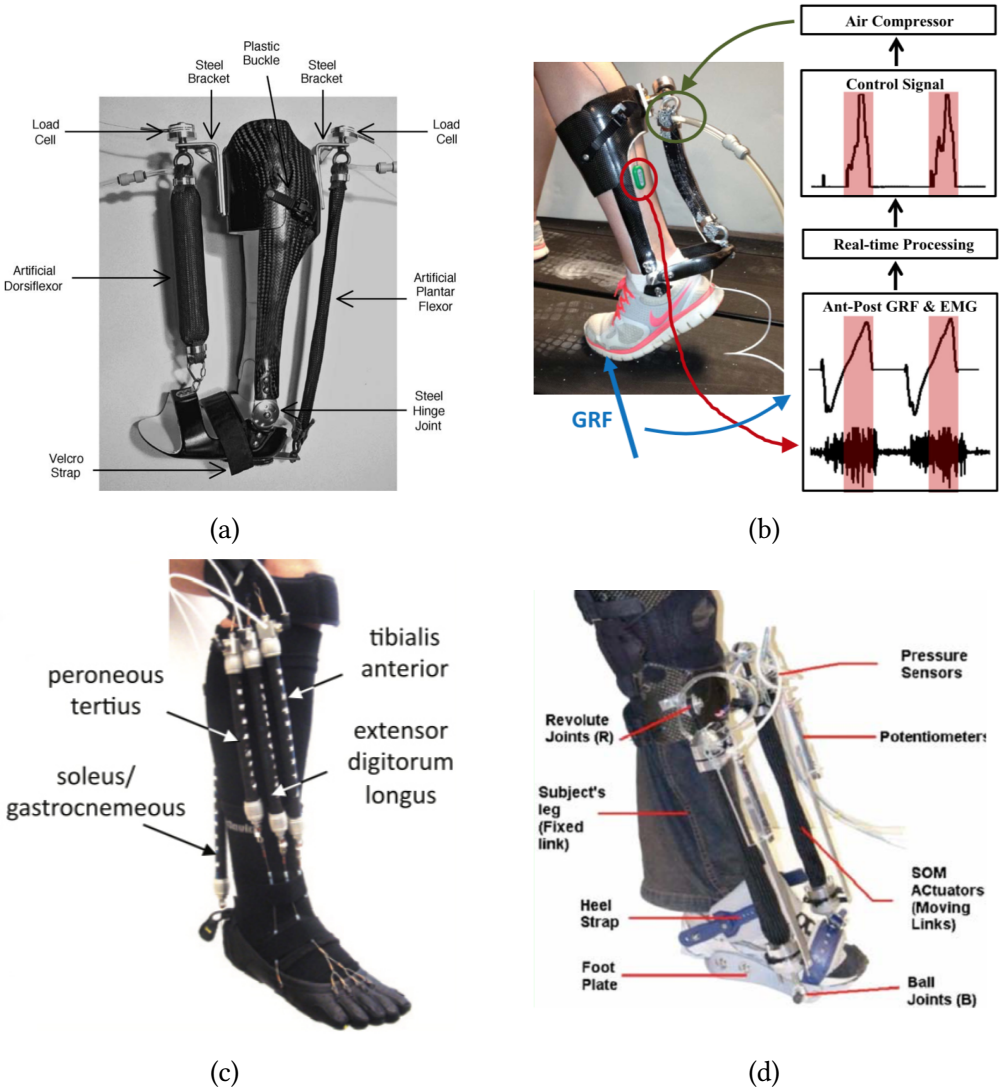

Figure 2.3 – AAFOs with pneumatic muscle actuators.

terials and actuators that mimics the biological muscle-tendon architecture (Fig. 2.3c). Four artificial muscles were placed on the lower leg (three anterior muscles for dorsiflexion, inversion, and eversion, as well as one posterior muscle for plantarflexion), with their artificial tendons anchored at the knee and foot braces. The artificial muscles were designed as counterparts to the biological muscles for dorsiflexion, plantarflexion, inversion, and eversion, respectively, so that the device could provide the supplementary forces to the corresponding muscles. Two custom-built strain sensors were used for measuring the ankle joint angles. Also, two inertia messurement units were used for measuring the orientations of the lower leg and the foot. Finally, four force sensitive resistors (FSR) were embedded in the shoe insole. The mechanical system was characterized to evaluate the response time, linearity, and repeatability of the actuation system.

Due to the nonlinearity of the pneumatic muscles, proportional control of the actuators was not as straightforward as for other linear actuators, such as DC motors. The prototype was tested for dorsi and plantar flexion motions while the wearer was seated, which have importance for rehabilitation, as a first proof of principle. From the initial results, the authors claim that a new controller that can assist walking gaits can be developed.

In [75], Ward et al. presented a robotic gait trainer that uses pneumatic muscles to produce plantar and dorsiflexion movements (Fig. 2.3d). This AAFO consists of a typical tripod mechanism consisting of a flat plate and bi-directional actuators. The uniqueness of this wearable device is that the fixed link in the tripod is the patient's leg. Such design reduces the complexity of the kinematics while still providing sufficient motion for all the degrees of freedom of the ankle joint. The study presents preliminary results of the AAFO assiting the gait movement of a healthy subject.

2.2.2.3. AAFO with electrical motors

It has been shown that the weight of the electric actuators is about twice of that of the hydraulic ones; however, the electric actuators are 92% more power efficient than the hydraulic ones during walking [76]. At the same time, unlike the hydraulic actuators that can have part of their weight located apart from the joints' axis of rotation, the weight of electrical joints is all centered at the actual joint. This may have some challenges for an efficient exoskeleton mechanical design. However, if the purpose of the robotic orthoses is not to assist the wearers to carry relatively heavy loads, electric actuators are generally more suitable to be used in exoskeletons. Indeed, the advantages of electric actuators can be highlighted with the decrease of the required torque output (i.e., decrease of actuators' size and weight). Additionally, since the required torques for lower limb robotic orthoses are relatively high and the speed is relatively low, it is usually hard for direct-drive electric actuators to satisfy the requirements of high torque output, low speed, small size, and lightweight simultaneously. Hence, geared drive and/or cable drive electric actuators are usually used to satisfy such requirements [16].

In [77], Zhu et al. presented a knee-ankle robotic orthosis consisting of a frameless electrical motor, a timing belt connecting the output shaft of the motor to the sun gear, and a planetary gear set (Fig. 2.4a). The ankle and knee are actuated to dynamically offload body weight from the affected leg of a stroke patient. The orthosis design was validated with two experiments with a healthy human subject wearing the orthosis while walking on a treadmill. The preliminary results affirm that the orthosis is a suitable platform for testing different rehabilitation control strategies.

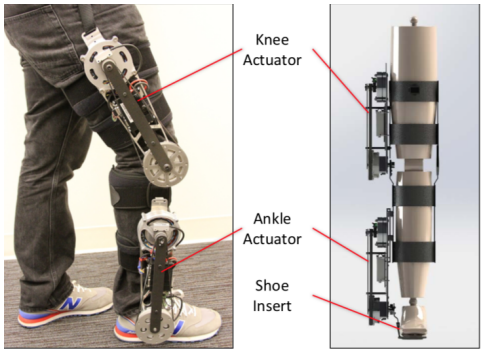

(a)

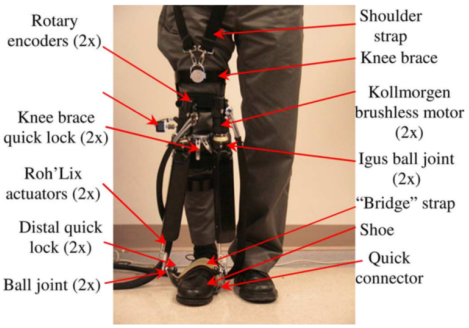

(b)

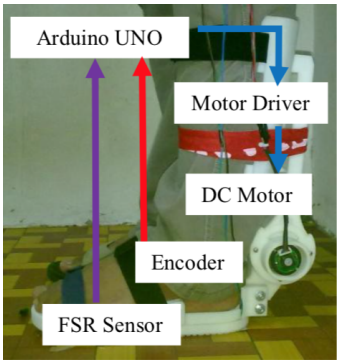

(c)

(d)

Figure 2.4 – AAFOs with electrical motor actuators.

Roy et al. [78, 79, 80] developed an ankle robot system (Anklebot). The Anklebot provides actuation in two degrees of freedom (DOF), namely plantar-dorsiflexion and inversion-eversion through two linear actuators mounted in parallel (Fig. 2.4b). Internal-external rotation is limited at the ankle with the orientation of the foot in the transverse plane being controlled primarily by rotation of the leg. The AAFO is actuated using two brushless DC motors, which provide torques that are amplified and transmitted to the foot via a pair of parallel linear traction drives. The traction drive consists of two linear screw actuators. Experimental results with a chronic stroke suffering from foot drop showed that the anklebot assisted gait training progressively while significantly reducing the foot drop effects after six weeks of training using the device.

In [81, 82], an AAFO is developed to assist the ankle joint in plantarflexion and dorsiflexion direction (Fig. 2.4c). The AAFO is equipped with two force sensitive resistors which act as switch sensors to actuate the DC motor enabling though the control of the dorsiflexion/plantarflexion of the ankle joint..

In [83], Veneva and Ferreira proposed an AAFO with a direct drive actuation using an

electric motor (Fig. 2.4d). The actuator joint torque is automatically modulated to optimize the heel-to-forefoot transition during the gait cycle. The study presents preliminary results with a healthy subject. The system controls the orthosis functionalities, records the data received from sensors during the gait and transfers recorded data to graphical user interface for visualization and future analysis.

2.2.2.4. AAFO with SEAs

Considering some limitations of the non-backdrivable actuators for robots, e.g., low power density, researchers started, since the 1990s, to develop series elastic actuators (SEAs). The SEA, previously developed for legged robots, was used to control the impedance of the orthotic ankle joint in sagittal plane. The SEA consists of a brushless DC motor in series with a spring and provides force control by controlling the extent to which the series spring is compressed. The advantages of the SEA are related to providing relatively low impedance, the motor is isolated from shock loads, and the effects of backlash, torque ripple, and friction are filtered by the spring. A further advantage is that the SEA exhibits stable behavior while in contact with external environments, particularly when in parallel with a human limb. Therefore, SEA-based actuators were then used as an important actuation mode for wearable robots [16].

In [29], Blaya et al. developed an AAFO using a SEA (Fig. 2.5a). The AAFO is developed to assist the wearer during loading response and swing phases to prevent drop foot and foot slap. A finite-state machine was implemented to address the gait diffeciencies. Three states were used, each with a specific control objective, across the gait cycle. From heel strike to midstance, the objective of the controller was to prevent foot slap. From midstance to toe-off, the controller minimized the overall impedance to not impede power plantar flexion movements. Finally, during the swing phase, the user's foot was lifted to prevent foot drop. Two unilateral drop-foot patients participated in the study. The results show that the number of occurrences of foot slap was reduced and the dorsiflexion angular range was increased during the swing phase.

In [84], Boehler et al. presented an actuated ankle foot orthosis using a SEA (Fig. 2.5b). Results from a test with a healthy subject showed that the robot is interacting with the wearer rather than forcing the wearer to perform a fixed movement. Although no predefined pattern was used to obtain the reference trajectories for the ankle joint angle, this angle matches a healthy subject's gait. Further, in [85], after several months of testing the system with three healthy subjects and two patients show that the control methodology is satisfactory for in-clinic use.

In [86], Moltedo et al. presented a mechanically adjustable compliance and controllable equilibrium position actuator (MACCEPA). The actuator is a torque-controlled, variable stiffness actuator that works as a torsion spring and allows controlling independently its equilibrium position and joint stiffness (Fig. 2.5c). The actuator is bidirectional, thus it can provide torques both in plantarflexion and dorsiflexion. Although several static characterization tests were performed with the actuator, the system is not connected yet to an ankle foot orthosis. In a future work, the complete AAFO will be tested with impaired subjects, to assess the performance of the actuator in assisting the ankle joint movements.

Zhang et al. [87] used an AAFO with a SEA actuator to compare nine different controllers during walking on a treadmill with one healthy subject (Fig. 2.5d). However, this AAFO can only produce assistance in the plantarflexion direction. Nevertheless, the results of the comparison between controllers offer an insight on the advantages and limitations of different control strategies for different rehabilitation purposes.

In [88, 89] Sugar et al. proposed a AAFO with a robotic tendon for gait assistance having a single degree of freedom in the sagittal plane (Fig. 2.5e). A robotic tendon is a spring based, linear actuator in which the stiffness of the spring is adapted. The robotic tendon uses its inherent elastic nature to reduce both peak power and energy requirements. The AAFO was tested with three hemiparetic patients. Results show that all subjects had some positive changes in their key gait variables while using the AAFO. These changes were less efficient while walking on a treadmill. Over ground robot data suggests that positive changes in gait variables do occur, but at a slower rate with respect to the walking on a treadmill.

Dijk et al. developed in [90] an AAFO called the Achilles exoskeleton that is intended to provide push-off assistance for healthy subjects during walking (Fig. 2.5f). The assistance is provided by a a SEA that has been optimized to provide maximal push-off power. The AAFO consists of three parts: two boot parts containing the motors, sensors and the mechanics to transfer power to the human and a backpack containing control hardware, batteries and power management.

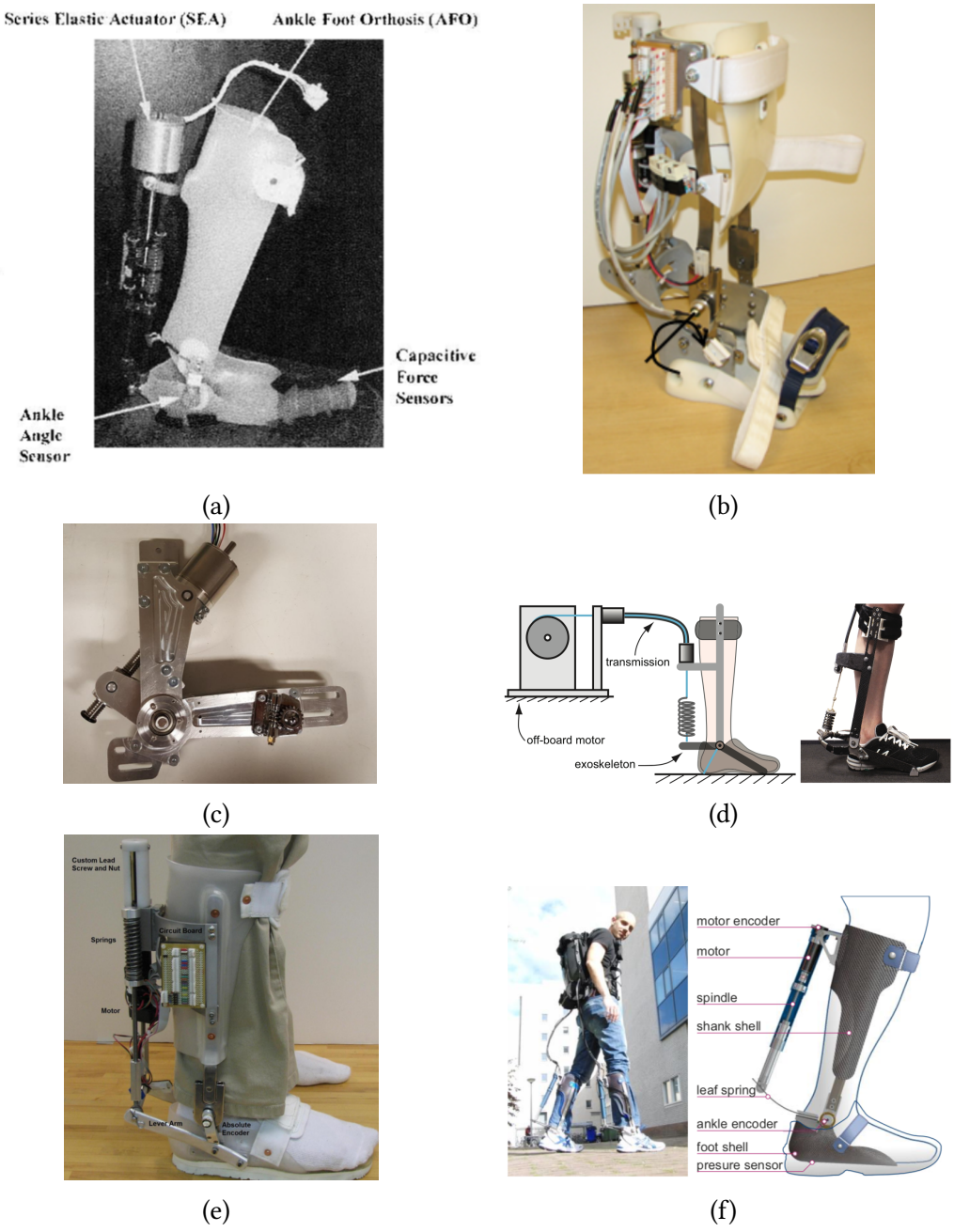

Figure 2.5 – AAFOs with series elastic actuators.

2.3 A review of control strategies

The control method applied to an exoskeleton or active orthosis has a direct impact on the level and rate of human adaptation to the active device; i.e., the central nervous system can adapt more easily to a continuous, smooth and proportionate stimulus [48]. In this sense, it is clear that there exist an close relationship between AAFO and the control strategies based on the rehabilitation purposes [20]. Control schemes are customized to the pathology characteristics as well as the mechanical configuration of the device. For example, there are several AAFO that are able to provide assistive torque only in the dorsiflexion direction to prevent foot drop and foot slap, or to provide assistive torque in the plantar-flexion direction to promote a more effective foot push-off power prior to the swing phase. Other AAFOs are able to produce torques in both directions of the sagittal plane of the ankle joint, to effectively assist during the push-off at the end of the stance phase, as well as providing assistance during the swing phase to prevent from foot drop.

Recent reviews of lower limb technologies [26, 46, 20, 91] show that the low level control strategies can be classified in four groups, based on the input signals of the controller: 1) those that pre-select the assistive torque value and apply it in a feedforward scheme with respect to the gait phase detected, 2) that provide the assistance as a function of EMG signals from the muscles spanning the ankle joint, 3) that adapt the stiffness, inertia or impedance of the coupled human-AAFO system based on different criteria, or 4) that provide the assistive torque as a function of the tracking error between the current ankle joint angle and a reference trajectory pattern commonly generated from healthy subject walking profiles.

In the following, a brief description of AAFO controllers is presented. The focus of this section is to review low level AAFO control algorithms, i.e., control algorithms that are explicitly designed to achieve the torque, position, impedance, or admittance control necessary to assist the ankle joint during the gait cycle.

2.3.1. Impedance control

The relationship between the force exerted by the actuators and resulting motion velocity is generally known as mechanical impedance. The concept of impedance control in the field of robotics is first introduced by Hogan [92]. Impedance controllers within an

AAFO aim to adapt the stiffness, inertia or impedance of the coupled human-AAFO system during walking activities as function of gait phase events detection. Such systems have the advantage of not requiring a predefined reference trajectory, however, they require a minimum residual voluntary effort to initiate movements and they require as well a prior identification of the human-AAFO parameters [80, 93].

For example, in [29], Blaya et al. used an adaptive control of a variable impedance AAFO to correct foot slap and foot drop. As mentioned before, this AAFO is actuated using a SEA, which effectively changes the stiffness of the assisted ankle joint. Selecting the preferred stiffness of the orthotic torsional spring is closely related to the ground reaction force generated at the moment of forefoot impact after each walking step. To detect the dual peaks and the occurrence of foot slap, the AAFO controller numerically differentiated the forefoot force if it was found to be negative, then the stiffness of the orthotic torsional spring was incremented. During each swing phase, stance time was estimated from the orthotic force transducers and the AAFO controller optimize the orthotic controlled toe landing stiffness. Also, a PD control was used to control the orthotic ankle joint during the swing phase to prevent foot drop. This was done by setting a reference desired ankle joint value that was sufficiently dorsiflexed.

In [79, 80], Roy et al. used the Anklebot to assist the ankle joint in two degrees of freedom. The anklebot delivered torques at the paretic ankle level during one or several key gait periods, based on a sub event-triggered method, each with unique functional needs: 1) concentric plantar flexion torque to enable push-off propulsion during terminal stance, 2) concentric dorsiflexion torque to facilitate swing clearance, starting at toe-off and continuing until mid-swing, and 3) velocity-dependent viscous torque (resistive) to attenuate the impact force at landing. The impedance controller generates ankle torques proportional to the magnitude of the tracking error between the desired and actual ankle trajectory through torsional stiffness and damping settings.

In [94, 95], Perez Ibarra et al. presented an impedance controller for the Anklebot. The robot stiffness is adapted online based on the patient's stiffness estimation and then it is optimized using a cost function that characterizes the assist-as-needed paradigm. To ensure patient involvment in the generated movement, an assistance factor is defined, limiting the robot action. The system was tested with four stroke patients. The results show that the proposed control strategies can effectively estimate the patient's stiffness and properly set the level of robot assistance to complete the desired task. The optimal solution seems to further stimulate the active participation of the patient by reducing the robot assistance during the task. Later, in [96], an EMG-driven musculoskeletal model

was used to compute the ankle joint stiffness and muscular force. The study showed that the activation of the tibialis anterior muscle during dorsiflexion was higher without the use of robotic assistance, compared to the adaptive-stiffness control.

2.3.2. Torque control

An example of torque control is presented in [64], where an electro-hydraulic actuated ankle foot orthosis is used to evaluate the adaptive ability of human locomotion when walking is challenged by different force field environments. For this purpose, a classical PID controller is used to control the system. The force delivered by the orthosis is measured using a load cell, located in series with the slave cylinder, which allows for torque control implementation. The control algorithm involved switching from force to position control in real time while applying rapid displacements.

In [57], a force control scheme is developed in order to stretch the ankle joint muscles in the sagittal plane for after acute stroke in-bed rehabilitation. The force control algorithms presented were developed for three purposes: the isometric torque generation, passive stretching and active movement training (with robotic assistance or resistance).

In [83], Veneva et al. used a torque control algorithm based on the biomechanical interpretation of the locomotion: during each gait cycle, the total time for the left and right legs when the foot remains in contact with the ground is measured, then the controller estimates the forward speed and modulates the swing phase flexion and extension in order to achieve lower limb dynamics similar to those found with healthy subjects. At the low level control, a PID controller was used to maintain stability when a foot load is applied.

In [77], Zhu et al. used a quasi-stiffness control method, which implements a virtual spring at each joint based on the slope of the desired torque-angle curve for healthy human walking. This desired torque was used as reference for the torque controller of the AAFO. Passive and high torque walking tests were conducted with a healthy subject.

2.3.3. EMG based control algorithms

Proportional myoelectric control uses the human's muscle activation signals to control external devices such as AAFO. This type of control relies on the detection of the wearer's intention to control the robotic device.

For example, in [62, 68, 70, 71, 97, 98], Ferris et al. developed an EMG based controller

that used the EMG signals from the soleus, gastrocnemius and tibialis anterior muscles to control the artificial muscles of the AAFO. Several test with healthy subjects have been conducted with this AAFO using the EMG based controller. It was found, in active assistance scenarios, that assiting the gait at specific moments could affect the muscle activation based on the type of the provided assistance, i.e. the AAFO reduced the muscle recruitment if the assistance was provided for the same function of the muscle. Furthermore, when the assistance provided directly counteracted the mechanical action of the wearer's soleus muscle, subjects adapted their walking control patterns by making significant reductions in soleus activation. Therefore, myoelectrically controlled, powered AAFOs have the potential to serve as a tool to investigate the locomotor adaptation process.

In [72], Takahashi et al. presented an AAFO that supplies plantarflexion assistance proportional to the user's paretic soleus electromyography amplitude during specific moments of the gait phase. Five subjects with stroke walked with a powered ankle orthosis for three sessions of five minutes each. The results show that the AAFO increased the paretic plantarflexion moment by 16% during the powered walking trials with repsect to unassisted walking condition. However, only in three subjects, the paretic soleus activation during push-off was reduced during the assisted sessions compared to unassisted walking.

2.3.4. Reference tracking control algorithms

Trajectory tracking or position control is widely implemented by robotic training devices. Trajectory tracking guides the patient's limbs towards a desired reference gait trajectories. It mainly consists of proportional feedback position controllers with joint angle gait trajectories as input. In this case, the issue of determining the optimal reference trajectory is of great importance. Mathematical models of normative gait trajectories and pre-recorded trajectories from healthy individuals are commonly used [91].

On the one hand, such reference tracking control systems have the advantage of potentially being able to assist the patient disregarding the level of the impairment. On the other hand, such control strategies are based on the use of predefined trajectories that may not fit to different profiles of patients, particularly in terms of walking speed, step length, movement range, etc.

For example, in [99], Holgate et al. proposed a trajectory tracking scheme to control a SEA actuator [84]. The trajectory pattern was generated based on the inclination of the

tibia during the gait cycle, or with a ”dynamic pace controller”, which uses the walking speed to adjust the magnitude and duration of the desired trajectory. Both approaches were tested with both healthy and stroke patients, respectively, with satisfactory results.

In [89], Ward et al. proposed a proportional controller for a SEA actuated AAFO. The control signals are derived from position feedback on the input side of the spring, while the output side is in open-loop. The system was tested with hemiparetic patients in two scenarios; treadmill and level walking. In both cases, the system was able to correct the ankle joint profile of the patients.

In [42], Martinez et al. used a lower limb exoskeleton with four active degrees of freedom at the hip and knee joints to assist walking during the swing phase of the gait cycle, the controller used a proportional derivative function based on the distance from the joint's path to a predefined healthy path, effectively achieving a torque field for the hip and knee joints that does not enforce a step duration.

To deal with foot drop, Zhang et al. [59, 60] presented an ankle rehabilitation robotic platform to stretch the ankle joint muscles following a predefined sine function, which amplitude and frequency were specified by a physiotherapist. The controller used a PD gain to follow the desired trajectory.

In [100], Kagawa et al. presented a joint trajectory generation algorithm that divides the gait cycle pattern into two curves crossing at specific ”via-points”; i.e., heel strike and midpoint of the swing phase. The algorithm then optimizes the joint trajectories by minimizing the square joint velocities. In simulations, Kagawa et al. reported that the algorithm required 0.16 seconds to be executed and produce the optimized trajectory.

Roy et al. [79, 80] proposed a gait event-triggered impedance control for an AAFO [78], where the generated assistive torque is proportional to the position and velocity error between a desired and actual ankle joint position. The swing ankle joint angle was selected to be over-dorsiflexed (20°) to deal with foot drop. The controller gains are calculated using a biomechanical model for landing, push-off and swing phases. The system was tested with both healthy and stroke subjects [79]. The patient achieving an increased walking speed in 6 weeks (from 30 to 36 cm/s), and an increased dorsiflexion angle during the swing phase (from $2.5\pm0.5^\circ$ to $7.6\pm0.8^\circ$).

In [85, 75], Hitt et al. presented a dynamically controlled ankle-foot-orthosis (DCO) controller that supports walking gait initiation, ending and speed modulation based on user intent on a treadmill. The DCO controller has a predetermined gait pattern expressed as a time-based function embedded in the controller. As the user initiates gait, the SEA's motor drives a lead screw nut through the pattern predetermined for each subject with

closed loop feedback. The ankle, however, is not forced to follow the specific pattern because a compliant spring is between the motor and user. The low-level controller used for the reference tracking is a PD controller. Several months of testing with three able-bodied and two subjects with gait deficits show that the control methodology is sufficient for clinical use.

Jamwal et al. [58] used an adaptive fuzzy controller to control the orientation and pose of a moving platform attached to the foot. Since the system uses pneumatic artificial muscles, the fuzzy control is capable of producing accurate trajectory tracking of the end effector. Furthermore, the adaptive scheme of the fuzzy control is able to compensate for the nonlinearity of the pneumatic muscle actuators as well as the external disturbances.

2.3.5. Gait phase based control algorithms

Feedforward controllers are the simplest to implement in AAFO, thus are common to find in preliminary studies or to test early prototypes [82]. Moreover, such strategies often used to select diferent control algorithms across the gait cycle. Only the AAFO controllers that use a feedforward control as the sole alorithm are described in this subsection. For such controllers, the assistive torque provided to the ankle joint depends on the detected gait phase and it is normally defined prior to the experiments and it remains constant for each detected gait phase. This control strategy has shown satisfactory results in assisting the gait cycle, as it can be seen in the following examples.

In [69], Gordon et al. proposed a ground reaction force based controller. The AAFO incorporated a foot switch, designed to fit only under the left forefoot inside the shoe. When the forefoot is in contact with the ground, a control signal activates maximal air pressure to the artificial pneumatic muscle through the pressure regulators. During active conditions with healthy subjects, the artificial pneumatic muscles produced large forces during stance and performed substantial concentric work. Further, the subjects walked with greater plantar flexion during active trials compared to unassisted ones.

In [84], the system switches between a velocity control and a stiffness control. The gait cycle is divided into seven different zones, which include one or more gait sub-phases, and each zone is governed by a given control law.

In [66], a heuristically tuned feedforward controller is presented. The control objectives at each gait phase are similar to those presented in [29], with the difference that plantar flexion assistance is provided during the late stance phase.

In [73] and [74], Park et al. used a feedforward and a feedback controllers to drive an

active soft orthotic device for the ankle joint. The feedforward controller uses look-up tables from previous experiments to calculate the assistive torque and the feedback controller uses a linear time-invariant controller that requires prior identification of the system.

2.4 Discussion

Based on the aforementioned review of the existing AAFO devices, it is noted that motor-actuated AAFOs have been widely used for applications were portability and low weight constraints are to be respected. In this thesis, a DC motor actuated AAFO was chosen to implement and test the proposed control strategies for assisting the gait movements.

To effectively assist the wearer of an AAFO in walking activities, several control strategies have been proposed in literature. From the overview of the control strategies, one can observe that feedforward strategies are simple to implement but the lack of feedback could produce an insufficient or excessive assistance. EMG based strategies provide a high rate of adaptation with respect to the central nervous system, but requires a minimum residual muscular activities to be effective, which might not be the case for some patients suffering from acute stroke. Furthermore, EMG sensor electrodes might easily become disconnected or detached from skin surfaces because human bodies are always in physical contact with the robot. In addition, sensor electrode misplacement due to human error is more likely when using multiple channels. Such effects may lead to significant errors in the estimation of the user's joint movements and may cause unstable torque generation by the robot and unconfortable movement to the wearer [101]. The systems that adapt their impedance have the advantage of not requiring a predefined trajectory but they require a minimum residual voluntary effort to initiate movements. Therefore, a trajectory tracking strategy could potentially provide more appropriate assistance when the wearer of the active orthosis is not fully able to initiate movements.

The potential issue with trajectory tracking based controllers is that the controller parameters are not tuned based on real time judgment of the patient's abilities. The term adaptation is used for real time tuning of the controllers designed for AAFO actuators to match patient's disability level and to actively involve the patient in the training process. As disability level varies from subject to subject, online compensation of the ankle-AAFO external and internal forces is of great importance in the adaptive assistance paradigm.

The effectiveness of AAFO to correct gait deficiencies at the ankle joint level, using trajectory tracking approaches, has not been extensively studied in the literature. Indeed, there is a lack of quantitative data of experimental results with subjects presenting gait deficiencies, such as paretic patients.

In this thesis, joint-level trajectory tracking control approaches that are able to compensate for the AAFO-ankle dynamic system changes are proposed. Furthermore, the ankle joint reference needs to be adjusted in real time based on the walking characteristics of the wearer, without imposing a predefined walking pace.

In the following chapter, the AAFO-human dynamic model is introduced and the hardware used to measure and actuate the ankle joint is described in detail.

3 — System modeling and hardware description

3.1 Introduction

In this chapter, a brief anatomical description of the ankle joint and the common pathologies present during the gait cycle is provided. Also, a dynamic model of the AAFO attached to the leg of the wearer is developed and described. Since different control strategies are used in this study, the dynamic model is presented in different forms.

Finally, a description of the harware used in the study is detailed. Starting with the system used for actuating the ankle joint during the gait cycle; an actuated ankle foot orthosis (AAFO). The amount of sensors depends on the number of gait variables required to be measured for each controller, and not all the control schemes presented in this study require the same experimental setup.

3.2 Anatomical description of the ankle joint

The muscles spanning in the lower limbs have to produce positive and negative work in a coordinated way in order to generate the walk motion. When there is a disruption in the walking task, either by a lack of coordination or power generation, some gait pathologies can appear, which, in part, are normally circumvented by the subject by modifying the gait pattern. Therefore, to correct the gait of paretic patients, a minimum understanding of the anatomy of the ankle joint and its pathologies is required.

Furthermore, it is important to analyze the gait in real time in order to detect any discrepancy of the ankle joint profile from a healthy pattern and provide assistive torque, directly or indirectly, in a effective manner. For this purpose, it is paramount to measure a minimum number of the variables involved in the gait cycle, which is done by adding sensors to the system.

It is convenient to have in mind the intrinsic dynamics of the ankle. The ankle-foot complex consists of different biological elements such as skin, muscles, tendons, ligaments, bones, cartilage, and connective tissue. The mechanical properties of these elements depend on several factors as the deformation rate, position, and motion speed [102]. Their behavior is inherently nonlinear. Moreover, the mechanical impedance of the ankle can be modified by the reaction of the muscles to the different electrical signals from the nervous system. This behavior also varies among different subjects and the wide variety of dysfunctional conditions that can affect the ankle motion [103]. The anatomy of the ankle joint complex shows that it is not just a simple hinge joint but that of multi-axial motions occurring simultaneously to facilitate human gait.

The majority of motion within the foot and ankle is produced by the twelve extrinsic muscles, which originate within the leg and insert within the foot. These muscles are contained within four compartments. The anterior compartment consists of four muscles: the tibialis anterior (TA), the extensor digitorum longus, the extensor hallucis longus, and the peroneus tertius. The tibialis anterior and the extensor hallucis longus produce dorsiflexion and inversion of the foot. The peroneus tertius produces dorsiflexion and eversion of the foot. The extensor digitorum longus only produces dorsiflexion of the foot. The lateral compartment is composed of two muscles: the peroneus longus and the peroneus brevis, which produce plantar flexion and eversion of the foot. The posterior compartment consists of three muscles: the gastrocnemius (GAS), the soleus (SOL), and the plantaris, which contribute to plantarflexion of the foot. The deep posterior compartment is composed of three muscles: the tibialis posterior, the flexor digitorum longus, and the flexor hallucis longus, which produce plantarflexion and inversion of the foot [104].

The key movements of the ankle joint complex are plantar and dorsiflexion, occurring in the sagittal plane; ab-/adduction occurring in the transverse plane and inversion-eversion, occurring in the frontal plane, as seen in Fig. 3.1. Combinations of these motions across both the subtalar and tibiotalar joints create three-dimensional motions called supination and pronation.

Lack of dorsiflexion in swing phase and at heel strike is a commonly reported kinematic

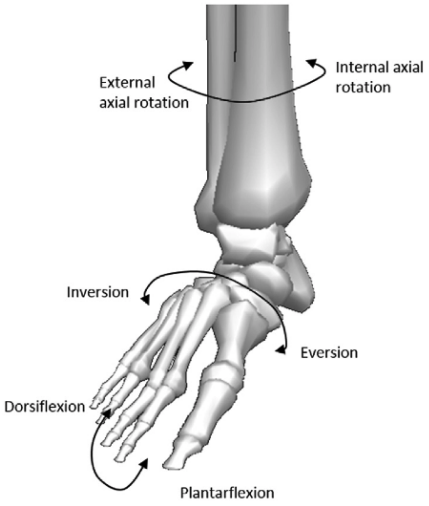

Figure 3.1 – Anatomy of the ankle joint and the main rotations.

deviation in people with hemiplegic stroke. As the foot normally clears the ground by less than a few centimetres during swing phase, a failure to dorsiflex the ankle during swing will effectively lengthen the lower limb. Unless compensations are made, this is likely to result in the foot hitting the ground as the hip flexes and the knee extends. To compensate for this increased lower limb length, people with hemiplegic stroke may excessively elevate the pelvis on the side of the swinging leg., i.e, abduct the contralateral hip in stance, abduct the swing hip, and they may laterally flex the trunk towards the unaffected side and restrict the lateral pelvic displacement towards the stance leg in much the same way as discussed under decreased peak knee flexion above [24, 25].

The net muscle moments acting at the ankle during swing phase are very small [105], however, EMG recordings of tibialis anterior muscle activity show peaks of activity at the beginning and end of swing. Hence, it is assumed that the tibialis anterior muscle produces a dorsiflexion moment which prevents the ankle accelerating into plantar flexion under the influence of motion dependent moments early in swing phase. Therefore, when the TA muscle is impaired in any way, a lack of dorsiflexion, especially during the swing phase, is evident and this could lead to a foot drop pathology. Also, and perhaps even more commonly, a reduced dorsiflexion in swing phase may be caused by an increased plantarflexor muscle moment attributable either to adaptive shortening or excessive activation of the plantarflexor muscles.

There are three main functions for the ankle plantar flexor group: 1) provide a controlled roll-off [106, 107], 2) actively provide forward progression or push-off [108, 109] and 3)

accelerate the leg into swing [110, 111].

The controlled roll-off theory describes forward progression during single-leg stance as a controlled fall [107]. Thus, the proposed primary action of the ankle plantar flexors during the controlled roll-off is to decelerate tibia rotation and prevent knee flexion as the body rotates over the stance leg. Forward progression is then the result of a passive mechanism as the body moves forward as a result of momentum and inertia.

The active push-off theory hypothesizes that the energy generated by the plantar flexor group is transferred to the trunk to provide support and forward progression. Supporting evidence was provided in a recent theoretical study that showed the plantar flexor moment was the primary contributor to the accelerations of the head-arms-trunk segment in both the horizontal (considered analogous to forward progression) and vertical (considered analogous to support) directions during the second-half of the single-leg stance phase [109].

The final theory suggests that the primary function of the ankle plantar flexors is to accelerate the leg into swing, and forward progression is provided later in the swing phase as energy from the swing leg is transferred to the trunk [110, 111].

Therefore, a lack of plantar flexion could also lead to gait pathologies such as a reduced push-off power, which in turn may lead to a reduction in walking speed. However, it has been proposed that a strong, well-timed ankle push-off occurring just prior to initial contact of the contralateral limb, can significantly reduce the energy required for step-to-step transition costs.

3.3 Dynamic model of the ankle joint

In order to model the AAFO system, a frame $\mathcal{F}(\vec{x}^f, \vec{y}^f, \vec{z}^f)$ is considered fixed to the left foot such that $\vec{x}^f$ has the same direction as the foot while the origin is located at the ankle joint; $\vec{z}^f$ is defined as the rotational axis of the ankle joint, and $\vec{y}^f$ is defined such that the three-sided frame $\mathcal{F}$ is direct. A second frame $\mathcal{G}(\vec{x}^g, \vec{y}^g, \vec{z}^g)$ is at the ground, with $\vec{x}^g$ parallel to the horizontal, $\vec{y}^g$ parallel to the vertical, and $\vec{z}^g$ defined such as the three-sided frame $(\vec{x}^g, \vec{y}^g, \vec{z}^g)$ is direct. Note that $\vec{z}^f$ and $\vec{z}^g$ are collinear.

Denote by θ the angle between the foot and the shank, by θ_s the angle between the shank and the vertical axis and by α the angle between the foot and the horizontal axis (Fig. 3.2). Using the embedded encoders in the AAFO and inertia measurement

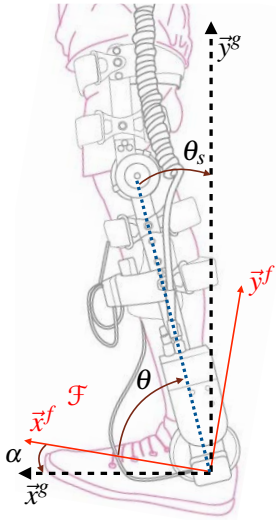

Figure 3.2 – The angles determining the foot and the shank orientations. Foot frame $\mathcal{F}(\vec{x}^f, \vec{y}^f, \vec{z}^f)$, where $\vec{x}^f$ is in the same plane as the heel-half of the insole. Ground frame $\mathcal{G}(\vec{x}^g, \vec{y}^g, \vec{z}^g)$.

units (IMUs), θ and θ_s are accessible to measurement and α is given by

$$\alpha = \theta + \theta_s - \frac{\pi}{2} \tag{3.1}$$

Several torques acting on the AAFO system at the ankle level are considered. They can be classified in endogenous (which are generated by the environment) and exogenous disturbances (which are dependent upon internal variables). The former group are the gravity torque, the solid and viscous friction torques, and system's joint stiffness torque. The later group are the torque induced by the translational acceleration of the foot, the torque developed by the ground reaction forces, and the torque produced by the plantar flexion and dorsiflexion muscle groups. Also, the torque developed by the AAFO's actuator, namely, the control torque, is considered. Since the AAFO used for this study has one degree of freedom only in the plantar and dorsiflexion direction, the modeling of the system is restricted to the sagittal plane. The AAFO system's dynamics can be expressed as follows:

$$J\ddot{\theta} = \tau_f + \tau_a + \tau_s + \tau_r + \tau_g + \tau_h + \tau \tag{3.2}$$

where τ_f is the solid and viscous friction torques, τ_a is the torque induced by the translational acceleration of the foot, τ_s is the system's joint stiffness torque, τ_r is the torque

induced by the ground reaction forces, τ_g is the gravity torque exerted by the foot on the ankle, τ_h is the torque produced by the plantar flexion and dorsiflexion muscle groups, and τ is the torque developed by the AAFO's actuator. All the torques are considered positive if they induce a counter clockwise rotation.

Remark 1 *The human torque τ_h is generated by the muscles actuating the ankle joint and is considered to be bounded by Δ_h: $|\tau_h| \leq \Delta_h$.*

Each of the aforementioned torques are defined as follows:

$$\begin{aligned}
\tau_f &= -k_{f_S}\text{sign}\dot{\theta} - k_{f_V}\dot{\theta} \\
\tau_a &= -k_a(a_y\cos\alpha - a_x\sin\alpha) \\
\tau_s &= -k_s(\theta - \theta_r) \\
\tau_r &= -k_r(x_g F_r)\cos\alpha \\
\tau_g &= -k_g\cos\alpha
\end{aligned} \tag{3.3}$$

where, k_{f_S} and k_{f_V} are the solid and viscous friction coefficients, k_s is the system's stiffness coefficient, k_a is the system's acceleration torque coefficient, a_x and a_y are the horizontal and vertical linear accelerations, expressed in the $\mathcal{G}$ frame, k_r is the ground reaction force coefficient, F_r is the equivalent GRF applied to the center of mass of the foot, x_g is the distance of the center of mass from the ankle joint expressed in the $\mathcal{F}$ frame, and $k_g = mgx_g$ is the system's gravity torque coefficient, where m and g, represent the mass of the foot and the gravity acceleration coefficient.

Note that the system's parameters described in (3.3) are difficult or impossible to measure directly, or require a mathematical model to estimate the values through prior experiments [112]. Furthermore, the values of these parameters may vary throughout a single session. For example, the torque generated by the interaction with the ground can be estimated using force sensitive resistors (FSR) embedded in the insoles of the shoes [113]. However, this estimation would be inaccurate if a small number of sensors is used and only the GRF perpendicular to the ground is considered. Nevertheless, the effects of these parameter variations are considered as external perturbations and are taken into account in the human torque variable τ_h. Consequently, these parameters are considered constant for this study.

By replacing (3.3) in (3.2), we obtain:

$$\begin{aligned} J\ddot{\theta} = & \underbrace{-k_g \cos\alpha - k_{f_S} sign\dot{\theta} - k_{f_V}\dot{\theta} - k_s(\theta - \theta_r)}_{:=\xi_{en}(\theta,\dot{\theta},\alpha,t)} \\ & \underbrace{-k_a(a_y\cos\alpha - a_x\sin\alpha) - k_r(x_g F_r)\cos\alpha + \tau_h}_{:=\xi_{ex}(\theta,\dot{\theta},\alpha,t)} + \tau \end{aligned} \tag{3.4}$$

where, $\xi_{en}(\theta,\dot{\theta},\alpha,t)$ and $\xi_{ex}(\theta,\dot{\theta},\alpha,t)$ represent the sum of all endogenous and exogenous torques, respectively.

The expression (3.4) of the AAFO dynamic model can be rewritten for different control schemes. For example, by adding FSR sensors in the insoles of the ipsilateral foot and multiplying the signals by the distance from the ankle joint to the sensor in the $\vec{x}^f$ direction, an estimation of the GRF ($x_g F_r$) can be obtained.

$$x_g F_r = R_1 x_1 + R_2 x_2 + R_3 x_3 + \ldots + R_n x_n \tag{3.5}$$

where R_w and x_w are the FSR signal of the wth ($w \in \{1,\ldots,n\}$) sensor and the distance from the ankle joint to the sensor, respectively, and n is the total number of FSR sensors. Although this estimation can be improved by using more sensors in the insole, doing so would yield in a bulky system, which require further computational time. It is a fair trade-off between the precision of the GRF estimation and the computational time to use three sensors. This has the further advantage of not requiring more FSR sensors than those already used for the gait detection algorithm described in section 4.2. Therefore, equation (3.4) can be rewritten as follows:

$$\begin{aligned} J\ddot{\theta} = & -k_{f_S}\text{sign}\dot{\theta} - k_{f_V}\dot{\theta} - k_a(a_y\cos\alpha - a_x\sin\alpha) \\ & - k_s(\theta - \theta_r) - k_r(R_1x_1 - R_2x_2 - R_3x_3)\cos\alpha \\ & - k_g\cos\alpha + \tau_h + \tau \end{aligned} \tag{3.6}$$

Also, by isolating the terms of the equation that are function of the ankle joint angle (θ,$\dot{\theta}$, and $\ddot{\theta}$), a cannonical expression is presented as follows:

$$\begin{aligned} J\ddot{\theta} + k_{f_V}\dot{\theta} + k_s\theta = & -k_g\cos\alpha - k_{f_S}sign\dot{\theta} + k_s\theta_r \\ & - k_a(a_y\cos\alpha - a_x\sin\alpha) \\ & - k_r(x_g F_r)\cos\alpha + \tau_h + \tau \end{aligned} \tag{3.7}$$

(a)

(b)

Figure 3.3 – (a), a healthy subject wearing the AAFO system. (b), the AAFO insole.

The right hand side terms of (3.7) are considered as disturbances to the system. Therefore, (3.7) can be rewritten as follows:

$$J\ddot{\theta} + B\dot{\theta} + K\theta = \tau + d, \tag{3.8}$$

with

$$\begin{aligned} d = &- k_g \cos\alpha - k_{fs} sign\dot{\theta} + k_s \theta_r \\ &- k_a(a_y \cos\alpha - a_x \sin\alpha) - k_r(x_g F_r)\cos\alpha + \tau_h \end{aligned} \tag{3.9}$$

where $B = k_{fv}$ and $K = k_s$. d represents all the non-linear disturbances.

3.4 Hardware description

3.4.1. Actuated Ankle Foot Orthosis (AAFO)

The orthosis used in this study is an AAFO as seen in 3.3. The AAFO is attached to the subject's left leg by means of straps to fix the robot to the calf and thigh, as shown in Fig. 3.3a. The orthosis has one active and one passive DOF, at the ankle and the knee joints, respectively. The active DoF is driven by a DC motor and a gearbox with a gear ratio of 114.4:1; the maximum output torque value is 15 Nm. It can produce assistive

torque in the platar and dorsiflexion directions. However, movement in the other axis of rotation is mechanically constrained, thus the AAFO system can only rotate on the sagittal plane.

The AAFO is equipped with an incremental encoder to measure the angle between the foot and the shank θ at sampling rate of 1 KHz. The angular velocity of the ankle joint $\dot{\theta}$ is derived and filtered numerically with a lowpass, fourth order Butterworth filter with a cutoff frequency of 50 Hz. The assistive torque is transmited via an insole that is rigid for the heel side of the foot and flexible on the toes, as explained in 3.3b. The AAFO is considered as rigidly fixed to the subject's leg. The foot and the AAFO are considered as one unit referred to as the AAFO system.

In this study, the problem of misalignment between the ankle joint and the AAFO's rotational axis when donning the device has been considerably reduced by adjusting manually the orthosis to every wearer's morphology using adaptable straps. Special cares have been taken during experiments in order to avoid reaching of the full ankle joint flexion/extension which considerably reduce the joint misalignment.

The electronics of the AAFO consist of a data acquisition card from National Instruments (NI myRIO-1900) and a controller card ESCON Module 50/5. This first card has the function to communicate to an outboard computer via wifi (802.11b,g,n) to receive the torque value the AAFO should produce and to send the readings from the two embedded encoders. The ESCON card can control the current of the DC motor, which allows for a torque control mode. An external battery is incorporated to the system that allows for a 2 hours autonomy.

The total weight of the system is 3.5 Kg, but only the motor, the gearbox and the ESCON card are attached to the side of the shank, with a weight of 2.35 Kg. The rest of the system is contained in a pounch that is securely fasted to the waist.

In order to ensure a sufficient torque generation accuracy of the AAFO's DC motor, a series of experiments were done. Such tests consisted in fixing a force sensor to the AAFO's solid foot insole at a known distance from the rotation axis of the ankle joint of the AAFO. With this experimental setup, the DC motor was characterized by measuring the produced torque at different desired torque values. The data obtained is used as a look-up table to estimate the generated AAFO's torque at a specific desired torque input.

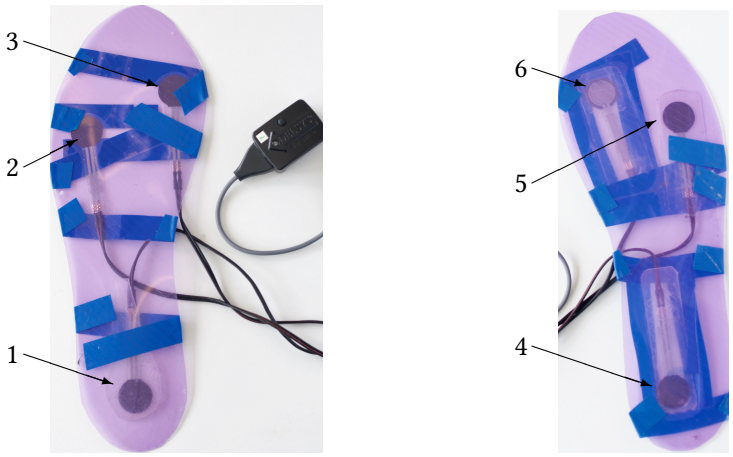

(a) Left insole. (b) Right insole.

Figure 3.4 – The insoles with the force sensitive resistors.

3.4.2. Sensors

In order to apply the assistive torque, the controllers require measurements of different angles, forces and/or accelerations. Extra sensors are added to the human-AAFO system. These include 1) inertia measurement units for measuring the orientation and accelerations of the lower limbs, 2) force sensitive resistors to estimate the forces applied between the foot and the ground, and 3) electromyography sensors to measure the muscular activity. These sensors are described in detail as follows.

3.4.2.1. Inertia Measurement Unit (IMU)

The inertia measurement system used is the MTx series from XSENS, Inc. It is composed of four inertia measurement units connected by wire to a hub which in turn connects wirelessly to the remote computer. The system uses batteries and has an autonomy of 2 hours. Each IMU has a 3-axis accelerameter, a 3-axis gyroscope, and a 3-axis magnetoscope, and can sample at 100 Hz. With the combination of the accelerameters, gyroscopes and magnetometers in the IMU it is possible to calculate the orientation of the unit and the angle between units. Therefore, two IMUs are attached to the shank and foot to determine the angle between the ground and the foot, and the angle between the vertical and the shank.

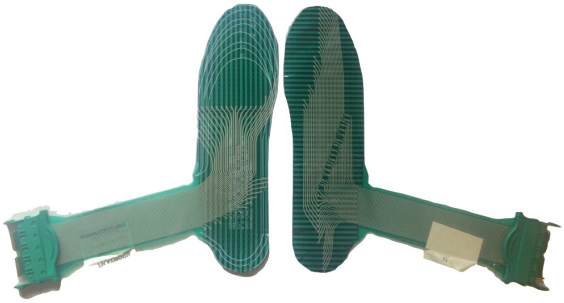

Figure 3.5 – The Tekscan FSR insoles.

3.4.2.2. Force Sensitive Resistors (FSR)

To measure the interaction of the foot with the ground, two systems are embedded in the insoles that go between the AAFO and the wearer's foot. These systems are consumer products, one is the Trigno wireless solution from Delsys, and the second one is the system from Tekscan, Inc.

The Trigno system consists of a main terminal that connects to the main computer via USB, and then connects wirelessly to different sensor adapters. Each adapter can be connected to four FSR that are embedded in each insole at specific positions in order to estimate the ground reaction force (GRF) under the foot, as shown in Fig. 3.4. This estimation is obtained at the heel level through the first FSR sensor and at the toes level through an average of the second and third FSR sensors measurements (located at the hallux and at the fifth metatarsal-phalange joints). Therefore, the GRF at the heel, middle foot, and toes levels can be measured.

The Tekscan system is composed of insoles embedded with several FSR in a grid array, as shown in Fig. 3.5. Therefore, each insole is divided into three regions: the heel, the middle foot, and the toes regions. The limits of each region can be tuned during the experiments. Then, all the FSR signals in each region are summed to determine the GRF. The GRF data are acquired with 100 Hz and sent to a Hub as shown in Fig. 3.5.

3.4.2.3. Electromyography (EMG)

The EMG sensors used for this study are also the Trigno wireless system from Delsys, Inc. Therefore, the EMG sensors are connected to the same main terminal as with the FSR adapters. The position for placing the EMG on the wearer's leg depends on the targeted muscle group. The movements of the ankle joint complex are plantar-dorsiflexion,

(a) (b)

Figure 3.6 – Electromyography sensor placement to measure the tibialis anterior and gastrocnemius muscular activities.

occurring in the sagittal plane; ab-adduction, occurring in the transverse plane, and inversion-eversion, occurring in the frontal plane [104]. Each movement is controlled by a combination of muscles spanning to the ankle joint. Therefore, in order to measure the muscular activity relevant to the plantar and dorsiflexion ankle joint movements, the EMG sensors need to be placed on top of the TA and GAS muscles, as shown in Fig. 3.6.

The sampling frequency of the EMG sensors is 100 Hz; such signal is filtered with a highpass second order Butterword filter with a cutoff frequency of 30 Hz, then it is rectified and then filtered again with a lowpass second order Butterword filter with a cutoff frequency of 5 Hz.

3.5 Conclusion

In this chapter, the description of the ankle joint is addressed. The main movements of the ankle complex include rotations on the three planes. However, only the plantar-/dorsiflexion and eversion/inversion movements are generated within the bones of the ankle joint. Therefore, the design of an AAFO has to consider these restrictions in order to promote an appropiate assistance of the joint.

For the AAFO used in this study, only the plantar and dorsiflexion rotations are assisted. Furthermore, the mechanical design of the orthotic device constrains the movement of the ankle joint in the sagital plane. Therefore, a dynamic model of the ankle joint for the sagittal plane is developed. This model considers internal and external disturbances to

the ankle joint system, e.g., torques generated by the muscles, ground reaction forces, joint stiffness, solid and viscous frictions, etc.

Finally, the harware systems used for this study are presented. These systems include the AAFO and the sensors; the IMU, FSR and EMG. The placement of the EMG sensors was obtained by evaluating the signal measured for different muscles spanning the ankle joint. The resulting EMG setup is illustrated in the chapter.

In the next chapter, a gait cycle analysis is presented and the reference trajectory generator algorithm is described, which adapts in real-time to the walking speed and step duration of the wearer of the AAFO.

4 — Gait cycle analysis

4.1 Introduction

The gait cycle is the result of a high level of coordination between the lower limbs and joints to ensure an efficient walking. Generally, the hip, knee and ankle joints are the focus of attention when studying the gait cycle and trajectory profiles have been observed for each joint. Furthermore, a decomposition of the gait cycle has been proposed based on different criteria, i.e., dividing the gait cycle in eight sub-phases. For this reason, ensuring that the lower limb joints produce a healthy trajectory profile could promote rehabilitation, especially when the subject suffers from a gait deficiency.

In rehabilitation, a common strategy to assist the lower limb joints during walking is the use of a reference tracking scheme, where the patients perform prescribed movements to recover their motor abilities. However, it is important that the reference used for the controller to be synchronized with the wearer's gait. For this purpose, two technics are mostly used; 1) to repeatedly generate the healthy ankle joint profile with a fixed periodicity, and use an audible or visual cue for the wearer to synchronize, or 2) to adapt in real-time the reference to the wearer's walking speed and step duration. Several actuated orthoses use gait event detection algorithms, the orientation of the tibia, or the gait parameter data from the previous step in order to generate a reference trajectory [99, 100]. The detection process is mainly based on the use of simple foot switches or force sensitive resistors [29, 79, 114], shoes with embedded pressure sensors [115] or with inertial sensors [116, 114]. Furthermore, different algorithms are used, such as finite-state machines [29, 114], fuzzy logic [115], model of the gait cycle as a function of the shank orientation [28], or regression models to identify the gait phases using in-shoe pressure mapping system [117].

This chapter presents the description of the gait cycle and how it is segmented. Also, a time-fixed ankle joint reference, calculated from 20 subjects, is explained and presented. Afterwards, an adaptive ankle reference generator (AARG) algorithm is presented. This ankle reference trajectory is updated as a function of the real-time gait cycle temporal evolution, in particular, the step and gait sub-phase durations. To prove the effectiveness of the generated profile, healthy subjects walk on a treadmill at different speeds and at their own self-selected step pace. The results show an ankle joint reference generated after the first five steps that is suitable for reference tracking controller applications.

4.2 Gait phases

The gait cycle is typically defined as starting with the heel strike of one foot and ending at the next heel strike of the same foot. This cycle is usually divided into two main phases: the stance phase and the swing phase, as it is shown in Fig. 4.1. The former represents the period of the cycle where the foot is in contact with the ground, and the latter phase represents the time when the leg is swinging forward to perform the step. During the gait cycle, specific events are defined based on the change of the interactions of the feet with the ground, e.g., the initial contact (IC), also called heel strike, toe landing (TL), heel off (HO), and toe off (TO). Note that these events occur for both feet, hence the stance phase can be segmented by the sequence of gait events triggered by both feet. Regarding the swing phase, it can be segmented based on the orientation and relative position of the lower limbs. Therefore, the sub-phases of the gait cycle are:

- Loading response (LR): begins at IC, ideally with the heel strike, and finishes with the TL event; from this point the foot is considered flat with the ground. Therefore, a double support period occurs during this sub-phase. The duration interval is 0-10% of the gait cycle.

- Early mid-stance (EMS): begins at the end of LR, and continues until the contralateral foot is lifted for the swing and a single support period starts. The duration interval is 10-20% of the gait cycle.

- Late mid-stance (LMS): begins at the EMS and finishes when the HO event is detected. The duration interval is 20-30% of the gait cycle.

- Terminal stance (TS): begins at the end of the LMS and continues until the contralateral foot strikes the ground. This sub-phase completes the period of single support. The duration interval is 30-50% of the gait cycle.
- Pre-swing (PS): begins with the contralateral IC, and finishes with the ipsilateral TO. The second period of the double support. The duration interval is 50-60% of the gait cycle.
- Initial swing (ISw): begins at the end of the PS sub-phase and finishes when the contralateral foot is aligned with the ipsilateral leg. The duration interval is 60-73% of the gait cycle.
- Mid-swing (MSw): begins after the ISw and finishes when the tibia is in a vertical orientation. The duration interval is 73-87% of the gait cycle.
- Terminal swing (TSw): begins with a vertical tibia and ends with the IC event. The duration interval is 87-100% of the gait cycle.

Since the foot has to clear the ground while the leg is swinging, it is important to define the maximum dorsiflexion (MD) during the swing phase. The time needed by the ankle joint to reach the MD varies from one subject to another. Generally, the MD occurs at around the 62% of the swing phase duration, that is about 85% of the whole gait cycle.

By detecting specific events during the gait cycle, it is possible to determine the key moments at which the ipsilateral ankle joint angle profile switches from dorsiflexion to plantar-flexion and vice-versa as shown in Fig. 4.1. Particularly, during the swing phase, the ankle joint rises the foot to avoid foot-drop and prepares the foot for the IC event. The ipsilateral foot terminates the stance phase with a push-off movement and then dorsiflexes to the MD value and then remains dorsiflexed until the IC event.

In this study, force sensitive resistors (FSR) are placed under each of the insoles of both feet to detect the gait events. These FSR sensors measure the interaction of the feet with the ground, allowing to estimate the ground reaction forces (GRF) and their distribution in the surface of the feet, i.e., the heel, mid-foot and toes contact with the ground. Moreover, an inertial measurement unit (IMU) is placed at the shank level to measure the acceleration of the shank along the longitudinal axis and accurately detect the IC event.

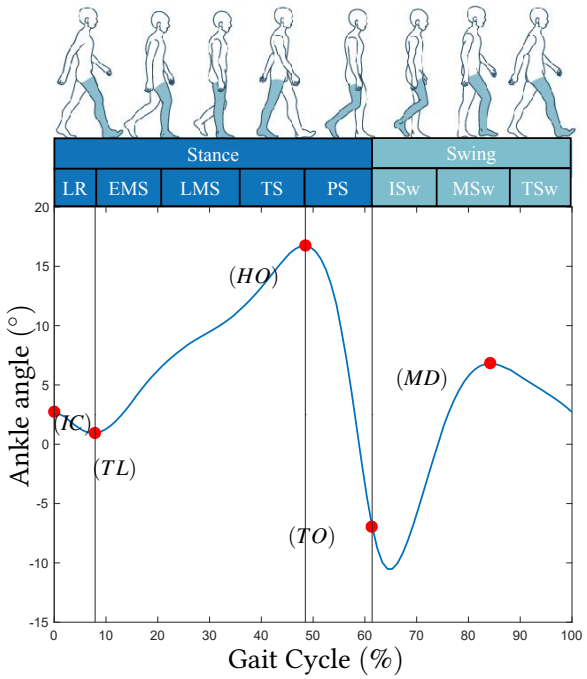

Figure 4.1 – On the top, the description of the gait by means of the gait sub-phases. On the bottom, the events in the gait cycle that correspond to the transitions between gait sub-phases or that describe a relative minimum or maximum in the ankle joint angle profile. The ankle angle is measured from the relaxed position, such that the positive values correspond to dorsiflexion and the negative values are plantar-flexion.

4.3 Gait phase detection

A Mamdani fuzzy inference system has been developed to detect the gait sub-phases based on the outputs of FSR sensors [118, 115]. The algorithm detects eight sub-phases including five sub-phases during the stance phase; the remaining three sub-phases during the swing phase are estimated. The algorithm to detect the gait sub-phases is described in four blocks, as shown in Fig. 4.2, and is described in the following. The human gait is analysed through all the sub-phases where the occurrence likelihood of each sub-phase is determined using a standard fuzzy membership value (μ_i).

Each foot is divided into three regions denoted by $j \in \{1,\ldots,6\}$; the heel, mid-foot and toes, with each region being measured by a FSR sensor, as described in block I, in Fig. 4.3.

In block II, six signals from the different areas of the feet are calibrated by detecting the minimum and maximum values since the begining of an experiment. Let $\vec{F}_{tj}$ be the vector that contains the acquired data from a given foot region FSR sensor j from the beginning of a session till a given time t. The magnitude range of the measurement from each sensor j is given by:

$$r_j = max(\vec{F}_{tj}) - min(\vec{F}_{tj}) \tag{4.1}$$

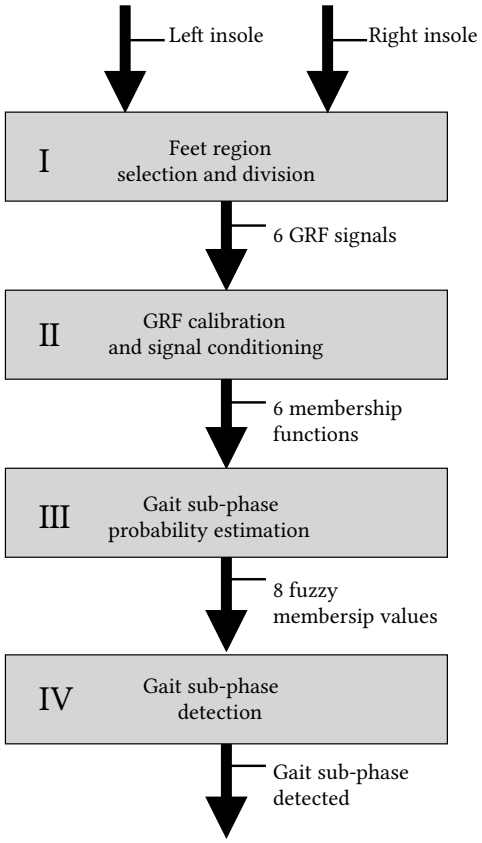

Figure 4.2 – The algorithm to detect the gait sub-phases based on the signals from the insoles embedded with force sensitive resistor matrices.

where $\max(\cdot)$ and $\min(\cdot)$ represent the maximum and minimum values of a vector. Let N_j be the threshold value for each region j, given by:

$$N_j = r_j \cdot h + min(\vec{F_{tj}}) \tag{4.2}$$

where h is the threshold percentage, an empirical value of 5% was found to be effective ($h = 0.05$). The membership function f_j for each sensor j is given by:

$$f_j = \frac{1}{2}\left(\tanh\left(\frac{k_j(F_{tj} - N_j)}{r_j} - 1\right) + 1\right) \tag{4.3}$$

where k_j represents the gain for each sensor j, and F_{tj} the measurement output of each FSR sensor j at a given time t during the session. Effective values for k_j were empirically tuned and were set to $k_{1,2,3} = 3$ and $k_{4,5,6} = 4$. This was done by increasing the sensibility gain k_j of each membership function f_j until every gait phase could be detected during level walking done by a healthy subject. Furthermore, once these values are set, they

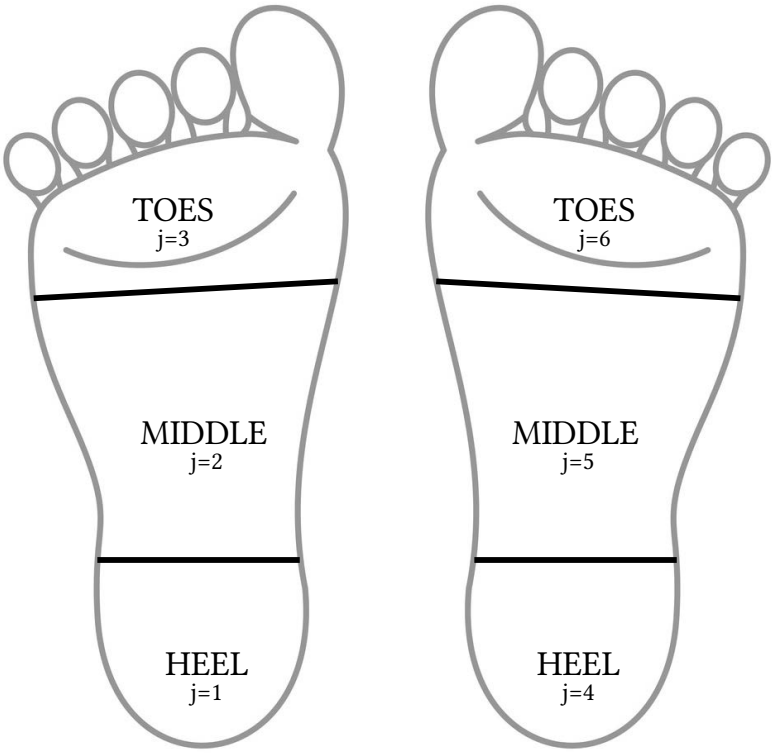

Figure 4.3 – The left heel, left middle, left toes, right heel, right middle, and right toes regions, where $j \in \{1, \ldots, 6\}$

allow the detection of each gait phase in a healthy gait pattern. However, if a paretic patient with a gait pathology would use the system, it would be expected that some gait phases are not executed and therefore not detected. Consequently, once the sensibility gains k_j are set and tested with the healthy subjects, these values are not changed for the paretic patient. Given that the paretic limb of the patient might not produce a normal GRF pattern, two FSR sensors are used to measure the GRF of the toes of the left foot, then the membership functions for the left middle and toes FSR sensors (f_2 and f_3) are processed by calculating the maximum value of the two FSRs. The rules that define each sub-phase's probability are described in Table 4.1; μ_{EMS}, μ_{LMS}, μ_{TS}, μ_{PS}, μ_{ISw}, μ_{MSw}, and μ_{TSw} correspond to the occurrence likelihood for the loading response, early mid-stance, late mid-stance, terminal stance, pre-swing, initial swing, mid-swing, and terminal swing sub-phases, respectively. This means that every sensor signal is defined as a large or small at any moment. In the block III, the fuzzy membership value (FMV)

Table 4.1 – *Fuzzy rules for Gait Phase Detection.* f_j *with* $j \in \{1,\dots,6\}$*, are the membership functions for the FSR sensors embedded in the insoles.* μ_i *represents the fuzzy variable that gives the probability for each sub-phase i (*$i \in \{1,\dots,8\}$

f_1	$max(f_2,f_3)$	f_4	f_5	f_6	μ_i
large	small	small	N/A	large	μ_{LR}
large	small	small	N/A	small	μ_{EMS}
large	large	small	N/A	small	μ_{LMS}
small	large	small	N/A	small	μ_{TS}
N/A	large	large	N/A	N/A	μ_{PS}
small	small	large	N/A	N/A	μ_{ISw}
small	small	small	large	N/A	μ_{MSw}
small	small	small	N/A	large	μ_{TSw}

is calculated for each sub-phase as follows:

$$\begin{aligned}
\mu_{LR} &= min(f_1, 1-max(f_2,f_3), 1-f_4, f_6)\\
\mu_{EMS} &= min(f_1, 1-max(f_2,f_3), 1-f_4, 1-f_6)\\
\mu_{LMS} &= min(f_1, max(f_2,f_3), 1-f_4, 1-f_6)\\
\mu_{TS} &= min(1-f_1, max(f_2,f_3), 1-f_4, 1-f_6)\\
\mu_{PS} &= min(f_1, f_4)\\
\mu_{ISw} &= min(1-f_1, 1-max(f_2,f_3), f_4)\\
\mu_{MSw} &= min(1-f_1, 1-max(f_2,f_3), 1-f_4, f_5)\\
\mu_{TSw} &= min(1-f_1, 1-max(f_2,f_3), 1-f_4, f_6)
\end{aligned} \tag{4.4}$$

Finally, in the block IV, the sub-phase with the maximum FMV value is selected. Also, to increase the accuracy of detecting the IC event, an additional IMU is placed at the shank level. If the TSw sub-phase is detected and the magnitude of the acceleration in the shank axis, measured by an IMU, crosses a certain threshold (a value of $a_{shank} > -11 m/s^2$ was found effective), the LR sub-phase is considered to have occurred instead. The threshold value of $11 m/s^2$ was empirically chosen from experiments. The fact of adding an additional IMU has considerably improved the results of detecting the IC event than simply using the FSR sensors.

To illustrate the gait phase detection algorithm, one session lasting 10 s with one halthy subject walking on a treadmill was conducted. The raw data from the FSR sensors are presented in Fig. 4.4a. Note that the measurement magnitudes for each sensor is different, therefore, the calibration (4.1) and (4.2) is required. Then, (4.3) is applied in real time and the output is presented in Fig. 4.4b, where $f_{2,3} = max(f_2, f_3)$. The FMV for

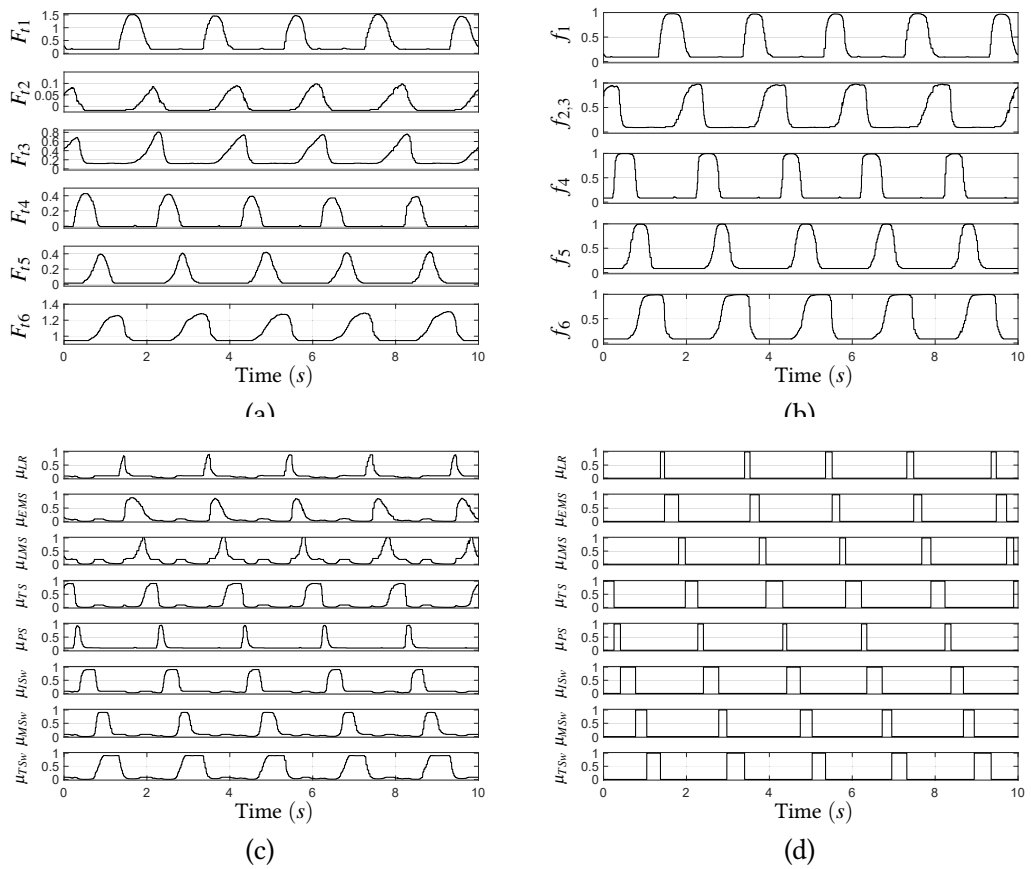

Figure 4.4 – Gait phase detection algorithm using FSR sensors. A session lasting 10 s. (a), the FSR signals from the left and right feet. (b), memberhip function value for each foot region, where $f_{2,3} = max(f_2, f_3)$. (c), fuzzy membership value for each gait sub-phase. (d), gait sub-phase detected in real time during the session.

each gait sub-phase is calculated using (4.4) and the result is shown in Fig. 4.4c. Finally, in Fig. 4.4d, one gait sub-phase is detected by using a $max()$ function to calculate the maximum FMV value between the gait sub-phases at any given time.

By calculating the duration of each sub-phase and of each step, it is possible to calculate in real time the duration percentage of each sub-phase with respect to the gait cycle, and the time between the gait events. At any given step, the average duration percentage for each sub-phase is calculated from the last five steps. The gait duration is then updated eight times per gait cycle, one time per sub-phase detected. The average duration percentage of each sub-phase is obtained after the first five steps and is then updated after each sub-phase detection.

Table 4.2 – *Key point values extracted from the average gait cycle of 20 healthy subjects.*

	IC (°)	TL (°)	HO (°)	TO (°)	MD (°)
Ankle angle θ	2.7	0.95	16.74	-6.92	6.8

4.4 Adaptive Ankle Reference Generator (AARG)

In order to generate a reference trajectory, an analysis of the gait of 20 healthy subjects has been performed in a clinical environment using a motion capture system (Motion Analysis Corporation, Santa Rosa, CA, USA, six cameras, Sampling Frequency 100 Hz) and two force plates (AMTI, Watertown, MA, USA, Sampling Frequency 1000 Hz). For more details on the experiment setup used for this analysis, please refer to [119]. From this analysis, an ankle joint angle profile, normalized with respect to the gait cycle, was calculated from the average of the 20 healthy subjects. It is possible to use this profile as the desired trajectory for the AAFO controllers, however, the duration of the gait cycle is fixed prior to the experiments and cannot be adapted during the session. Constraining the step duration of the reference could enforce a specific walking pace on the wearer of the AAFO, which is not ideal as it can lead to issues to synchronize the reference to the subject's walking pace. Therefore, a desired trajectory that adapts in real time to the subject's gait presents a clear advantage. For this purpose, the ankle joint angle values at the gait events (IC, TL, HO, TO and MD) are followed in a timely manner, defined by the measured step duration and the proportions of the gait sub-phases. In this section, an adaptive ankle reference generator (AARG) is presented.

The adaptive reference trajectory is calculated at the moment of the occurrence of any of the gait events using a cubic spline function; if no event is detected, the previously calculated reference trajectory is followed, as shown in the flow chart in Fig. 4.5a. The use of a cubic spline function to produce the desired trajectory ensures the existance of a smooth ankle joint angle and its derivatives; velocity and acceleration profiles. To update the reference trajectory, the beginning of the cubic spline function is the current reference ankle joint angle, and is calculated until reaching the next key point value in the gait cycle. For example, if the TL event is detected, a cubic spline trajectory that connects the current value of the reference to the HO key point value is calculated. The duration of the cubic spline is given by the duration of the sub-phases involved between the initial and final events conforming the cubic spline. In the given example, the duration of the cubic spline is the sum of the duration of the MS and TS sub-phases. The

Table 4.3 – *Experimental ankle joint angle key points values in degrees* (°) *for the AARG.*

	IC	TL	HO	TO	MD
Healthy subjects	-1	-3	6	-8.5	0

current ankle joint velocity reference is used as the initial condition for the cubic spline, and an ankle joint velocity value of zero is used as the final condition. This process for updating the ankle joint reference profile is illustrated in the flow chart in Fig. 4.5b. The adaptive reference ankle joint angular velocity and accelerations are calculated afterwards by numerically deriving the calculated cubic spline trajectory. In the case where the cubic spline trajectory is completed before the next event occurs, the ankle joint reference profile remains at the last value of the cubic spline until the next event is detected and the process continues. For the swing phase, if the TO event is detected, the cubic spline is calculated from the current ankle joint angle reference, then follows the MD key point in the middle of the path, and ends with the IC event. The ankle joint angle values at the gait events from the averaged ankle joint profile of the 20 subjects are showed in Table 4.2.

With this approach, the AARG calculates paths connecting the main key points of the healthy ankle profile and updates the adaptive reference trajectory after the detection of each of the main gait events. The advantage of this algorithm is that it does not impose any specific walking speed to the wearer but rather adapts to the generated desired kinematic trajectory as a function of the sub-phase durations.

4.4.1. Experimental evaluation

In this section, the efficiency of the ankle reference trajectory generator algorithm during gait cycles is assessed through real-time experiments. The AARG is evaluated with one healthy subject with the objective to evaluate the accuracy and repeatability of the AARG algorithm. Since the system is intended to modify the ankle joint profile of the healthy subjects, the IC, TL, HO, TO, and MD ankle joint angle values at the gait events for the AARG algorithm are set to generate a ankle joint profile different from the healthy pattern. These new IC, TL, HO, TO, and MD key point values are shown in Table 4.3. The experiments with the healthy subject have been performed according to the following protocol. The first subject walks on a treadmill at different speeds, 1.6 Km/hr, 2 Km/hr, 2.4 Km/hr, and 3 Km/hr.

For all sessions, the gait detection algorithm updates routines for the reference generator,

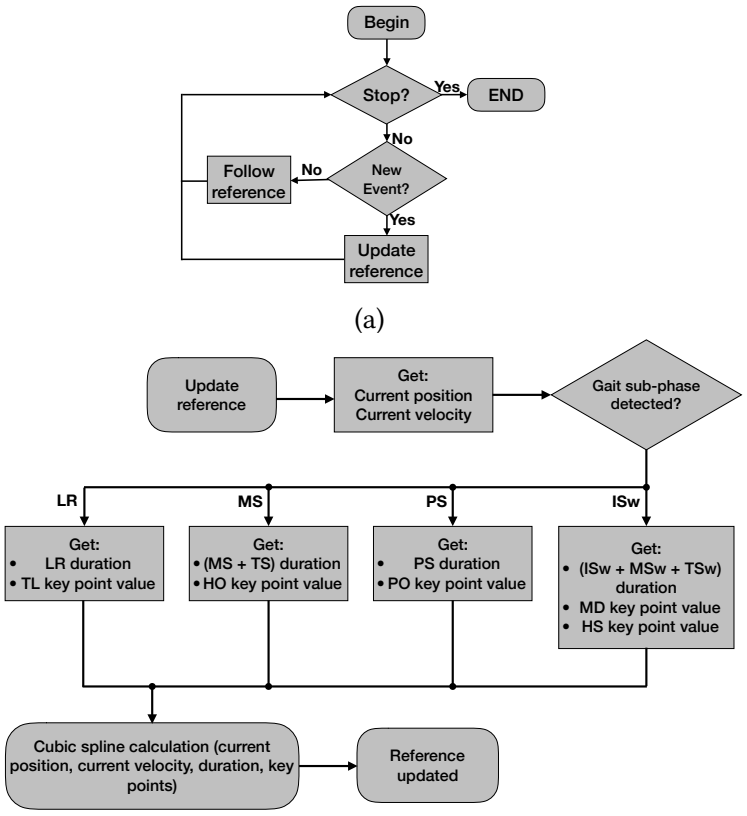

Figure 4.5 – On the top, the flow chart for the ankle reference generator program. On the bottom, the flow chart for the ankle reference update program.

e.g., the calculation for the step duration, the duration percentages of each gait sub-phase, and the ankle reference trajectory. The measured ankle angle, the ankle reference position and velocity data were normalized with respect to the gait cycle, measured from one IC event to the next one, and the average was calculated thereafter. Each sub-phase is detected using the algorithm described in section 4.3 and each sub-phase duration is then averaged for the whole session and normalized with respect to the gait cycle in order to calculate the mean proportions of the gait sub-phases. Fig. 4.6 shows the mean ankle joint angle reference generated by the AARG algorithm during an unassisted session with a healthy subject while on a treadmill at 2 Km/hr. The key points used for the AARG are highlighted in the figure. All the key points correspond to the description shown in Fig. 4.1. The increased value of the standard deviation after the transition between the TS and PS sub-phases correspond to the high variability of the gait kinematics at every step.

Fig. 4.7 shows the generated ankle profile during the four sessions. It is worth noting,

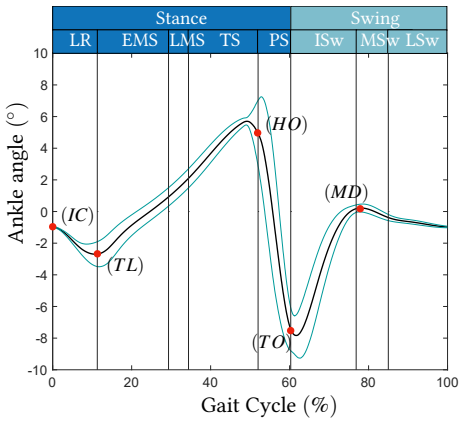

Figure 4.6 – Mean ankle joint angle reference generated by the AARG algorithm during an unassisted session with a healthy subject. The cyan lines represent the standard deviation and the vertical lines dividing the gait cycle are the detected gait phases.

Table 4.4 – *Mean step duration (MSD) and standard deviations in milliseconds (ms) for sessions with one healthy subject on a treadmill at different walking speeds.*

	Session 1	Session 2	Session 3	Session 4
MSD (*ms*)	3630±158	2058±43	1670±50	1282±23

as shown in Fig. 4.7a, that the ankle joint angle reference trajectory is similar during all sessions, independently of the gait speed, which makes the algorithm more robust with respect to changes in the step durations within a single or multiple session. Fig. 4.7b shows that the reference ankle joint velocity is updated with respect to the gait speed. However, the ankle joint kinematics changes slightly for different gait speeds and the amplitude of the ankle joint range of motion is reduced at the lowest speed while it is increased at the highest speed, as it can be seen in Fig. 4.7c. For this reason, and in order to compare the results in similar conditions, the sessions where assistive torque from the AAFO is provided to the subjects are performed on a treadmill at a fixed speed of 2 Km/hr (see chapter 7). It can be observed in Fig. 4.7d that all the sub-phases are correctly identified. The average measured step duration for each session is presented in Table 4.4.

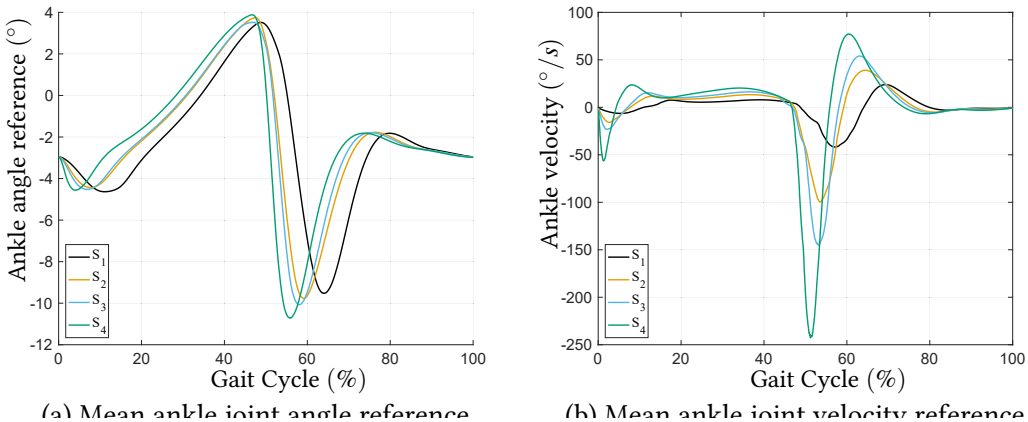

(a) Mean ankle joint angle reference

(b) Mean ankle joint velocity reference

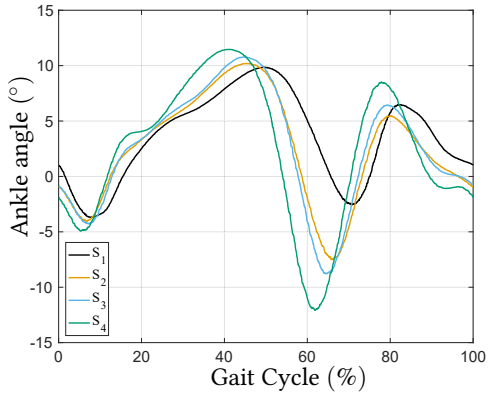

(c) Mean real ankle joint angle.

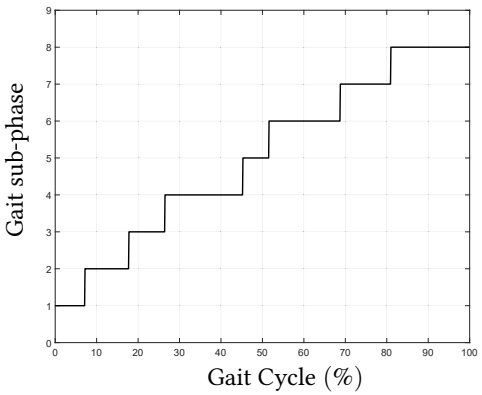

(d) Mean real ankle joint angle.

Figure 4.7 – Generated ankle profile and steps duration at 4 different walking speeds. (a) and (b) show the mean ankle joint angle and velocity reference profiles for each session, normalized to the gait cycle. (c) shows the mean ankle joint angle performed by the subject during each session, normalized to the gait cycle. (d) shows the gait phase durations normalized to the gait cycle (1:LR; 2:EMS; 3:LMS; 4:TS; 5:PS; 6:ISw; 7:MSw; 8:LSw).

4.5 Conclusion

Human walking is a complex task that involves the correct coordination of different muscle groups. Since this task describes a periodic cycle, it can be segmented according to different criteria, e.g., the interaction with the ground, or the specific functional objectives of the ankle joint. Hence, the gait cycle is divided into gait phases which can be further divided into sub-phases. This division is commonly used for controlling the lower limbs robotic exoskeletons as a high level controller scheme. Therefore, it is important to accurately detect every gait sub-phase for controlling a wearable assistive robot. For this purpose, several gait phase detection algorithms have been proposed in

the literature. For exmple, IMU based approaches allow for fast detection of different gait modes, e.g., sit-to-stand, climb stairs, level walking, etc. [120]. However, it is difficult to divide the stance phase of the gait cycle using IMUs, since the movement of the foot, when in contact with the ground, is not enough for an accurate detection of the sub-phases. FSR based approaches can divide the stance phase with greater accuracy since the criteria to describe these sub-phases is based on the interaction between the foot and the ground. However, these approaches can not detect the swing sub-phases of the gait cycle.

The ankle joint angle profile, normalized relative to the gait cycle, presents gait events (IC, TL, HO, and TO) that correspond to the division of the gait stance sub-phases. Therefore, accurately detecting these sub-phases allows for the detection of the gait events, and viceversa. Furthermore, it is possible to recreate the ankle joint profile by tracing spline curves that connect specific points that are defined by the gait event and a preselected ankle joint angle value.

Relying on a predefined desired trajectory may not be comfortable for subjects due to the fact that patient profiles are very different. Therefore, the ankle joint reference needs to be updated online and it should be adapted with respect to the wearer's walking speed and the gait phase durations. The former is satisfied by adjusting the reference velocity and the latter by adjusting the different proportions on the sub-phase durations. The algorithm was evaluated on a healthy subject at different walking speeds on a treadmill. The results obtained show that the AARG is able to accurately generate an ankle joint reference that is suitable to be used as the desired trajectory for tracking control schemes. Moreover, only ground reaction forces and shank acceleration in the longitudinal axis are used for the AARG algorithm, making the system portable and lightweight.

In the next chapter, an adaptive model reference control (MRAC) and a adaptive proxy-based sliding mode control (APSMC) are introduced. Such controllers are based on the dynamic model presented in chapter 3. Further, the stability is analyzed for two cases; an active and a passive wearer.

5 — Adaptive control strategies

5.1 Introduction

Paretic patients following a gait rehabilitation process require active assistance of their lower limbs to approach healthy joint movement profiles. Depending on the impairment level, the approach to generate the assistance could be different. As reported in chapter 2, there are several strategies to determine the assistance level provided by the AAFOs during gait rehabilitation [20, 26, 84]: 1) by pre-selecting the assistive torque magnitude and applying it in a feedforward scheme with respect to the gait phase detected [84, 82, 66, 118, 121], 2) as a function of electromyography (EMG) signals recorded from the lower limbs skeletal muscles [68, 96], 3) by adapting the stiffness, inertia or impedance of the augmented human-exoskeleton system based on the gait phase detected [29, 80, 122, 123], or 4) as a function of the tracking error between the current ankle joint angle and a reference trajectory pattern commonly generated from healthy subject walking profiles [58, 60, 85, 89, 83, 99, 113, 124, 125, 126, 127, 128]. Feedforward strategies are simple to implement but the lack of feedback could lead to an insufficient or excessive assistance while the stability of the overall system could not be guaranteed. EMG based strategies provide a high rate of adaptation for the nervous system, but requires a minimum residual muscular activities in order to be effective, which might not be the case for some patients with acute stroke symptoms. The systems that adapt their impedance have the advantage of not requiring a predefined trajectory but require a minimum residual voluntary effort to initiate the movement. Therefore, a trajectory tracking strategy could potentially provide more appropriate assistance when the wearer of the active orthosis is not fully able to initiate the movement. This is generally the case in the process of a gait rehabilitation. For example, for a paretic patient suffering from foot drop, the reference trajectory could be defined with an higher dorsiflexion during the swing phase and

loading response sub-phase, or an increased plantar flexion profile during the late stance for a patient suffering from a reduced push-off power generation at toe off. Therefore, the design of the desired trajectory is closely related to the requirements of the wearer to compensate for gait defficiencies, which could promote appropriate and meaningful assistance provided by the AAFO.

From a control point of view, the challenges of using an AAFO for assistance and rehabilitation purposes are mainly related to: i) a high nonlinearity of the AAFO; ii) the human-robot transparency as the interaction dynamics and power transfer from the robot to the human joint vary from one wearer to another, and iii) uncertainties related to the human-exoskeleton modeling as well as external disturbance resulting from voluntary human movement and interactions with the environment. In addition to the foregoing, intrinsic safety is crucial when using an assitive device such as AAFO in a close interaction with patients [129]. Traditional proportional, integral derivative (PID) controllers have been widely used with robotic orthoses in a rehabilitation environment [85, 89, 80, 83, 75, 99, 127]. While such controllers can be used to track predefined trajectories of the ankle joint, they usually lack the performances achieved by model based controllers. However, model-based control strategies require accurate knowledge of the system's parameters, i.e. wearer-active AAFO parameters, to calculate the required assistive torque to achieve an appropriate rehabilitation task. This is due to the fact that the identification process has to be done prior to each session and with each subject, which is time and effort consuming. Furthermore, unexpected external perturbations could increase the risk of inappropriate assistance, reduce the rehabilitation benefits, or may even cause injuries. Adaptive Control (AC) is quite effective in dealing with model parameter uncertainties and has gained wide applications in practical engineering. The successful applications of AC methods usually depend highly on the design of identification or estimation laws on time-varying model parameters [130] and has been recently applied to AAFO in [131]. Therefore, an adaptive, model based control strategy presents a clear advantage over the classical PID and traditional model based control approaches.

In the context of nonlinear control systems, sliding mode control (SMC) has gained much attention due to its design simplicity and robustness with respect to external disturbances [132]. However, it is well known that the discontinuous switching of the controller is prone to induce high-frequency chattering of mechanical systems which would be unconfortable and unsafe for the wearer and harmful for the AAFO. Proxy-based sliding mode control (PSMC), introduced in [133], efficiently combines the conventional SMC with PID control methods to increase the safety of the closed-loop system compared

to the traditional PID control method. In other words, PSMC guarantees the safety when large tracking error occurs and ensures similar tracking performance during normal operation similar to that of the PID control. However, since the AAFO system parameters and external disturbances vary from subject to subject, the fixed PID control gains in PSMC may limit its tracking and robustness performances.

This chapter deals with the adaptive control of an AAFO to assist the gait of paretic patients. The AAFO system is driven by both, the residual human torque generated by the muscles spanning the ankle joint as well as the AAFO's actuator's torque. Two adaptive control approaches are presented. First, a model reference adaptive control (MRAC) is proposed to assist dorsiflexion and plantar-flexion movements of the ankle joint during level walking. Unlike most classical model-based controllers, the proposed one does not require any prior estimation of the system's (AAFO-wearer) parameters. Moreover, the basic MRAC model is enhanced by adding a projection function to the adaptive law and by replacing the poportional derivative term of the control law by a saturation operator in order to improve the convergence rate of the adaptive parameters while maintaining the system's safety. The input-to-state stability of the AAFO-wearer system with respect to a bounded human muscular torque is proved in closed-loop based on a Lyapunov analysis.

Second, an adaptive proxy based sliding mode control (APSMC) applied to the AAFO by introducing an adaptation method [134], which allows online tuning of the PID gains in the PSMC scheme. Therefore, the proposed APSMC is able to adapt to the changes in the system's dynamics as well as external disturbances, while providing a better tracking performance with respect to standard PSMC while the safety characteristics are preserved.

5.2 Preliminaries

5.2.1. Input-to-State Stability (ISS)

The notion of Input-to-State Stability (ISS) is now recognized as a central concept in linear and nonlinear systems analysis [135, 136]. It provides a nonlinear generalization of finite gains with respect to supremum norms and also of finite L_2 gains. ISS allows to quantify sensitivity to disturbances, and, more generally, of the dependence of state

trajectories on actuator and measurement errors, magnitudes of tracking signals, and the like. It plays a central role in recursive design, controllers for non-minimum phase systems, observers, and many other areas.

In the following, $\|\cdot\|$ denotes Euclidean norm for vectors and the induced 2-norm for matrices, respectively. A scalar continuous function $\gamma(r)$ defined for $r \in [0,a]$ is said to belong to class $\mathcal{K}$ if it is strictly increasing and $\gamma(0) = 0$, and it is said to belong to class $\mathcal{K}_\infty$ if it is defined for all $r \geq 0$ and $\gamma(r) \longrightarrow \infty$ as $r \longrightarrow \infty$. A scalar continuous function $\beta(r,s)$ defined for $r \in [0,a]$, $s \in [0,\infty]$ is said to belong to class $\mathcal{KL}$ if for each fixed s it belongs to class $\mathcal{K}$ and for each fixed r it is decreasing in s and $\beta(r,s) \longrightarrow 0$ as $s \longrightarrow \infty$. A dynamical system with state x and input w is called ISS if there exist a class $\mathcal{KL}$ function β and a class $\mathcal{K}$ function γ such that $\|x(t)\| \leq \beta(\|x(0)\|, t) + \gamma(\left\|w_{|0.t|}\right\|_\infty)$ for all $t \geq 0$. For a signal w, $\|\cdot\|_\infty$ denotes the $\mathcal{L}_\infty$ -norm: $\left\|w_{|0.s|}\right\|_\infty = \sup_{0 \leq t \leq s} \|w(t)\|$. For linear systems, ISS is equivalent to global asymptotic stability of the unforced system [137].

Definition 1 *[137] A smooth function $V : \mathbb{R}^n \longrightarrow \mathbb{R}_{\geq 0}$ is called an ISS-Lyapunov function for system $\dot{x} = f(x,u)$ if there exist $\mathcal{K}_\infty$-functions (α_1, α_2), and $\mathcal{K}$-functions α_3 and χ, such that*

$$\alpha_1(|\xi|) \leq V(\xi) \leq \alpha_2(|\xi|) \tag{5.1}$$

for any $x(0) = \xi \in \mathbb{R}^n$ and

$$\nabla V(\xi) \cdot f(\xi, \mu) \leq -\alpha_3(|\xi|) \tag{5.2}$$

for any $\xi \in \mathbb{R}^n$ and any $\mu \in \mathbb{R}^m$ so that $|\xi| \geq \chi(|\mu|)$.

Theorem 2 *[137] The following properties are equivalent for any system:*

1. *It is ISS.*
2. *It admits an ISS-Lyapunov function.*
3. *It is robustly stable.*

5.2.2. Stability via Control Lyapunov Functions

Consider the affine system in the control dynamical systems defined by:

$$\dot{x} \quad = \quad f(x) + g(x)u \tag{5.3}$$

where $x \in \mathcal{X} \subset \mathbb{R}^n$, $u \in \mathcal{U} \subset \mathbb{R}^p$, and f and g are Lipschitz functions vanishing at the origin. If the system (5.3) admits an asymptotic stabilizing feedback $k : \mathcal{X} \to \mathcal{U}$ then there exists a Control Lyapunov Function (CLF) $V : \mathcal{X} \to \mathbb{R}$, that is a smooth function, positive definite such that:

$$\dot{V} = \underbrace{\frac{\partial V}{\partial x} f(x)}_{:=a(x)} + \underbrace{\frac{\partial V}{\partial x} g(x)}_{:=b(x)} k(x) < 0 \tag{5.4}$$

It is worth noting that if k is assumed to be smooth, then V is known to exist and to be as smooth as k. In the present work, only the smoothness of V is required which is less restrictive than the one of k. An equivalent requirement on the time derivative of V is that:

$$b(x) = 0 \Rightarrow a(x) < 0$$

Theorem 3 (Sontag's universal formula [135]) *Assume that system (5.3) admits V as CLF. For any real analytic function $\bar{q} : \mathbb{R} \to \mathbb{R}$ such that $\bar{q}(0) = 0$ and $b\bar{q}(b) > 0$ for $b \neq 0$, let $\gamma_C : \mathbb{R}^2 \to \mathbb{R}$ be defined as*

$$\gamma_C(a,b) := \begin{cases} \frac{a(x)+\sqrt{a(x)^2+b(x)\bar{q}(b(x))}}{b(x)} & \text{if } b \neq 0 \\ 0 & \text{if } b = 0 \end{cases} \tag{5.5}$$

Let the feedback $u : \mathcal{X} \to \mathcal{U}$, smooth on $\mathcal{X} \setminus \{0\}$ be defined by

$$u_i(x) := -b_i(x)\gamma_C(a(x), \beta(x)),\ i \in \{1, \ldots, p\} \tag{5.6}$$

with $\beta(x) := \|b(x)\|^2$. Then u is such that for all non zero x, $\frac{\partial V}{\partial x} f(x) + \frac{\partial V}{\partial x} g(x)u(x) < 0$. Moreover, if the CLF satisfies the so called small control property *[135], then taking*

$$\bar{q}(b(x)) := b(x),$$

the control is continuous at the origin.

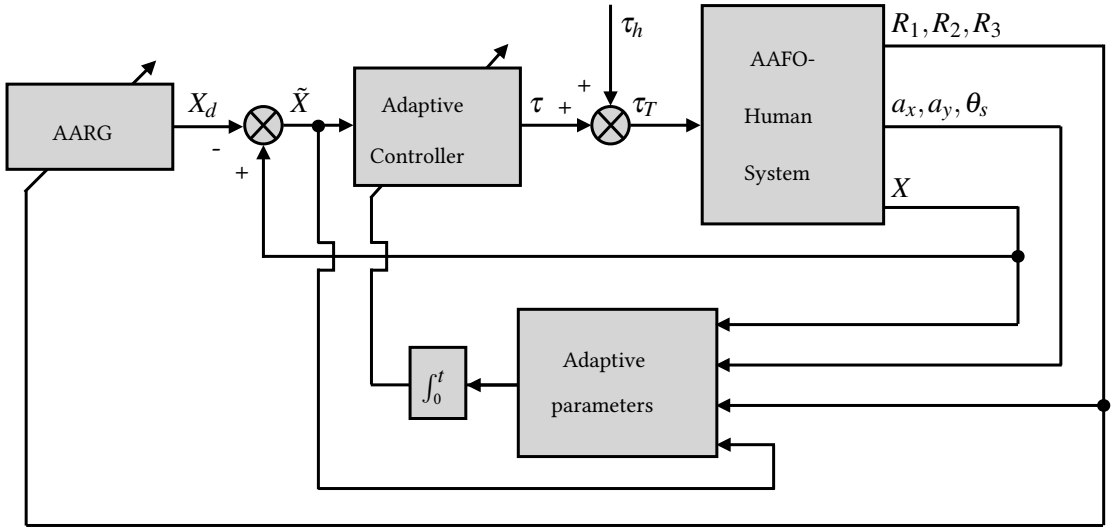

Figure 5.1 – MRAC's block diagram; where X, X_d and $\tilde{X}$ are respectively the current state, the desired and the state error vectors.

5.3 Model reference adaptive control

The model reference adaptive control (MRAC) structure proposed in [138] is depicted in Fig. 5.1. The AAFO dynamic model defined in equation (3.6) depends on the parameters defined in eq. (3.3). Each of these parameters depend on the individual foot's as well as the orthosis' parameters. While the orthosis' parameters can be identified once, the foot's parameters depend on the subject and should be identified at the beginning of each experiment with new subject. Moreover, the foot's parameters are subject to changes during the experiment, such as the subject's muscular fatigue, for example. To avoid a time and efforts consuming identification process prior to the experiments, which is often a complex task, the approach adopted in this work is based on the use of an adaptive controller to drive the ankle joint angle towards the desired trajectory generated using the adaptive reference generator, section 4.4 of chapter 4.

Let θ_d, $\dot{\theta}_d$ and $\ddot{\theta}_d$ be the desired angle, angular velocity and acceleration of the ankle joint respectively. Define $s = \dot{\tilde{\theta}} + \lambda\tilde{\theta}$ where λ is a scalar positive parameter; $\tilde{\theta}$ and $\dot{\tilde{\theta}}$ are the position and velocity errors respectively ($\tilde{\theta} = \theta - \theta_d$, $\dot{\tilde{\theta}} = \dot{\theta} - \dot{\theta}_d$).

Assumption 1 *The current and desired ankle joint angles and their derivatives up to the second order (θ, $\dot{\theta}$, $\ddot{\theta}$, θ_d, $\dot{\theta}_d$, $\ddot{\theta}_d$) are considered well known and bounded.*

The proposed adaptive control torque is applied during the whole gait cycle, including

the swing phase and the stance phase. It has the following expression:

$$\begin{aligned}\tau =& \hat{J}(\ddot{\theta}_d - \lambda\dot{\tilde{\theta}}) + \hat{k}_{f_S}\text{sign}\dot{\theta} + \hat{k}_{f_V}\dot{\theta} + \hat{k}_s(\theta - \theta_r) \\ &+ \hat{k}_a(a_y\cos\alpha - a_x\sin\alpha) + \hat{k}_g\cos\alpha \\ &+ \hat{k}_r(R_1x_1 - R_2x_2 - R_3x_3)\cos\alpha - \kappa s\end{aligned} \tag{5.7}$$

where κ is a scalar positive gain and $\hat{J}$, $\hat{k}_{f_S}$, $\hat{k}_{f_V}$, $\hat{k}_s$, $\hat{k}_a$, $\hat{k}_g$, and $\hat{k}_r$ are respectively the estimated torque coefficients for the inertia, solid and viscous friction, stiffness, acceleration, gravity, and ground reaction. The parameters adaptation law is given as follows:

$$\begin{aligned}\dot{\hat{k}}_{f_S} &= -a_1\text{sign}\dot{\theta}s \\ \dot{\hat{k}}_{f_V} &= -a_2\dot{\theta}s \\ \dot{\hat{k}}_a &= -a_3(a_y\cos\alpha - a_x\sin\alpha)s \\ \dot{\hat{k}}_s &= -a_4(\theta - \theta_r)s \\ \dot{\hat{J}} &= -a_5(\ddot{\theta}_d - \lambda\dot{\tilde{\theta}})s \\ \dot{\hat{k}}_r &= -a_6(R_1x_1 - R_2x_2 - R_3x_3)\cos\alpha s \\ \dot{\hat{k}}_g &= -a_7\cos\alpha s\end{aligned} \tag{5.8}$$

where $a_n, n \in \{1,\ldots,7\}$ are positive scalar gains. Applying the adaptive control torque (5.7) to the AAFO system as expressed by (3.6), the dynamics of the closed loop system during the whole gait cycle can be determined as follows:

$$\begin{aligned}\tilde{J}(\ddot{\theta}_d - \lambda\dot{\tilde{\theta}}) =& \tilde{k}_{f_S}\text{sign}\dot{\theta} + \tilde{k}_{f_V}\dot{\theta} + \tilde{k}_s(\theta - \theta_r) \\ &+ \tilde{k}_a(a_y\cos\alpha - a_x\sin\alpha) + \tilde{k}_g\cos\alpha \\ &+ \tilde{k}_r(R_1x_1 - R_2x_2 - R_3x_3)\cos\alpha - \kappa s\end{aligned} \tag{5.9}$$

where $\tilde{J}$, $\tilde{k}_{f_S}$, $\tilde{k}_{f_V}$, $\tilde{k}_s$, $\tilde{k}_a$, $\tilde{k}_g$, and $\tilde{k}_r$ represent the estimation error of the inertia, solid and viscous friction, stiffness, acceleration, gravity, and ground reaction parameters, respectively.

Remark 2 *The purpose of the controller gains λ and κ is to adjust the response of the motor torque as a function of the position and velocity errors. While the scalar gains of the adaptive law a_n adjust the convergence speed of the estimated torque coefficients $\hat{k}_{f_S}, \hat{k}_{f_V}, \hat{k}_a, \hat{k}_s, \hat{J}, \hat{k}_r$, and $\hat{k}_g$. These scalar gains need to be tuned manually, by trial and error, as opposed to the system's parameters defined in (3.3).*

5.3.1. Stability analysis

For the MRAC controllers, the stability analysis of the closed-loop AAFO system is presented for two cases; i.e. passive and active wearers. In the first case, the wearer is in passive mode, and is not exerting any active muscular torque at the ankle level ($\tau_h = 0$). The equilibrium point in this case study is proved to be asymptotically stable. In the second case, the wearer is in active mode and able to deliver a muscular activity actuating the ankle joint ($\tau_h \neq 0$). The AAFO system is proved to be input-to-state stable with respect to a bounded human muscular torque τ_h, i.e., the system is globally asymptotically stable in the absence of external inputs τ_h and its trajectory θ stays below certain bound.

5.3.1.1. Passive wearer

Proposition 1 *Consider the AAFO system modeled by (3.6) with a completely passive wearer at the ankle joint level ($\tau_h = 0$). Assume that the current and desired ankle joint angles and their derivatives up to the second order are bounded (Assumption 1). Applying the control torque (5.7), with the adaptation law defined in (5.8), ensures that the equilibrium point $\tilde{x} = [\tilde{\theta},\ \dot{\tilde{\theta}}]^T = [0,\ 0]^T$ is globally asymptotically stable.*

Proof 1 *Consider the Lyapunov function V defined by:*

$$\begin{aligned} V =& \frac{1}{2}Js^2 + \frac{1}{2a_1}\tilde{k}_{fs}^2 + \frac{1}{2a_2}\tilde{k}_{fv}^2 + \frac{1}{2a_3}\tilde{k}_a^2 + \frac{1}{2a_4}\tilde{k}_s^2 \\ &+ \frac{1}{2a_5}\tilde{J}^2 + \frac{1}{2a_6}\tilde{k}_r^2 + \frac{1}{2a_7}\tilde{k}_g^2 + \kappa\lambda\tilde{\theta}^2 \end{aligned} \tag{5.10}$$

The derivative of V is given by:

$$\begin{aligned} \dot{V} =& sJ\dot{s} - \frac{1}{a_1}\tilde{k}_{fs}\dot{\tilde{k}}_{fs} - \frac{1}{a_2}\tilde{k}_{fv}\dot{\tilde{k}}_{fv} - \frac{1}{a_3}\tilde{k}_a\dot{\tilde{k}}_a - \frac{1}{a_4}\tilde{k}_s\dot{\tilde{k}}_s - \frac{1}{a_5}\tilde{J}\dot{\tilde{J}} \\ &- \frac{1}{a_6}\tilde{k}_r\dot{\tilde{k}}_r - \frac{1}{a_7}\tilde{k}_g\dot{\tilde{k}}_g + 2\kappa\lambda\tilde{\theta}\dot{\tilde{\theta}} \end{aligned} \tag{5.11}$$

Replacing (5.8) and (5.9) into (5.11), the derivative of the Lyapunov function V with $\tau_h = 0$ becomes:

$$\dot{V} \quad = \quad -\kappa s^2 + 2\kappa\lambda\tilde{\theta}\dot{\tilde{\theta}} = -\kappa\dot{\tilde{\theta}}^2 - \kappa\lambda^2\tilde{\theta}^2 \tag{5.12}$$

Therefore, the Lyapunov function V is strictly decreasing. Based on Assumption 1, $\tilde{\theta}$ and $\dot{\tilde{\theta}}$

are bounded. Therefore, the second derivative $\ddot{V}$ of the Lyapunov function is bounded and $\dot{V}$ is uniformly continuous. Using Barbalat Lemma [139], the equilibrium point

$$\tilde{x} = [\tilde{\theta},\ \dot{\tilde{\theta}}]^T = [0,\ 0]^T$$

is globally asymptotically stable [138]. Consequently, the ankle joint angle tracks the desired one and the angular position and velocity trajectories remain bounded.

Since $\tilde{\theta}$ and $\dot{\tilde{\theta}}$ converge to zero then s and the system's parameters dynamics (5.8) converge also to zero. Therefore, the system's parameters (5.8) converge to constant values.

5.3.1.2. Active wearer

In the following, the wearer is exerting a muscular torque $\tau_h \neq 0$, that is partially actuating the ankle joint. This torque can be observed through the muscular activity measurements of the tibialis anterior (TA) muscle, responsible for dorsiflexion, and gastrocnemius (GAS) muscle, responsible for plantarflexion. τ_h is considered as an external input to the AAFO system.

Proposition 2 *Consider the AAFO system defined by (3.6) with an active wearer: $\tau_h \neq 0$. Assume that Assumption 1 holds and that the wearer's muscular torque τ_h actuating the ankle joint is bounded, i.e. $|\tau_h| \leq \Delta_h$ (Remark 1). By applying the control torque (5.7, 5.8) to the AAFO, and in view of the equilibrium point's asymptotic stability, the AAFO system is input-to-state stable with respect to the wearer's muscular torque τ_h.*

Proof 2 *Consider the Lyapunov function V defined in (5.10). The derivative of V considering the human torque τ_h is given by:*

$$\begin{aligned} \dot{V} = & \quad -\kappa\dot{\tilde{\theta}}^2 - \kappa\lambda^2\tilde{\theta}^2 + \tau_h s \\ \leq & \quad -\kappa|\dot{\tilde{\theta}}|^2 - \kappa\lambda^2|\tilde{\theta}|^2 + \tau_h(|\dot{\tilde{\theta}} + \lambda\tilde{\theta}|) \end{aligned}$$

Let $m = \min(1, \lambda^2)$. It can be verified that $|\dot{\tilde{\theta}} + \lambda\tilde{\theta}| \leq \sqrt{1+\lambda^2}||\tilde{x}||$ where $\tilde{x} = [\tilde{\theta},\ \dot{\tilde{\theta}}]^T$.

$$\begin{aligned} \dot{V} & \leq -\kappa m||\tilde{x}||^2 + \tau_h\sqrt{1+\lambda^2}||\tilde{x}|| \\ & \leq -\kappa m(1-\delta)||\tilde{x}||^2 - \kappa m\delta||\tilde{x}||^2 + \tau_h\sqrt{1+\lambda^2}||\tilde{x}|| \\ & \leq -\kappa m(1-\delta)||\tilde{x}||^2 \quad \forall\ ||\tilde{x}|| \geq \frac{\tau_h\sqrt{1+\lambda^2}}{\kappa m\delta} \end{aligned} \tag{5.13}$$

where $0 < \delta < 1$. *In view of (5.10, 5.13) and the asymptotic stability of the free moving AAFO's states, the system is input-to-state stable with respect to the bounded external input* τ_h *with* $\gamma(r) = \frac{r\sqrt{1+\lambda^2}}{km\delta}$ *([139]).*

5.4 Projection based adaptive control

Given that the MRAC is proven to be ISS, the tracking error remains bounded, however, this implies that the adaptive parameters might not converge to a final value in a finite time as the error may not vanish. In other words, the adaptation of the estimated parameters depend on the magnitude of the tracking error, if this error does not converge to zero, the parameters will continue adapting during the walking of the subject [139]. For this reason, a projection-based MRAC is proposed which is based on the MRAC strategy but further ensures that the adative parameters remain bounded using a projection operator [140].

Based on the dynamic model presented in 3.6 and the adaptive control torque (5.7), denote by W the vector of the system's parameters:

$$W = [k_{f_S}, k_{f_V}, k_a, k_s, J, k_r, k_g]^T \tag{5.14}$$

and $\hat{W}$ the vector of the estimated ones:

$$\hat{W} = [\hat{k}_{f_S}, \hat{k}_{f_V}, \hat{k}_a, \hat{k}_s, \hat{J}, \hat{k}_r, \hat{k}_g]^T \tag{5.15}$$

Then, the parameters estimation error vector is defined as: $\tilde{W} = W - \hat{W}$. Denote by Y the vector:

$$\begin{aligned} Y = &[\text{sign}\dot{\theta},\ \dot{\theta},\ (a_y \cos\alpha - a_x \sin\alpha),\ (\theta - \theta_r), \\ &(\ddot{\theta}_d - \lambda\dot{\tilde{\theta}}),\ (R_1 x_1 - R_2 x_2 - R_3 x_3)\cos\alpha,\ \cos\alpha] \end{aligned} \tag{5.16}$$

The parameters adaptation law is given by:

$$\dot{\hat{W}} = -\Gamma \text{Proj}(Y^T s, \hat{W}) \tag{5.17}$$

where Y and $\hat{W}$ are defined in (5.15) and (5.16) and Γ is a positive definite scaling diagonal matrix: $\Gamma = \text{diag}(\Gamma_n), n \in \{1, \ldots, 7\}$. $\text{Proj}(y, \hat{W})$ is a projection operator defined in [140].

This projection operator is a robustness augmentation technique that bounds the output of a non-linear adaptive controller while conforming to the Lyapunov stability rules. It is given by:

$$\text{Proj}(y,\hat{W}) = \begin{cases} y & \text{if} \quad ||\hat{W}|| < W_M \text{ or } \hat{W}^T y \geq 0 \\ (I - \frac{\hat{W}\hat{W}^T}{||\hat{W}||^2})y & \text{if} \quad ||\hat{W}|| \geq W_M \text{ and } \hat{W}^T y < 0 \end{cases} \tag{5.18}$$

The proposed adaptation law and projection operator have the following properties [140, 141]:

1. $\hat{W}(t)$ is uniformly continuous,
2. If $||W(0)|| \leq W_M$, then $||W(t)|| \leq W_M, \forall t > 0$,
3. $||\text{Proj}(y,\hat{W})|| \leq ||y||$,
4. $\tilde{W}^T \text{Proj}(y,\hat{W}) \leq \tilde{W}^T y$,
5. $||\text{Proj}(y,\hat{W})||$ is bounded if $||y||$ is also bounded.

Applying the adaptive control torque (5.7, 5.17) to the AAFO system modeled by (3.6), the dynamics of the closed loop system are given by:

$$\begin{aligned} J\dot{s} = &-\tilde{J}(\ddot{\theta}_d - \lambda\dot{\tilde{\theta}}) - \tilde{k}_g \cos\alpha - \tilde{k}_a(a_y\cos\alpha - a_x\sin\alpha) \\ &- \tilde{k}_s(\theta - \theta_r) - \tilde{k}_{fS}\text{sign}\dot{\theta} - \tilde{k}_{fV}\dot{\theta} \\ &- \tilde{k}_r(R_1x_1 - R_2x_2 - R_3x_3)\cos\alpha - \kappa s + \tau_h \end{aligned} \tag{5.19}$$

5.4.1. Stability analysis

Following the stability analysis for the basic MRAC, the stability analysis of the closed-loop AAFO system is presented for two cases; passive and active wearer.

5.4.1.1. Passive wearer

Proposition 3 *Consider the AAFO system modeled by (3.6) with a completely passive wearer ($\tau_h = 0$). Suppose that the current and desired ankle joint angles and their derivatives up to the third order are bounded (Assumption 1). Applying the control torque (5.7) and (5.17) ensures that the equilibrium point $\tilde{x} = [\tilde{\theta},\ \dot{\tilde{\theta}}]^T = [0,\ 0]^T$ is asymptotically stable.*

Proof 3 *Consider the Lyapunov function V defined by:*

$$V = \frac{1}{2}Js^2 + \frac{1}{2}\tilde{W}^T\Gamma^{-1}\tilde{W} + \kappa\lambda\,\tilde{\theta}^2 \tag{5.20}$$

The derivative of V is given by:

$$\dot{V} = sJ\dot{s} + \tilde{W}\Gamma^{-1}\dot{\tilde{W}} + 2\kappa\lambda\,\tilde{\theta}\,\dot{\tilde{\theta}} \tag{5.21}$$

Replacing (5.17) and (5.19) into (5.21), the derivative of V becomes ($\tau_h = 0$):

$$\begin{aligned} \dot{V} &= \underbrace{-\tilde{W}Y^T s + \tilde{W}\,Proj(Y^T s, \hat{W})}_{\leq 0} - \kappa(\dot{\tilde{\theta}} + \lambda\,\tilde{\theta})^2 + 2\kappa\lambda\,\tilde{\theta}\,\dot{\tilde{\theta}} \\ &\leq -\kappa\dot{\tilde{\theta}}^2 - \kappa\lambda^2\tilde{\theta}^2 \end{aligned} \tag{5.22}$$

Therefore, the Lyapunov function V is strictly decreasing. Given that all the signals and their derivatives are bounded (Assumption 1), the second derivative of the Lyapunov function $\ddot{V}$ is also bounded and $\dot{V}$ is therefore uniformly continuous. Consequently, by Barbalat Lemma, the equilibrium point $\tilde{x} = [\tilde{\theta},\ \dot{\tilde{\theta}}]^T = [0,\ 0]^T$ is asymptotically stable [139, 138]. As a result, the control law ensures that the AAFO system's states (θ, $\dot{\theta}$, $\ddot{\theta}$) asymptotically track the reference (θ_d, $\dot{\theta}_d$, $\ddot{\theta}_d$) and the solution trajectories remain bounded.

5.4.1.2. Active wearer

For the case when the wearer is considered active and exerting a muscular torque $\tau_h \neq 0$ (τ_h is considered as an external torque to the AAFO system), the stability analysis is as follows.

Proposition 4 *Consider the AAFO system defined by (3.6) with an active wearer: $\tau_h \neq 0$ (Remark 1). Assume that the derivatives of the desired ankle joint angle $\dot{\theta}_d$, $\ddot{\theta}_d$ are bounded (Assumption 1). By applying the control torque (5.7, 5.17) to the AAFO system, and in view of the equilibrium point's asymptotic stability, the AAFO system is input-to-state stable with respect to the wearer's torque τ_h.*

Proof 4 *Consider the Lyapunov function V defined in (5.20). The derivative of V considering the human torque τ_h is given by:*

$$\begin{aligned}\dot{V} = & \underbrace{-\tilde{W}Y^T s + \tilde{W}Proj(Y^T s, \hat{W})}_{\leq 0} - k\dot{\tilde{\theta}}^2 - k\lambda^2\tilde{\theta}^2 + \tau_h s \\ \leq & \quad -k|\dot{\tilde{\theta}}|^2 - k\lambda^2|\tilde{\theta}|^2 + \tau_h(|\dot{\tilde{\theta}} + \lambda\tilde{\theta}|)\end{aligned}$$

Let $m = \min(1, \lambda^2)$. *It can be verified that* $|\dot{\tilde{\theta}} + \lambda\tilde{\theta}| \leq \sqrt{1+\lambda^2}||\tilde{x}||$ *where* $\tilde{x} = [\tilde{\theta},\ \dot{\tilde{\theta}}]^T$.

$$\begin{aligned}\dot{V} &\leq -km||\tilde{x}||^2 + \tau_h\sqrt{1+\lambda^2}||\tilde{x}|| \\ &\leq -km(1-\delta)||\tilde{x}||^2 - km\delta||\tilde{x}||^2 + \tau_h\sqrt{1+\lambda^2}||\tilde{x}|| \\ &\leq -km(1-\delta)||\tilde{x}||^2 \quad \forall\ ||\tilde{x}|| \geq \frac{\tau_h\sqrt{1+\lambda^2}}{km\delta}\end{aligned} \tag{5.23}$$

where $0 < \delta < 1$. *In view of (5.20, 5.23) and the asymptotic stability of the non human controlled orthosis' states, the system is input-to-state stable with respect to the bounded external input* τ_h *with* $\gamma(r) = \frac{r\sqrt{1+\lambda^2}}{km\delta}$ *[139].*

5.5 Adaptive controller with PD saturation

Improving the robbustness of the MRAC by bounding the adaptive parameters is one way to achieve better tracking performance and improve the stability. However, in (5.7), the control law has two main parts; i.e., the adaptive parameters that are sensitive to the error function s, and the proportional and derivative (PD) gains (denoted by the κs term). It is well known that a high proportional gain increases the input torque to reduce the error, but if the tracking error is beyond a given tolerable value, this could potentially lead to unstability. Also, the derivative gain can reduce the overshooting effects in the tracking performance but is sensitive to the noise introduced when numerically deriving the ankle joint angle. Hence, a high derivative gain could also lead to unstability. Therefore, a compromise has to be made between the magnitude of the PD gains and the chattering produced at the AAFO's ankle joint torque generation. A possible solution is to introduce relatively high PD gains but limiting their effects on the control law by using a saturation function. The MRAC is improved by saturating the PD gains of the control law (5.8) with the intention to have a higher PD gain values and at the same time reduce the chattering effects.

Using the dynamic model of the AAFO system (3.6), the proposed adaptive control torque has the following expression:

$$\begin{aligned}\tau =& \hat{J}(\ddot{\theta}_d - \lambda\dot{\tilde{\theta}}) + \hat{k}_{fS}\text{sign}\dot{\theta} + \hat{k}_{fV}\dot{\theta} + \hat{k}_s(\theta - \theta_r) \\ &+ \hat{k}_a(a_y\cos\alpha - a_x\sin\alpha) + \hat{k}_g\cos\alpha \\ &+ \hat{k}_r(R_1x_1 - R_2x_2 - R_3x_3)\cos\alpha \\ &- \alpha_p\text{sat}_{N_1}(k_p\tilde{\theta}) - \alpha_v\text{sat}_{N_2}(k_v\dot{\tilde{\theta}})\end{aligned} \tag{5.24}$$

where $\alpha_p,\ \alpha_v,\ k_p,\ k_v$ are scalar positive gains and N_1, N_2 the bounds of the proportional and derivative actions.
$\text{sat}_N(\cdot)$ is a saturation function, bounded between $\pm N$, defined such as:

$$\text{sat}_N(x) = \begin{cases} x & \text{if} \quad |x| \leq N \\ N\text{sign}(x) & \text{if} \quad |x| > N \end{cases} \tag{5.25}$$

with $\text{sign}(\cdot)$ is the classical signum function. The parameters, related to the adaptation law, are the same as in (5.8). Applying the adaptive control torque (5.24) to the AAFO system modeled by (3.6), the dynamics of the closed loop system can be determined as follows:

$$\begin{aligned}J\dot{s} =& -\tilde{J}(\ddot{\theta}_d - \lambda\dot{\tilde{\theta}}) - \tilde{k}_{fS}\text{sign}\dot{\theta} - \tilde{k}_{fS}\dot{\theta} - \tilde{k}_s(\theta - \theta_r) \\ &- \tilde{k}_a(a_y\cos\alpha - a_x\sin\alpha) - \tilde{k}_g\cos\alpha \\ &- \tilde{k}_r(R_1x_1 - R_2x_2 - R_3x_3)\cos\alpha \\ &- \alpha_p\text{sat}_{N_1}(k_p\tilde{\theta}) - \alpha_v\text{sat}_{N_2}(k_v\dot{\tilde{\theta}}) + \tau_h\end{aligned} \tag{5.26}$$

5.5.1. Stability analysis

5.5.1.1. Passive wearer

Proposition 5 *Consider the AAFO system modeled by (3.6) with a completely passive wearer ($\tau_h = 0$). Suppose that the current and desired ankle joint angles and their derivatives up to the second order are bounded (Assumption 1). Applying the control torque (5.7) and (5.8) ensures that the equilibrium point $X = [\tilde{\theta},\ \dot{\tilde{\theta}}]^T = [0,\ 0]^T$ is asymptotically stable.*

Proof 5 *Consider the Lyapunov function V defined by:*

$$V = \frac{1}{2}Js^2 + \tilde{W}^T\Gamma^{-1}\tilde{W} + \varepsilon\int_0^{\tilde{\theta}} sat_{N_1}(k_px)dx \tag{5.27}$$

with $\Gamma = diag(a_n),\ i \in \{1,\ldots,7\}$ *and* ε *a positive scalar parameter.. The derivative of* V *is given by:*

$$\dot{V} = sJ\dot{s} - \tilde{W}^T\Gamma^{-1}\dot{\hat{W}} + \varepsilon sat_{N_1}(k_p\tilde{\theta})\dot{\tilde{\theta}} \tag{5.28}$$

Replacing (5.8) and (5.26) into (5.28), the derivative of the Lyapunov function V *becomes:*

$$\begin{aligned}
\dot{V} &= -\left(\alpha_p sat_{N_1}(k_p\tilde{\theta}) + \alpha_v sat_{N_2}(k_v\dot{\tilde{\theta}})\right)\left(\dot{\tilde{\theta}} + \lambda\tilde{\theta}\right) \\
&\quad +\varepsilon sat_{N_1}(k_p\tilde{\theta})\dot{\tilde{\theta}} \\
&= -\begin{bmatrix}\tilde{\theta} & \dot{\tilde{\theta}}\end{bmatrix}\begin{bmatrix}\alpha_p\lambda & \alpha_v\lambda \\ \alpha_p - \varepsilon & \alpha_v\end{bmatrix}\begin{bmatrix}sat_{N_1}(k_p\tilde{\theta}) \\ sat_{N_2}(k_v\dot{\tilde{\theta}})\end{bmatrix} \\
&= -X^T\Delta Sat(KX)
\end{aligned}$$

with

$$\Delta = \begin{bmatrix}\alpha_p\lambda & \alpha_v\lambda \\ \alpha_p - \varepsilon & \alpha_v\end{bmatrix} \tag{5.29}$$

and

$$K = diag(k_p, k_v) \tag{5.30}$$

are two positive definite matrices $X = \begin{bmatrix}\tilde{\theta} & \dot{\tilde{\theta}}\end{bmatrix}^T$ *and* $Sat(Y) = [sat(y_1)\ldots sat(y_n)]$, *for* $Y = [y_1, y_2, \ldots, y_n]$ *and* $n \in \mathbb{R}^+$.

Let $\lambda_{\min}(\cdot)$ *be the minimum eigenvalue of the embedded matrix. Since* X *and* $sat(KX)$ *have the same sign,* $\dot{V}$ *can be bounded by:*

$$\begin{aligned}
\dot{V} &\leq -\lambda_{\min}(\Delta)\min(k_p, k_v)\|X\|^2 &(5.31)\\
&\leq -\delta\|X\|^2 &(5.32)
\end{aligned}$$

with $\delta = \lambda_{\min}(\Delta)\min(k_p, k_v)$. *Therefore, the Lyapunov function is strictly decreasing. Considering Assumption 1,* $\tilde{\theta},\ \dot{\tilde{\theta}}$ *are bounded. Having that all the variables and their derivatives are bounded, the second derivative of the Lyapunov function* $\ddot{V}$ *is bounded and* $\dot{V}$ *is therefore uniformly continuous. Using Barbalat Lemma, the equilibrium point* $X = [\tilde{\theta},\ \dot{\tilde{\theta}}]^T = [0,\ 0]^T$ *is asymptotically stable [139, 138]. As a sequel, one can state that the control law ensures that the free moving AAFO system's states track asymptotically the desired ones (*$\theta \to \theta_d$ *and* $\dot{\theta} \to \dot{\theta}_d$*) and the solution trajectories remain bounded.*

5.5.1.2. Active wearer

An active wearer, exerting a muscular torque $\tau_h \neq 0$, is considered. τ_h is considered as an external torque to the AAFO system.

Proposition 6 *Consider the AAFO system defined by (3.6) with an active wearer: $\tau_h \neq 0$. Consider that assumption 1 holds. Assume also that the wearer's muscular torque τ_h actuating the ankle joint is bounded, i.e. $|\tau_h| \leq \Delta_h$ (Remark 1). By applying the control torque (5.8) and (5.24) to the AAFO, and in view of the equilibrium point's asymptotic stability, the AAFO system is input-to-state stable with respect to the wearer's torque τ_h.*

Proof 6 *Consider the Lyapunov function V defined in (5.27). The derivative of V considering the human torque τ_h is given by:*

$$\begin{aligned}
\dot{V} &= -\left(\alpha_p sat_{N_1}(k_p\tilde{\theta}) + \alpha_v sat_{N_2}(k_v\dot{\tilde{\theta}})\right)\left(\dot{\tilde{\theta}} + \lambda\tilde{\theta}\right) \\
&\quad +\varepsilon sat_{N_1}(k_p\tilde{\theta})\dot{\tilde{\theta}} + \tau_h\left(\dot{\tilde{\theta}} + \lambda\tilde{\theta}\right) \\
&= -\begin{bmatrix}\tilde{\theta} & \dot{\tilde{\theta}}\end{bmatrix}\begin{bmatrix}\alpha_p\lambda & \alpha_v\lambda \\ \alpha_p - \varepsilon & \alpha_v\end{bmatrix}\begin{bmatrix}sat_{N_1}(k_p\tilde{\theta}) \\ sat_{N_2}(k_v\dot{\tilde{\theta}})\end{bmatrix} + \tau_h\begin{bmatrix}\lambda & 0 \\ 0 & 1\end{bmatrix}\begin{bmatrix}\tilde{\theta} \\ \dot{\tilde{\theta}}\end{bmatrix} \\
&= -X^T\Delta Sat(KX) + \tau_h\Lambda X
\end{aligned}$$

with Δ and K defined in (5.29) and (5.30) respectively, and

$$\Lambda = \begin{bmatrix}\lambda & 0 \\ 0 & 1\end{bmatrix} \tag{5.33}$$

The derivative of the Lyapunov function in presence of the human torque τ_h is bounded by:

$$\dot{V} \leq -\lambda_{\min}(\Delta)\min(k_p, k_v)\|X\|^2 + \tau_h\sqrt{1+\lambda^2}\|X\| \tag{5.34}$$

Taking $0 < m < 1$ and $\delta = \lambda_{\min}(\Delta)\min(k_p, k_v)$, then the derivative of the Lyapunov function can be bounded by:

$$\begin{aligned}
\dot{V} &\leq -\delta\|X\|^2 + \tau_h\sqrt{1+\lambda^2}\|X\| \\
&\leq -\delta(1-m)\|X\|^2 - m\delta\|X\|^2 + \tau_h\sqrt{1+\lambda^2}\|X\|
\end{aligned}$$

and therefore:

$$\dot{V} \leq -\delta(1-m)\|X\|^2 \quad \forall\|X\| \geq \frac{\tau_h\sqrt{1+\lambda^2}}{m\delta} \tag{5.35}$$

Since $|\tau_h| \leq \Delta_h$ *then* $\frac{\tau_h\sqrt{1+\lambda^2}}{m\delta}$ *is bounded and vanishes if* τ_h *vanishes. In view of (5.27, 5.35) and the asymptotic stability of the free moving orthosis' states, the system is input-to-state stable with respect to the bounded external input* τ_h *with* $\rho(r) = \frac{r\sqrt{1+\lambda^2}}{m\delta}$ *[139].*

5.6 Adaptive proxy-based sliding mode controller

The advantage of the proxy-based sliding mode control (PSMC) structure is that a over-damping motion can be obtained to avoid large actuator torque when a large position error occurs and a relatively accurate tracking performance can be guaranteed by the inner PID controller. The PSMC structure proposed in [142] is depicted in Fig. 5.2. A virtual object, referred as proxy, was used to connect a first-order sliding mode controller and a conventional PID controller. To further improve the robustness of the traditional PSMC with respect to disturbances from the wearer or the environment, an adaptive tuning algorithm is introduced to tune the parameters the inner PID controller. The whole structure of the proposed APSMC is shown in Fig. 5.3.

Since the AAFO system parameters and external disturbances vary from subject to subject, the fixed PID control parameters' values in PSMC limit its tracking and robustness performances. In [143], the authors proposed a neural-network-based method to tune the PID parameters in PSMC and higher robustness was observed when implementing the method in a robotic orthosis for gait training conducted with healthy subjects.

The sliding mode controller (SMC) shown in Fig. 5.3 is designed as

$$\tau_{smc} = F\,\text{sign}(e_\sigma + H\dot{e}_\sigma) \tag{5.36}$$

with

$$e_\sigma = \theta_d - \theta_p \tag{5.37}$$

where $H > 0$ and $F > 0$ denote scalar design parameters. θ_d and θ_p represent the desired ankle angle and the proxy angle.

The adaptive PID controller is designed as follows:

$$\tau_{pid} = K_p e_p + K_i \int_0^t e_p dt + K_d \dot{e}_p, \tag{5.38}$$

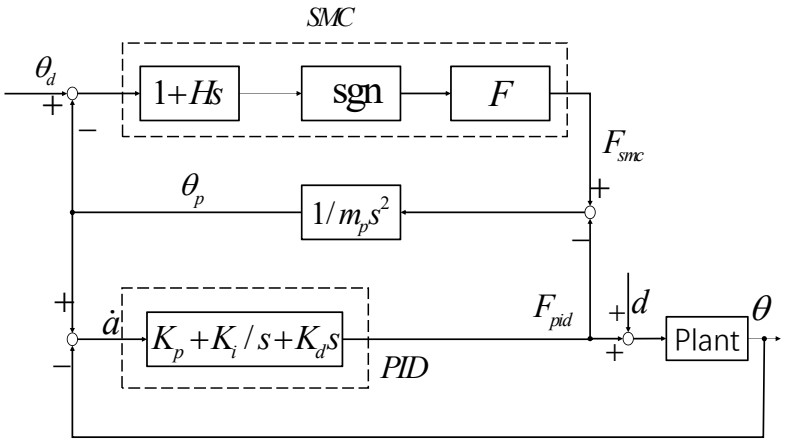

Figure 5.2 – Principal of PSMC.

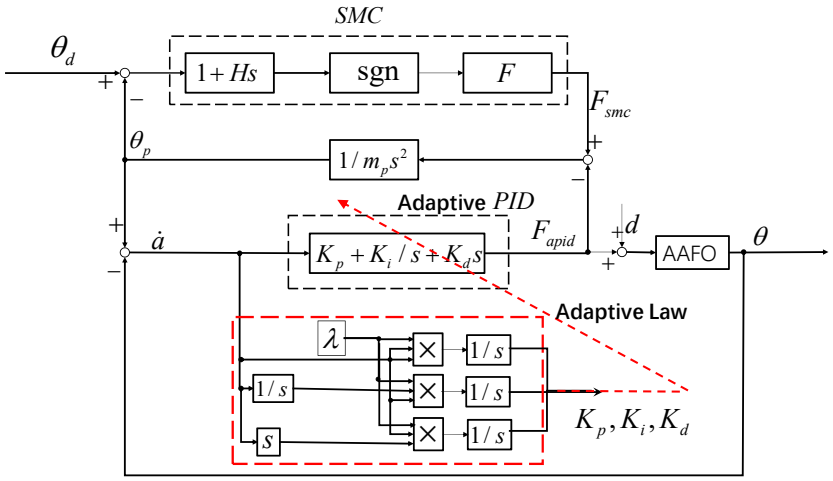

Figure 5.3 – Control block of two PSMCs. (a) Conventional PSMC control block. (b) APSMC control block.

with

$$e_p = \theta_p - \theta. \tag{5.39}$$

where θ shows the real ankle angle. K_p, K_i and K_d denote the adaptive proportional, integral and differential gains, respectively.

By defining

$$a = \int_0^t (\theta_p - \theta) d\tau \tag{5.40}$$

and

$$\mu = \theta_d - \theta + H(\dot{\theta}_d - \dot{\theta}), \tag{5.41}$$

then, the SMC (5.36) and adaptive PID (5.38) controllers can be re-expressed as:

$$F_{smc} = F\,\text{sign}(\sigma - \dot{a} - H\ddot{a}) \tag{5.42}$$

and

$$F_{pid} = K_p\dot{a} + K_i a + K_d\ddot{a}. \tag{5.43}$$

According to the analysis in [142], The dynamics of the proxy (see Fig. 5.2) can then be expressed as follows:

$$m_p\ddot{\theta}_p = \tau_{smc} - \tau_{pid}, \tag{5.44}$$

where m_p is the proxy mass which is assumed to zero. Then, we have

$$\tau_{smc} = \tau_{pid} = \tau_m \tag{5.45}$$

By applying the following relation between the signum function $\text{sign}(\cdot)$ and the saturation function $sat(\cdot)$:

$$y + X = Y\,\text{sign}(z - Zy) \Leftrightarrow y = -X + Y\,sat(\tfrac{z/Z+X}{Y}), \tag{5.46}$$

where $Y, Z > 0$ and $X, y, z \in R$.

Therefore, the whole control law can be rewritten as follows:

$$\tau_m = F\,sat\Big(\frac{K_d}{F}\Big(\frac{\sigma - \dot{a}}{H} + \frac{K_p\dot{a} + K_i a}{K_d}\Big)\Big) \tag{5.47}$$

with

$$\ddot{a} = -\frac{K_p\dot{a} + K_i a}{K_d} + \frac{F}{K_d}sat\Big(\frac{K_d}{F}\Big(\frac{\sigma - \dot{a}}{H} + \frac{K_p\dot{a} + K_i a}{K_d}\Big)\Big) \tag{5.48}$$

5.6.1. Adaptive Tuning Algorithm

During walking with the assistance of the AAFO, the parameters of model (3.7) change from subject to another as the wearer varies his/her ankle joint stiffness. Moreover, the human-exoskeleton is subject to external disturbances such as the interaction with the ground through the GRF which is varying with gait evolution. To deal with such effects, an on-line tuning PID controller is used. Leading up to the application of the adaptation interaction theory to the inner PID controller (see Fig. 5.3), the inner PID based human-exoskeleton closed-loop system is divided into four independent subsystems such as the

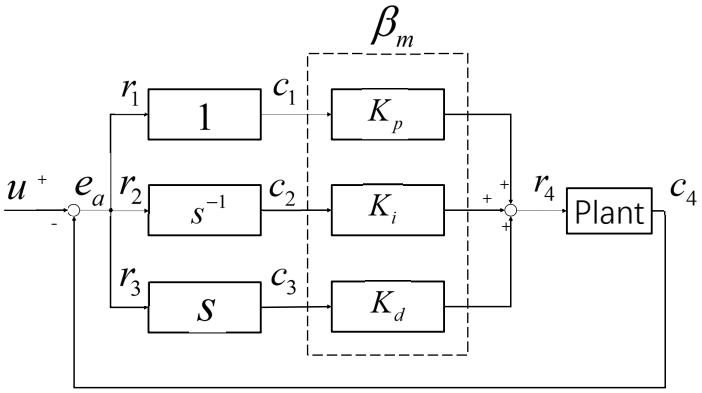

Figure 5.4 – PID subsystem interaction of APSMC.

proportional part, integral part, derivative part and the human-exoskeleton system as shown in Fig. 5.4. The PID parameters, $\beta = \{K_p\ K_i\ K_d\}$, are considered as the connection weights between subsystems. Based on the adaptive interaction theory presented in [144], the tuning of the PID parameters β can be considered as a minimum problem and associated performance index $\mathscr{E}$ is designed as follows:

$$\mathscr{E} = e_a^2 = (p - y_4)^2. \tag{5.49}$$

where $y_4 = \theta$ shows the output of the fourth subsystem, i.e., the human-exoskeleton system.

According to the analysis shown in [144], $\mathscr{E}$ monotonically decreases with time, if the connection weight β is adapted as:

$$\dot{\beta} = -\gamma \frac{d\mathscr{E}}{d\beta} \tag{5.50}$$

with $\gamma > 0$,

Applying (5.50) to the on-line tuning of the PID parameters, we have:

$$\dot{\beta} = -\gamma \frac{d\mathscr{E}}{de_a} \circ G'(\tau_{pid}) \circ y_i. \tag{5.51}$$

where y_i, $i \in 1,2,3$ shows the input of each subsystem as shown in Fig. 5.4. $G'(\tau_{pid})$ represents the Frechet derivative of the human-exoskeleton system model G with input τ_{pid} and output θ.

From (5.43) and (5.51), the on-line tuning algorithm of the PID parameters is given by:

$$\begin{aligned}\dot{K}_p &= -\gamma \frac{d\mathscr{E}}{de_a} \circ G'(\tau_{pid}) \circ \dot{a} \\ \dot{K}_i &= -\gamma \frac{d\mathscr{E}}{de_a} \circ G'(\tau_{pid}) \circ a. \\ \dot{K}_d &= -\gamma \frac{d\mathscr{E}}{de_a} \circ G'(\tau_{pid}) \circ \ddot{a}\end{aligned} \tag{5.52}$$

According to approximation tuning method proposed in [144], the Frechet derivative for the second order system, e.g., G, can be further simplified as:

$$G'(\tau_{pid}) \circ y_i = k y_i, \tag{5.53}$$

where k is a constant. Thus, (5.52) becomes:

$$\begin{cases} \dot{K}_p = 2\gamma k e_a \dot{a} \\ \dot{K}_i = 2\gamma k e_a a \\ \dot{K}_d = 2\gamma k e_a \ddot{a} \end{cases}. \tag{5.54}$$

Since $e_a = \theta_p - \theta = \dot{a}$, (5.54) can be further rewritten as:

$$\begin{cases} \dot{K}_p = \lambda \dot{a} \dot{a} \\ \dot{K}_i = \lambda \dot{a} a \\ \dot{K}_d = \lambda \dot{a} \ddot{a} \end{cases}. \tag{5.55}$$

where $\lambda = 2\gamma k$.

It should be noted that using the approximation tuning method (5.55), $\dot{K}_p$ is always positive when the error a in not zero. Hence, the upper limit of the K_p should be limited in practice.

Compared to the Frechet tuning algorithm [145], a common method for tuning PID controller, an advantage of the use of approximation tuning algorithm (5.54) is that the human-exoskeleton model is not required. However, an upper limitation of the proportional parameter K_p is needed to ensure the stability of the closed-loop system if these always exists a tracking error, which is inevitable in practice. Moreover, it can be observed that only one parameter is used for tuning the PID controller using the approximation tuning algorithm, which makes it easier to use compared to other existing methods such as fuzzy based approaches, e.g., [146] and neural network based ones, e.g., [143].

5.6.2. Stability Analysis

Define the tracking error $e = \theta_d - \theta$ and the error vector as:

$$E = [e \quad E_1] \tag{5.56}$$

where $E_1 = [\dot{e}\ \dot{a}\ a]$. By substituting $e = \theta_d - \theta$ to (3.8), the error dynamics equation is obtained:

$$J\ddot{e} + k_{fV}\dot{e} + k_s e = -\tau + \varphi, \tag{5.57}$$

with

$$\varphi = J\ddot{\theta}_d + k_{fV}\dot{\theta}_d + k_s\theta_d - d, \tag{5.58}$$

where $|\varphi| \leq \delta_0$ with $\delta_0 > 0$. To demonstrate the stability of the APSMC for the system (3.8), the following lemma is introduced.

Lemma 1 ([142]) *Considering the closed-loop system composed of system (3.8) and an adaptive PID controller (5.43) and (5.55) that accepts an input $u = \dot{\theta}_p - \dot{\theta}_d$, there exists K_p, K_i, K_d that allow that the function V_p satisfies:*

$$V_p(E_1) \geq \delta \|E_1\|^2, \tag{5.59}$$

and

$$\dot{V}_p(E_1) \leq \tau u + \delta_0 \Xi E_1 - \rho_E \|E_1\|^2 - \rho_u \|u\|^2, \tag{5.60}$$

where ρ_E, ρ_u and δ are positice numbers, and Ξ a constraint matrix.

Since the on-line tuning algorithm (5.55) is able to guarantee appropriate gains for the PID controller designed for a second order nonlinear system e.g., (3.8), which has been proved in [147], the Lemma 1 holds true according to analysis shown in [142]. For more details, please refer to [142]. Based on Lemma 1, the stability of the proposed APSMC controller can be stated as:

Proposition: Considering the closed-loop system composed of system (3.8) and an APSMC controller, i.e., (5.47), (5.48) and (5.55), and the Lemma 1 holds true. Then, there exists a closed set ξ including the origin with which $E \to \xi$ is achieved as $t \to \infty$.

Proof:

To analyze the stability of the APSMC, a Lyapunov function candidate is chosen as:

$$V(E) = V_p(E_1) + \|F(e - \dot{a})\|_1 \tag{5.61}$$

Obviously, $V(E) > 0$ for any $E \neq 0$ and $V(E) = 0$ when $E = 0$. The derivative of (5.61) can be expressed as follows:

$$\dot{V}(E) = \dot{V}_p(E_1) + (\dot{e} - \ddot{a})F\text{sign}(e - \dot{a}). \tag{5.62}$$

From (5.60) and (5.62), we obtain:

$$\begin{aligned} \dot{V}(E) \leq & fu + \delta_0 \Xi E_1 - \rho_E \|E_1\|^2 - \rho_u \|u\|^2 \\ & + (\dot{e} - \ddot{a})F\text{sign}(e - \dot{a}) \end{aligned}. \tag{5.63}$$

By substituting (5.40) into (5.62) and using the fact $u = \dot{\theta}_p - \dot{\theta}_d = \ddot{a} - \dot{e}$, we obtain:

$$\begin{aligned} \dot{V}(E) \leq & (\ddot{a} - \dot{e})F\text{sign}(\sigma - \dot{a} - H\ddot{a}) + \delta_0 \Xi E_1 - \rho_E \|E_1\|^2 \\ & - \rho_u \|u\|^2 + (\dot{e} - \ddot{a})F\text{sign}(e - \dot{a}) \end{aligned}. \tag{5.64}$$

Considering $\sigma - \dot{a} - H\ddot{a} = e - \dot{a} + H(\dot{e} - \ddot{a})$, (5.63) becomes

$$\begin{aligned} \dot{V}(E) \leq & H(\dot{e} - \ddot{a})\frac{F}{H}[\text{sign}(e - \dot{a}) - \text{sign}(e - \dot{a} + H(\dot{e} - \ddot{a}))] \\ & + \delta_0 \Xi E_1 - \rho_E \|E_1\|^2 - \rho_u \|u\|^2 \\ \leq & \delta_0 \Xi \|E_1\| - \rho_E \|E_1\|^2 - \rho_u \|u\|^2 \end{aligned}. \tag{5.65}$$

Therefore, the tracking error $E \to \xi$ is satisfied as $t \to \infty$.

Note that the following relation has been used in the above equation

$$y^T X[\text{sign}(z + y) - \text{sign}(z)] \geq 0, \tag{5.66}$$

where $X > 0$, and $y, z \in R$.

5.7 Conclusion

Traditional PID controllers have been widely used with robotic orthoses in the rehabilitation environment [80, 83, 89]. While these controllers are simple to implement and can be used to track a predefined trajectory for the ankle joint, they usually lack the performance achieved by model-based controllers.

Model based control approaches need to handle the innate changes of the parameters of the AAFO-human system that occur during the gait activity, especially with paretic patients. Such changes can occur due to different factors, such fatigue or movement defficiencies with paretic patients. Failing to adapt to these changes can produce inappropriate assistance, negatively impacts the rehabilitation benefits, or can even cause injury. Furthermore, by adapting to the changes in the parameters of the AAFO-human system, a prior identification session is not required. Therefore, an adaptive control approach presents a clear advantage over the classical model based control approaches.

In this chapter, a MRAC stratey was developed. This control approach requires the measurement of different system parameters in order to adapt the controller parameters as a function of the tracking error. Therefore, such adaptation can affect the adaptation rate for each controller parameter individually and allows for a compensation the gait deficiencies during walking. Moreover, the stability of the system was proved to be ISS with respect to the muscular torque τ_h. However, in practice, the adaptation rate of the controller parameters could be limited to the sampling and control loop frequencies, i.e., a relatively high adaptation gain a_n, $n \in \{1, \ldots, 7\}$, could lead to the adaptive parameters not converging to a final value. For this reason, a projection function was implemented to the adaptation law of the basic MRAC in order to bound the magnitude of the adaptive parameters. Also, when a big tracking error ocurrs, the AAFO with the basic MRAC produces a big assistive torque which could lead to unstability due to the limited control loop frequency. To prevent the AAFO system from producing such a torque, a saturation operator was proposed to bound the PD gain of the basic MRAC.

Safety is crucial for an AAFO system, particulary when applied with paretic patients. PSMC is an effective way that combines safety and relatively good tracking performance. APSMC is achieved by introducing a suitable adaptation of the PID gains of the conventional PSMC. Thus APSMC is able to improve the tracking performance of the PSMC. Furthermore, the APSMC does not require the online measurement of the system parameters other than the ankle joint angle and velocity, which presents an advantage

compared to the MRAC.

The control strategies proposed in this chapter use an adaptation approach to compensate for the changes in the AAFO-human dynamics during walking. However, in the next chapter, a control strategy that uses an observer to estimate the disturbances exerted on the system is developed.

6 — Active disturbance rejection control

6.1 Introduction

Since the seminal works of Artstein and Sontag [135], Control Lyapunov Functions, so called CLFs, have become central to feedback design. A main reason is that the existence of a CLF is necessary and sufficient for the stabilizability of a system with a control input. Domains of application include robust nonlinear feedback design [148], receding horizon control of nonlinear systems [149], stabilization of hybrid systems [150] and stabilization of nonlinear system with event-based control [151], to name only a few. In the bipedal walking robot framework, CLF approach has been successful used to exponentially stabilize periodic orbits of the hybrid zero dynamics by shaping the energy [152, 153], where the control laws are based on the Sontag's formula which is well known to possess robustness to static and dynamic input uncertainties [154]. Former properties represent a main motivation to use CLFs in the present work.

The objective of the above-mentioned control approaches is to reject disturbances through feedback, which is based on the tracking error between the measured outputs and their setpoints or desired trajectories. As a consequence, such controllers cannot react fast enough in the presence of strong disturbances. In order to overcome this limitation, Active Disturbance Rejection Control (ADRC) was introduced by Han [155]. ADRC is fundamentally based on the possibility of on-line estimating adverse effects so called "total disturbance" caused by the coupling between unknown system dynamics (endogenous) and external (exogenous) disturbances. This estimation is then canceled via an appropriate feedback-feedforward control law [156]. The most remarkable feature of ADRC

lies in its estimation/cancellation nature, where the total disturbance is considered as an extended state and is estimated, in real-time, through an Extended State Observer (ESO) [157, 158, 159] so called disturbance-observer [160]. ADRC has been exploited in almost all domains of control engineering for example: motion control of humanoid robots [161], power filter design [162], energy storage [163], power plants [164], DC Converters [165], electric machines and servomechanisms [166, 167, 168], renewable energy together with cooperative control [169].

Recently, ADRC was applied to the area of biped locomotion [170] and rehabilitation systems [171, 172]. Where the ADRC have been designed by combining ESO with different control methods, such as PID control, optimal control, backstepping, sliding modes, adaptive control, predictive control. Actually, the main idea of the ADRC methodology lies on the need for having a flatness property [173] or of a partially linearizable structure with stable zero dynamics (minimum phase systems) [156]. Flatness is natural in the ADRC design and offers no obstacle to either observer-based design or direct disturbance cancellation.

In this chapter, an Active Disturbance Rejection Control (ADRC) is developed. Compared to the adaptive controllers introduced in the previous chapter, the ADRC is able to reduce the chattering effects of the AAFO's DC motor while producing a relatively good tracking performance. For this purpose, an Extended State Observer (ESO) is designed to estimate on-line the unknown disturbances and canceled by injecting the output of ESO into the feedback loop. A stability analysis of the estimation error dynamics is carried out in the input-to state stability (ISS) framework. Moreover, the feedback design is based on the existence of a Control Lyapunov Function (CLF). The stability analysis discloses that the tracking trajectory controller is ISS.

6.2 Preliminaries

6.2.1. Flatness and feedback linearization revisited

A single input nonlinear system is said to be differentially flat if there exists a differential function of the state, called *flat output* such that all variables in the system (i.e. states, outputs, inputs, etc.) are, in turn, expressible as differential functions of the flat output. It is a property that trivializes the exact linearization problem in a nonlinear system.

Furthermore, flatness immediately yields the required open-loop (nominal) behavior of the system for a particular desired trajectory tracking.

Theorem 4 *[173] A single input nonlinear system of the form $\dot{x} = f(x,u)$ with $x \in \mathbb{R}^n$ and $u \in \mathbb{R}$ is differentially flat if and only if it is feedback linearizable.*

6.2.2. Flatness differential of the AAFO

Let $y = \theta$ be an associated output for the AAFO system (3.4). This results in:

$$\ddot{y} = \frac{1}{J}\left(\xi(\theta,\dot{\theta},\alpha,t) + \tau\right) \tag{6.1}$$

where, $\xi(\theta,\dot{\theta},\alpha,t) = \xi_{en}(\theta,\dot{\theta},\alpha,t) + \xi_{ex}(\theta,\dot{\theta},\alpha,t)$. Inspection of (6.1) shows that choosing $\tau = -\xi(\theta,\dot{\theta},\alpha,t) + Jv$ results in the linear system $\ddot{y} = v$, where v is a feedback component. From the Theorem 4, the AAFO system (3.4) is differentially flat, such that its *Flat Output* is the angular position θ. The flatness of the system implies that all variables of the system and the control vector τ can be parameterizable in terms of $R = \theta$ and a finite number of its derivatives with respect to time, that is:

$$\theta = R \tag{6.2}$$
$$\dot{\theta} = \dot{R} \tag{6.3}$$
$$\ddot{\theta} = \ddot{R} \tag{6.4}$$
$$\tau = J\ddot{R} - \xi(R,\dot{R},\alpha,t) \tag{6.5}$$

The function, $\xi(R,\dot{R},\alpha,t)$ represents the included endogenous and exogenous disturbances which are unknown, but are assumed to be uniformly absolutely bounded.

6.3 ADRC design for the AAFO

In this section a position trajectory tracking of the AAFO is addressed by using a control strategy based on the ADRC technique. The function, $\xi(R,\dot{R},\alpha,t)$, will be estimated through the use of the ESO, that is based on the system's dynamic:

$$\ddot{R} = \frac{1}{J}\left[\tau + \xi(R,\dot{R},\alpha,t)\right] \tag{6.6}$$

For this purpose, the following is assumed:

- Only the flat output is measured, i.e. the angular position $R = \theta$;
- The nominal value of inertia moment J is known;
- The perturbation function $\xi(R, \dot{R}, \alpha, t)$ is a uniformly absolutely bounded disturbance, i.e. $\sup_t \mid \xi(\cdot) \mid = \|\xi(R, \dot{R}, \alpha, t)\|_\infty \leq K_0$.

6.3.1. ESO design for the AAFO

Let $e = R - R_1$ be the estimation error, through (6.6), the following extended state observer is proposed:

$$\Sigma_{ESO} := \begin{cases} \dot{R}_1 = R_2 + l_3 e \\ \dot{R}_2 = \frac{1}{J} u + \eta_1 + l_2 e \\ \dot{\eta}_1 = \eta_2 + l_1 e \\ \dot{\eta}_2 = l_0 e \end{cases} \tag{6.7}$$

where R_1, R_2 are the estimated variable of the flat output R and its derivative, respectively. η_1 and η_2 represent the disturbance estimation and its time derivative, respectively, and τ is the control input. The set of coefficients $\{l_3, l_2, l_1, l_0\}$ are constant values.

Proposition 7 *Consider the ESO (6.7) and the AAFO system (6.6). Then, the estimation error behavior satisfies the ISO property (Input to Output Stability) [137], i.e. the error dynamics converges to a sphere centered at the origin of the estimation error phase space with radius*

$$\rho = \frac{\alpha K_0}{J \lambda_1} \tag{6.8}$$

where α and λ_1 are parameters that depend of the selection of the set of coefficients $\{l_3, l_2, l_1, l_0\}$. Furthermore, the error dynamics exhibits asymptotic stability to $e = 0$ for $\xi = 0$.

Proof 7 *Consider the estimation error $e = R - R_1$ and its successive derivatives together with the observer dynamics (6.7) and the AAFO dynamics (6.6). Then, the estimation error e satisfies the following linear differential equation*

$$e^{(4)} + l_3 e^{(3)} + l_2 \ddot{e} + l_1 \dot{e} + l_0 e = \frac{1}{J} \ddot{\xi} \tag{6.9}$$

The space state of (6.9) could be expressed as follows:

$$\Sigma_{EO} := \begin{cases} \dot{x} = Ax + B\xi \\ e = Cx \end{cases} \tag{6.10}$$

where

$$A = \begin{pmatrix} 0 & 1 & 0 & 0 \\ 0 & 0 & 1 & 0 \\ 0 & 0 & 0 & 1 \\ -l_0 & -l_1 & -l_2 & -l_3 \end{pmatrix} \quad B = \begin{pmatrix} 0 \\ 0 \\ 0 \\ \frac{1}{J} \end{pmatrix} \quad C = \begin{pmatrix} 0 & 0 & 1 & 0 \end{pmatrix} \tag{6.11}$$

The variation of parameters formula gives the following solution

$$\begin{aligned} x(t) &= \exp(At)\,x(0) + \int_0^t \exp(A(t-q))B\xi\,dq \\ e(t) &= C\exp(At)\,x(0) + C\int_0^t \exp(A(t-q))B\xi\,dq \end{aligned} \tag{6.12}$$

If the set of coefficients $\{l_3,\, l_2,\, l_1,\, l_0\}$ are selected such that the matrix A is Hurwitz, the following inequality is obtained:

$$\begin{aligned} \|e(t)\| &\leq \|\exp(At)\,e(0)\| + \int_0^t \|\exp(A(t-q))B\xi\,dq\| \\ &\leq \underbrace{\|\exp(At)\,\|\|e(0)\|}_{\beta(\|x(0)\|,t)\in\mathcal{KL}} + \underbrace{|\xi|\|B\|\int_0^t \|\exp(A(t-q))\|dq}_{\gamma(\|\xi\|_\infty)\in\mathcal{K}_\infty} \end{aligned} \tag{6.13}$$

Since there exist $\beta \in \mathcal{KL}$ and $\rho \in \mathcal{K}_\infty$ the error dynamics is ISO [137], i.e. the error dynamics are ultimately bounded by $\gamma(\|\xi\|_\infty)$ and the system exhibits asymptotic stability to $e(t) = 0$ for $\xi = 0$. Furthermore, if the set of coefficients $\{l_3,\, l_2,\, l_1,\, l_0\}$ are selected such that the matrix A is Hurwitz, with real eigenvalues listed in increasing order $\lambda_1(A) < \lambda_2(A) < \lambda_3(A) < \lambda_4(A)$, one knows that, $\|\exp(At)\| \leq \alpha\exp(-\lambda_1 t)$ with $\alpha = \|T\|\|T^{-1}\|$ where T is a matrix such that $T^{-1}AT$ is diagonal. Using this fact in (6.13), one obtains:

$$\begin{aligned} \|e(t)\| &\leq \exp(-\lambda_1 t)\,\|x(0)\| + \frac{\alpha K_0}{J}\int_0^t \exp(-\lambda_1(t-q))\,dq \\ &\leq \exp(-\lambda_1 t)\,\|x(0)\| + \frac{\alpha K_0}{J\lambda_1}(1-\exp(-\lambda_1 t)) \end{aligned} \tag{6.14}$$

Consequently $\|e(t)\|$ *converges exponentially to a sphere with radius* $\rho = \frac{\alpha K_0}{J\lambda_1}$ *when* $t \to \infty$.
■

Remark 3 *The first term in (6.14) may dominate for small* t*, and this serves to quantify the magnitude of the observer's transient behavior as a function of the size of the initial state* $x(0)$ *and the value of* λ_1*. This property allow us choosing a judicious set of coefficients* $\{l_3, l_2, l_1, l_0\}$ *in order to provide an acceptable transient term.*

Remark 4 *The first term in (6.13) vanishes for a* t *sufficiently large. Thus the dynamics of estimation error satisfies the asymptotic gain (AG) property. That is, for all large enough* t*, the trajectory exists, and it approaches arbitrarily close to a sphere whose radius is proportional to the bound of* ξ *and inversely proportional to* λ_1*. The estimate AG is ultimately bounded.*

6.3.2. Tracking control design for the AAFO

It is desired to drive the flat output $R = \theta$ of the system (6.6), to track a given reference trajectory R^*, defined by a healthy profile of the ankle joint during the gait cycle, regardless of the unknown but uniformly bounded nature of ξ. Then, the objective is to design a control law using the estimated disturbance in order to cancel it. Since the state is available, it will be used in the feedback. The proposed trajectory tracking controller with disturbance rejector is formulated as follows:

$$\tau = J\left(\ddot{R}^*(t) - v\right) \tag{6.15}$$

$\ddot{R}^*(t)$ represents the feed-forward component and v shows the feedback component to be determined. Let $z_1 = R - R^*$ and $z_2 = \dot{R} - \dot{R}^*$ be the flat output tracking error and its derivative, the AAFO system (6.6) can be expressed as

$$\Sigma_{EC} := \begin{cases} \dot{z}_1 = z_2 \\ \dot{z}_2 = v + \dfrac{\xi}{J} \end{cases} \tag{6.16}$$

which has the form $\dot{z} = Az + B\left(v + \frac{\xi}{J}\right)$. Since the proposed control law in this study is based on an CLF approach, the first step is to find an appropriate CLF for the system (6.16). This is summarized in the following proposition.

Proposition 8 *The function $V : \mathbb{R}^2 \longrightarrow \mathbb{R}$ defined by*

$$V(z) = z^T P z \tag{6.17}$$

is a CLF for the system (6.16) relative to the equilibrium state $z^e = (0\ 0)^T$ with the stabilizing control:

$$v = -\varepsilon B^T P z - \frac{\xi}{J} \tag{6.18}$$

where P shows the solution of the Ricatti equation:

$$A^T P + PA - 2\varepsilon PBB^T P = -Q \tag{6.19}$$

Proof 8 *V is smooth and positive definite. Now, consider the derivative of (6.17) along the trajectories of the closed-loop*

$$\begin{aligned} \dot{V}(z) &= \dot{z}^T P z + z^T P \dot{z} \\ &= \underbrace{z^T (A^T P + PA) z}_{:=a(z)} + \underbrace{2 z^T PB}_{:=b(z)} \left(v + \frac{\xi}{J} \right) \\ &= z^T \underbrace{(A^T P + PA - 2\varepsilon PBB^T P)}_{-Q} z < 0 \end{aligned} \tag{6.20}$$

Furthermore, for $Q = diag(q_1, q_2)$ and $\varepsilon > 0$, the solution of the Ricatti equation is satisfied for P given in (6.21)

$$P = \begin{pmatrix} p_{11} & p_{12} \\ p_{21} & p_{22} \end{pmatrix} \tag{6.21}$$

where

$$p_{11} = 2\varepsilon \sqrt{\frac{q_1}{2\varepsilon}} \sqrt{\frac{1}{\varepsilon} \sqrt{\frac{q_1}{2\varepsilon}} + \frac{q_2}{2\varepsilon}},$$

$$p_{12} = p_{21} = \sqrt{\frac{q_1}{2\varepsilon}}, \quad \textit{and}$$

$$p_{22} = \sqrt{\frac{1}{\varepsilon} \sqrt{\frac{q_1}{2\varepsilon}}}.$$

Besides, from (6.20), note that $b(x) = 0$ implies $z_1 = -\frac{p_{22}}{p_{12}} z_2$, as a consequence

$$a(x) = -2(\sqrt{\frac{q_1}{2\varepsilon}} + q_2) z_2^2 < 0$$

Thus, the time derivative of V meets the following requirement:

$$b(x) = 0 \Rightarrow a(x) < 0 \ \ \textit{for all } z \neq z^e$$

Then V given by (6.17) is a CLF for the system (6.16) relative to the equilibrium state $z^e = (0\ 0)^T$.
■

The Proposition 8 was used only to design a CLF where the ADRC and the observer (6.7), used as a rejector, are designed. Then, the feedback component v is defined as:

$$v(z) = -b(z)\left(\gamma_C(a(z), b(z)) + \kappa\right) - \eta_1(t) \tag{6.22}$$

where $\kappa \in \mathbb{R}_{>0}$. Using (5.5):

$$\gamma_C(a(z), b(z)) := \begin{cases} \frac{a(z)+\sqrt{a^2(z)+b^4(z)}}{b^2(z)} & \text{if } b(z) \neq 0 \\ 0 & \text{if } b(z) = 0 \end{cases} \tag{6.23}$$

Furthermore, the system exhibits asymptotic stability to the origin of the state space tracking error for $\Delta = 0$.

Proposition 9 *The AAFO system (6.6) and its control (6.15) with v given by (6.22) is ISS with respect to Δ, where $\Delta = (\xi/J - \eta_1)$, i.e. the difference between the total unknown disturbance and its estimation obtained by (6.7).*

Proof 9 *Let $V : \mathbb{R}^2 \longrightarrow \mathbb{R}$ be a CLF for the system (6.16) defined by (6.17). The derivative*

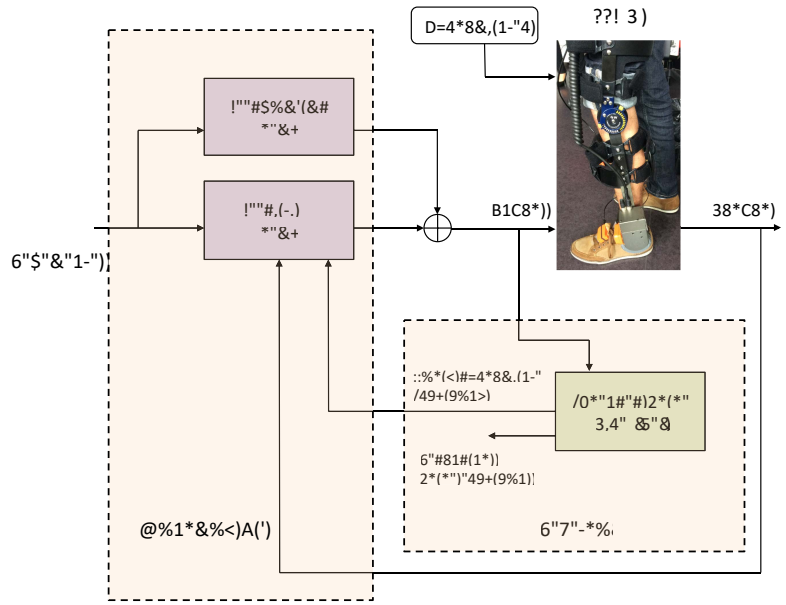

Figure 6.1 – ADRC: ESO and control law based on CLF approach

of (6.17) along the trajectories of the closed-loop becomes

$$
\begin{aligned}
\dot{V}(z) &= \dot{z}^T P z + z^T P \dot{z} \\
&= \underbrace{z^T (A^T P + PA) z}_{:=a(z)} + \underbrace{2 z^T P B}_{:=b(z)} \left(v + \frac{\xi}{J} \right) \\
&= a(z) + b(z) \left(-b(z) \left(\gamma_C(a(z), b(z)) + \kappa \right) - \eta_1(t) + \frac{\xi}{J} \right) \\
&= -\sqrt{a^2(z) + b^4(z)} - \kappa b^2(z) + b(z) \underbrace{\left(\frac{\xi}{J} - \eta_1 \right)}_{\Delta} \\
&= -\sqrt{a^2(z) + b^4(z)} - \kappa \left[b^2(z) - \frac{2b(z)\Delta}{2\kappa} + \frac{\Delta^2}{4k^2} \right] + \frac{\Delta^2}{4k} \\
&= -\sqrt{a^2(z) + b^4(z)} - \kappa \left[b(z) - \frac{\Delta}{2k} \right]^2 + \frac{\Delta^2}{4k} \\
&\leq -\underbrace{\sqrt{a^2(z) + b^4(z)}}_{W(z)} + \frac{\Delta^2}{4k}
\end{aligned}
\tag{6.24}
$$

since $W(z)$ is positive definite and radially unbounded, there exist a class $\mathcal{K}_\infty$ function $\bar{\rho}$ such that $W(z) \geq \bar{\rho}(|z|)$ and therefore

$$
\dot{V}(z) \leq -\bar{\rho}(|z|) + \frac{\Delta^2}{4k} \tag{6.25}
$$

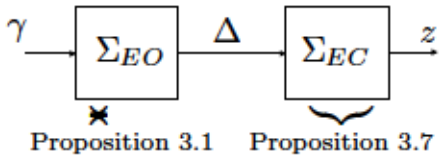

Figure 6.2 – ISS interpretation for the ADRC

It follows that if $|z| \geq \bar{\rho}^{-1}\left(\frac{\Delta^2}{2k}\right)$, *the* $\dot{V}(z) \leq -\frac{1}{2}\bar{\rho}(|z|)$. *By Definition 1 and Theorem 2, the AAFO system (6.6) with control (6.15), (6.22) and (6.23) is ISS with respect to* Δ.

Consider the ADRC composed of the ESO (6.7) and the trajectory tracking controller (6.15) driving together the AAFO system (6.6) to follow a desired angular trajectory (see Fig. 6.1). From (6.10) and (6.16) the observer dynamics error and the tracking dynamics error can be viewed as two ISS systems in cascade (see Fig. 6.2). Then, the following proposition for the ADRC stands.

Proposition 10 *The ADRC composed of the ESO (6.7) and the trajectory tracking controller (6.15) is ISS, when the unknown total disturbance* ξ *is viewed as the input and the tracking error* z *viewed as the output.*

Proof 10 *The claim follows from the properties for the interconnection of nonlinear systems that are ISS [135, 136]. Consider the estimation error dynamics (6.10) and the tracking error dynamics (6.16), which can be viewed as a cascade system, as shown in Fig. 6.2. Since each system is ISS as was proven in Proposition 7 and 9 , then the overall system is ISS. That is, the ADRC is ISS when the unknown total disturbance* ξ *is the input and the tracking error* z *the output.*

6.4 Conclusion

In this chapter, an active disturbance rejection control (ADRC) is developed. An extended state observer (ESO) is used to estimate the total endogenous and exogenous disturbances exerted on the AAFO-human system. Such estimation is then used to cancel the dynamics of the AAFO-human model and a control Lyapunov function (CLF) is proposed as the control law of the ADRC approach. Furthermore, the properties of the CLF include a relatively good tracking with high robustness to external perturbations and

estimation errors of the ESO. The combination of the ESO with the CLF features a low chattering effect of the AAFO's DC motor.

This control approach requires only the measurement of the ankle joint angle, since the ESO is able to estimate the velocity of the ankle joint. Furthermore, no additional sensors are necesary, which is an advantage over the MRAC approaches introduced in the previous chapter.

In the next chapter, the proposed control strategies; the MRAC, APSMC, and the ADRC, are evaluated in experiments with healthy subjects and paretic patients in a clinical environment.

7 — Experimental Results: Aplication to an AAFO for gait assistance

7.1 Introduction

Assisting the ankle joint during walking while using a reference trajectory, requires a correct synchronization between the desired ankle joint profile and the generated assistive torque by the AAFO while taking into account the wearer participation to the movement achievement. In this chapter, the different control strategies presented in chapters 5 and 6 are assessed for their effectiveness to assist the gait through experiments performed by healthy subjects and paretic patients wearing the AAFO either walking on a treadmill or on level ground, respectively. Each controller is evaluated for its performance to follow a desired ankle joint profile, as described in chapter 4, hence, different quantitative assessment methods are implemented, e.g., electromyography measurements, tracking errors, and assistive torque.

Firstly, the model reference adaptive controller (MRAC) is assessed. Starting with the basic MRAC, three case studies were analyzed: 1) with no ground reaction forces and no musculoskeletal torque, 2) with assistive torque provided only during the swing phase, and 3) with assistive torque provided through the whole gait cycle. The results obtained with one healthy subject and one paretic patient are reported. Then, the projection based model reference adaptive controller (PMRAC) is assessed for its tracking performance. The assistive torque is provided during the whole gait cycle, and the results of three healthy subjects are presented. Subsequently, a saturation approach of the proportional

and derivative control element of the MRAC is implemented and applied to the AAFO system. One healthy subject and one paretic patient participated in the experiments to assess the tracking performance of the controller.

Secondly, an adaptive proxy-based sliding mode control (APSMC) is assessed with two healthy subjects and two paretic patients while assistive torque is provided during the whole gait cycle.

Finally, an active disturbance rejection control (ADRC) with a Lypunov function control is assessed with one healthy subject while walking on a treadmill.

7.2 Experimental protocols

In total, four healthy subjects and three paretic patients have undertaken experiments throughout the study. However, the different control strategies were not tested with every subject. The subjects recruited for each controller are reported in the results. The subjects' features are shown in Table 7.1.

All healthy and patient subjects were informed of the experimental protocols and gave their consent before participating in the experiments that were approved by the department of Neurorehabilitation at Henri Mondor University Hospital. All precautions were taken to not adversely affect the health of the participants who served as research subjects. Precautions were also taken to protect the privacy of the subjects and the confidentiality of their personal information. All healthy subjects were able to perform complete dorsiflexion and plantar flexion of the ankle joint with no spasticity or contracture. The paretic patients presented a unilateral foot drop condition with a reduced range of motion in the plantar flexion direction during the second half of the stance phase. The patients also had an absence of strongly manifesting spasticity and co-contracture in lower extremity joints. To guarantee the safety of the subjects while walking, the mechanical design of the AAFO ensures an ankle joint movement within a limited range set to -32° for the dorsiflexion and 22° for the plantar flexion.

The objectives of testing the system's with healthy subjects are: 1) to prove that the system is able to modify the natural ankle joint profile at targeted moments of the gait cycle with a high level of repeatability, 2) the safety of the wearer during experiments, and 3) to evaluate the accuracy of the adaptive ankle reference generator (AARG) algorithm. Experiments with the healthy subjects were done prior to the experiments with

Table 7.1 – *Subjects' characteristics*

	Subject	Gender	Age (years)	Weight (Kg)	Height (cm)
Healthy	H1	Male	30	63	180
	H2	Male	25	64	175
	H3	Male	27	67	185
	H4	Male	31	76	170
Patient	P1	Female	57	50	160
	P2	Male	23	57	170
	P3	Male	58	79	176

the paretic patients.

Since the system is intended to modify the ankle joint profile of the healthy subjects, at first, each subject walks on a treadmill at a predefined walking speed while no assistive torque is provided to adjust the reference trajectory to promote dorsiflexion or plantar flexion at specific moments of the gait cycle.

For experiments using a time-fixed ankle joint desired profile, the adjustment of the reference is done by modifying the range of motion of the ankle joint and the duration of the gait cycle (step duration). An audible cue is provided as feedback to the subject in order to synchronize the walking pace to the duration of the gait cycle. This cue is triggered by the reference every time a new gait cycle starts (IC event), i.e. every 2 s. Therefore, the subjects need to land the ipsolateral heel at the same moment the audible cue is provided.

For the rest of the experiments, the ankle reference trajectory is updated online based on the main gait cycle events and is adapted with respect to the self-selected speed of the wearer (chapter 4) with no need to an audible cue.. In order to adjust the ankle joint profile, the initial contact (IC), toe landing (TL), heel-off (HO), toe-off (TO), and maximum dorsiflexion (MD) key points values for the AARG algorithm are set to generate a personalized ankle joint profile for each subject.

The experiments with the healthy subjects have been performed according to the following scenario. A session, lasting several seconds, starts when the ankle joint AARG algorithm has measured 5 steps to produce the online reference trajectory, or the subject has correctly synchronized with the time-fixed reference. Several sessions per subject are performed to evaluate the repeatability and the consistency of the results. A resting time of 60 s between the sessions is provided. Finally, several additional sessions per subject are performed without the AAFO's assistance in order to compare the results with those recorded during the assistance sessions. The session duration, and number

of assisted and unassisted sessions depend on the used controller.

Since asking the patients to synchronize with a audible cue is not feasible, only the AARG algorithm is used to calculate the desired trajectory. Initially, each patient wears the AAFO and walks on level ground without the orthosis assistance for the FSR calibration process using (4.1) and (4.2). The ankle joint angle is measured to define the values of the IC, TL, HO, TO, and MD key points needed for the adaptive reference. Afterwards, 3 sessions without assistance and 3 sessions with assistance are conducted. All sessions are performed at a slow self-selected walking speed for improved safety and to generate an ankle joint angle profile similar with the one produced by healthy subjects walking at 2 m/s. One session consists of a 8 m or 60 s walking on level ground (depending on the controller used) with the first 5 steps used to calibrate the FSR measurements. A resting period of 1 minute is provided between sessions. The experiments with the paretic patients were performed under the supervision of the medical staff at the Henri Mondor hospital, Créteil, France.

As described in chapter 3, the AAFO is equipped with an incremental encoder that measures the angle θ between the foot and the shank. The angular velocity of the ankle joint $\dot{\theta}$ is derived numerically with a sampling frequency of 1 KHz. The control torque and any the extra sensors are sampled at the same frequency.

A gait cycle is considered from the heel strike of the left foot to the next heel strike of the same foot. All data were time normalized to 100% of the gait cycle. At the end of the experiments, the ankle joint angle, the reference profile, and the assistive torque have been resampled at 2000 samples per gait cycle in order to calculate the average profile, normalized with respect to the gait cycle. Furthermore, in order to homologize the presentation of the ankle joint angle and velocity to the literature (Fig. 4.1), the ankle angle and velocity were plotted using $\theta_{fig} = -(\theta - 90^{\circ})$ and $\dot{\theta}_{fig} = -\dot{\theta}$, where θ_{fig} and $\dot{\theta}_{fig}$ represent the ankle joint angle and velocity presented in the figures of this chapter.

7.3 Experimental setup

The MRAC relies on the measurement of the ground reaction forces, the orientation of the shank, and the translational accelerations of the foot in order to estimate the system parameters (5.8). In Fig. 7.1a, the AAFO system is worn by a healthy subject. The experimental setup depicted in the figure consist of the AAFO in combination with two inertial

measurement units (XSENS): one is used to estimate the angle θ_s between the shank and the vertical axis (Fig. 3.2), and the other one is used to measure the translational accelerations at the ankle level a_x, a_y in the horizontal and vertical directions, respectively. Also, six force sensitive resistors (FSR) are embedded in the left and right insoles and are connected to a wireless system (Trigno, Delsys), as seen in Fig. 3.4. Finally, since the tibialis-anterior (TA) and gastrocnemius (GAS) muscles are mainly responsible of the dorsiflexion and plantar flexion movements respectively, placing electromyography (EMG) sensors at these muscles provides a template of the muscular activities developed by the subject in both directions of the ankle movement. It should be noted that the human muscular torque does not need to be estimated within this control strategy, but it is used only for the assessment of the effectiveness of the control strategy. Note that this hardware configuration is also used for experiments with the paretic patients but the EMG sensors were removed, as shown in Fig. 7.1b, due to time constrains during the experimental setup in the hospital.

Regarding the adaptive proxy-based sliding mode controller and the active disturbance rejection control, fewer sensors were required. Indeed, both controllers used only the ankle joint angle and velocity measurements. However, the generation of the adadptive desired trajectory requires the use of embedded FSR elements (Delsys or Tekscan systems). In Fig. 7.1c, the configuration of the AAFO with the Tekscan system is shown for one paretic patient.

For all the experimental setups, the AAFO and the extra sensors are connected to a host PC using WIFI. The control algorithm is running in labview on the host PC, where the data measured from both the AAFO and the sensors are synchronized.

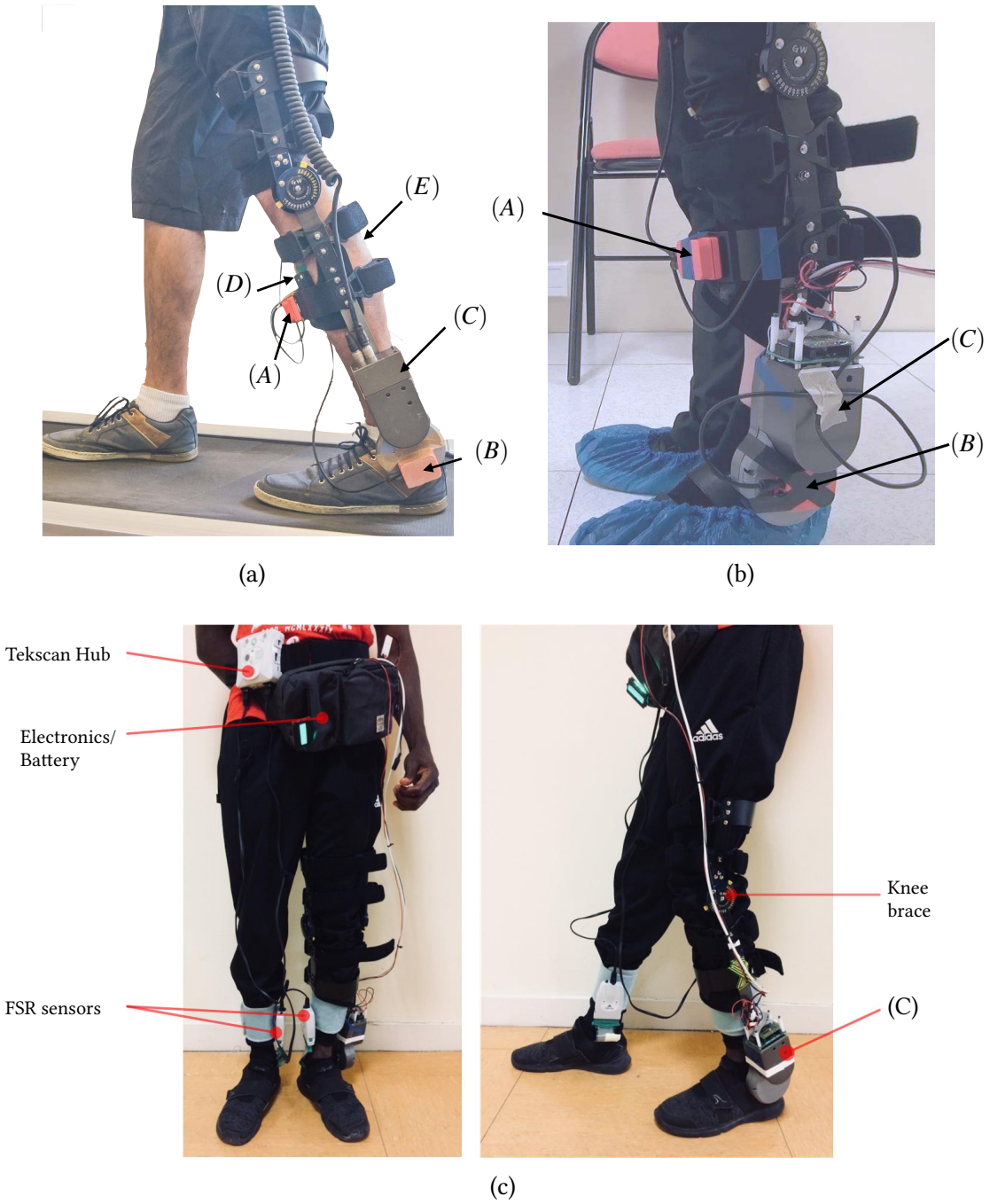

Figure 7.1 – (a), a healthy subject wearing the AAFO with the Trigno (EMG plus FSR sensors) and XSENS systems. (b), a paretic patient wearing the AAFO with the Trigno (FSR sensors) and XSENS systems. (c), a paretic patient wearing the AAFO with the Tekscan system. The setup of the system is: (A) IMU used to estimate the angle between the shank and the vertical axis, (B) IMU measuring the translational accelerations, (C) AAFO, and (D) and (E) are the EMG sensors for measuring the TA and GAS muscular activities, respectively.

7.4 Model reference adaptive control

The first control strategy to assess is the basic MRAC, the stability of the system is evaluated by tracking a sinusoidal ankle angle profile while the subject is seated with both legs hanging without contact with the ground (τ_g). Furthermore, the subject is asked to remain passive, i.e., to not move his foot during this session in order to guarantee a null muscular torque ($\tau_h = 0$, the EMG signals of the TA and GAS muscles were used to ensure that there is no voluntary human activity at the ankle level). The objective of this session is to ensure adaptive parameters convergence while maintaining satisfactory tracking performance. In this case study, the controller's parameters (5.7) and (5.8) were set empirically by trial and error to: $\kappa = 1$, $\lambda = 1$ and $a_n = 1$ with $i \in \{1, 2, 3, ..., 6\}$, all the adaptive parameters were initialized to zero, which stress the no need of a prior identification process, and $\theta_r = \frac{\pi}{2}$. The controller was able to correctly track the position within the first seconds, and gradually improve its performance until reaching excellent tracking, as seen in Fig. 7.2. Furthermore, all the adaptive parameters have converged to a bounded range of values as shown in Fig. 7.3.

7.4.1. Swing phase assistance

Once the stability of the system has been proven experimentaly when no human torque or GRF are present as external disturbances to the system, the MRAC controller is used to assist the gait of subject H1 (see table 7.1) only during the swing phase. The reference trajectory matches a healthy ankle angle profile corresponding to the swing phase of a gait cycle. This profile was obtained by conducting experiments with healthy subjects in a clinical set, as described in section 4.4. The subject is asked to walk on a treadmill, effectively activating his muscles ($\tau_h \neq 0$). The controller is triggered when the swing phase is detected. This is done by measuring the ground reaction forces (GRF) at three points of the left foot and calculating the gait phase probability using the fuzzy logic based algorithm presented in section 4.3. Therefore, if the subject's left foot is in contact with the ground, no torque will be generated by the AAFO's actuator. When the left leg starts the swing phase, the AAFO is controlled to track the desired trajectory and the estimated parameters are adapted according to (5.8). For this part, the subject walks on a treadmill at a fixed speed of 1 Km/h with no inclination.

The controller's parameters were set empirically by trial and error to: $\kappa = 1.2$, $\lambda = 0.7$,

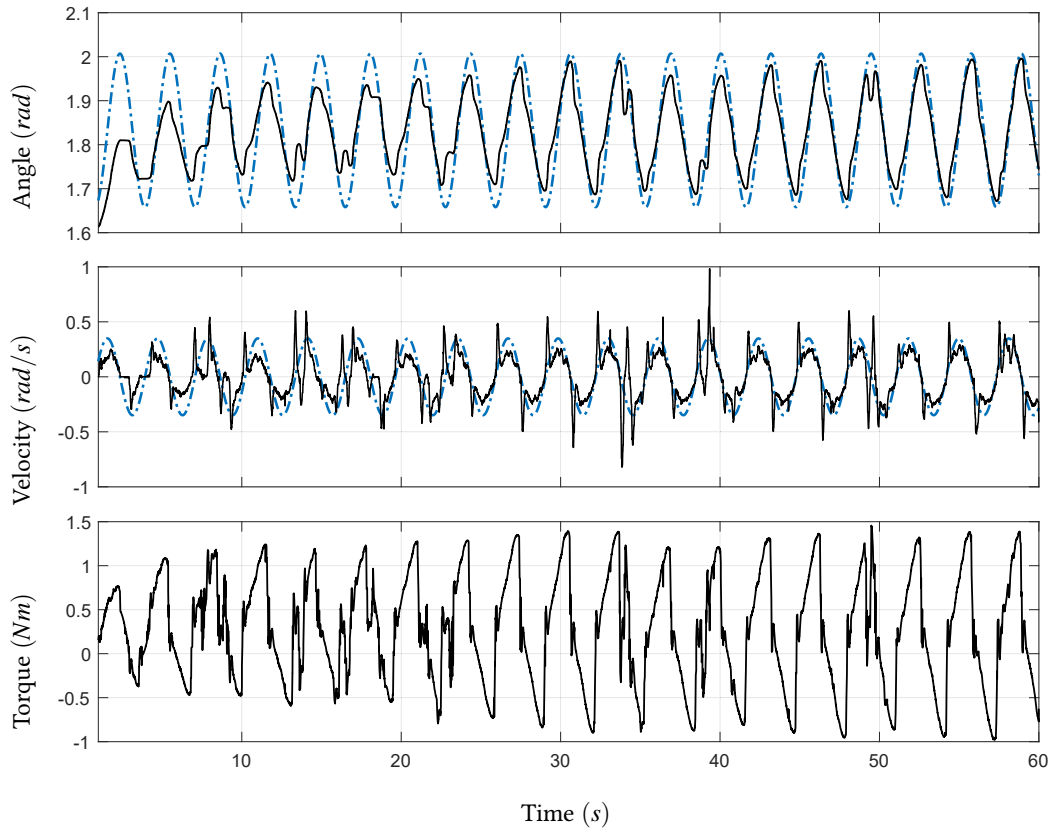

Figure 7.2 – System's performance tracking a sinusoidal ankle angle profile. In the first two plots, the dash-dotted blue line represents the desired profile and the solid black line is the current profile. In the last plot (bottom), the control torque is represented. The subject is seated on a chair with the leg free to swing above ground. There is no interaction with the ground and neither TA nor GAS muscular activity.

$a_1 = 0.15$, $a_2 = 0.15$, $a_3 = 0.5$, $a_4 = 0.7$, $a_5 = 0.8$, and $a_6 = 0.5$, all the adaptive parameters were initialized to zero and $\theta_r = \frac{\pi}{2}$. Since the adaptive parameters are adjusted only during the swing phase and in the case of an error on the position and velocity tracking, as described in (5.8), the adaptive parameters do not converge to the real values of the AAFO-human system.

7.4.1.1. Gait kinematic results

The AAFO was able to assist the wearer during the swing phase of the gait cycle. After a few steps, the range of motion has increased and closely tracks the desired ankle angle trajectory as seen in Fig. 7.4. With an average position error of 0.04 (*rad*) and a maximum error of 0.1 (*rad*), during the swing phase. After 30 *s*, most of the adaptive parameters have converged to a bounded range, as seen in Fig. 7.5. The relatively slow adaptation is

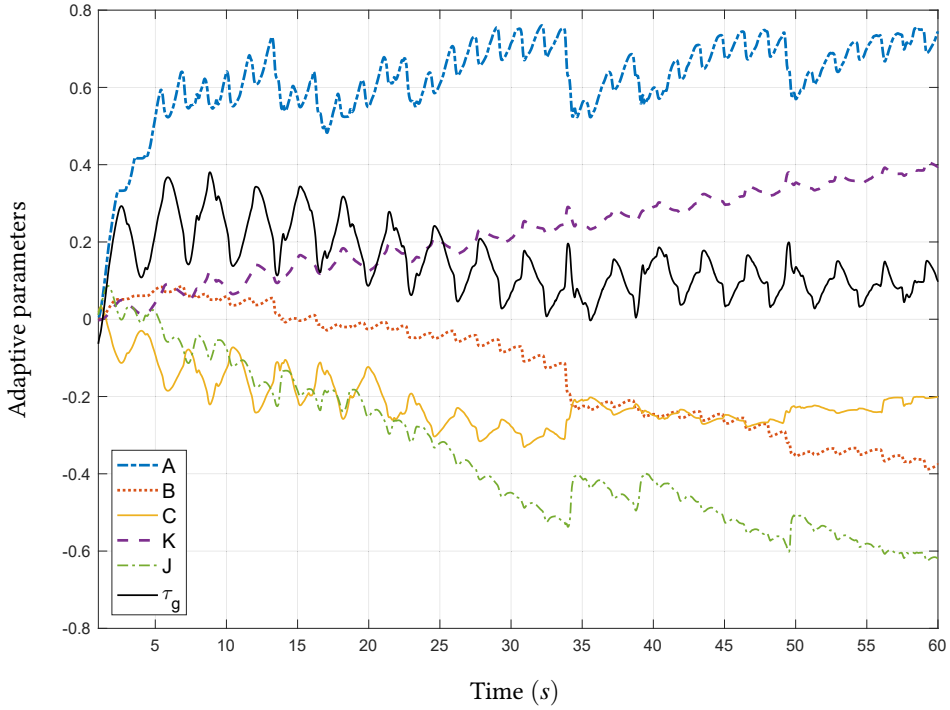

Figure 7.3 – System's adaptive parameters values during the passive case study.

related to the fact that following each heel strike (stance phase), the current and desired ankle angles need to match again. Nevertheless, the torque applied by the AAFO is able to assist in both directions of the ankle motion (dorsiflexion and plantar-flexion), without needing to identify the system's parameters.

While the proposed method shows a satisfactory tracking performance over time, the adaptive parameters were not able to converge to their final values due to the discontinuous desired trajectory and the intermittent assistance being provided. Therefore, the adaptive desired trajectory was defined for the whole gait cycle and the assistance was provided continuously.

7.4.1.2. Muscular activity analysis

A common measurement to assess the assistance using actuated orthoses is the muscular activity monitoring. Normally, an assistance of a healthy subject provided by an AAFO should produce a reduction of the amplitude of EMG signals when compared to the case of the subject wearing the AAFO with no assistance. The activities of the TA and GAS muscles were reduced by 30% and 12% respectively, compared to the walking sessions with/without the controller activated during the swing phase, as seen in Fig 7.6. Since the TA muscle is activated during the swing phase along with the controller, it is expected

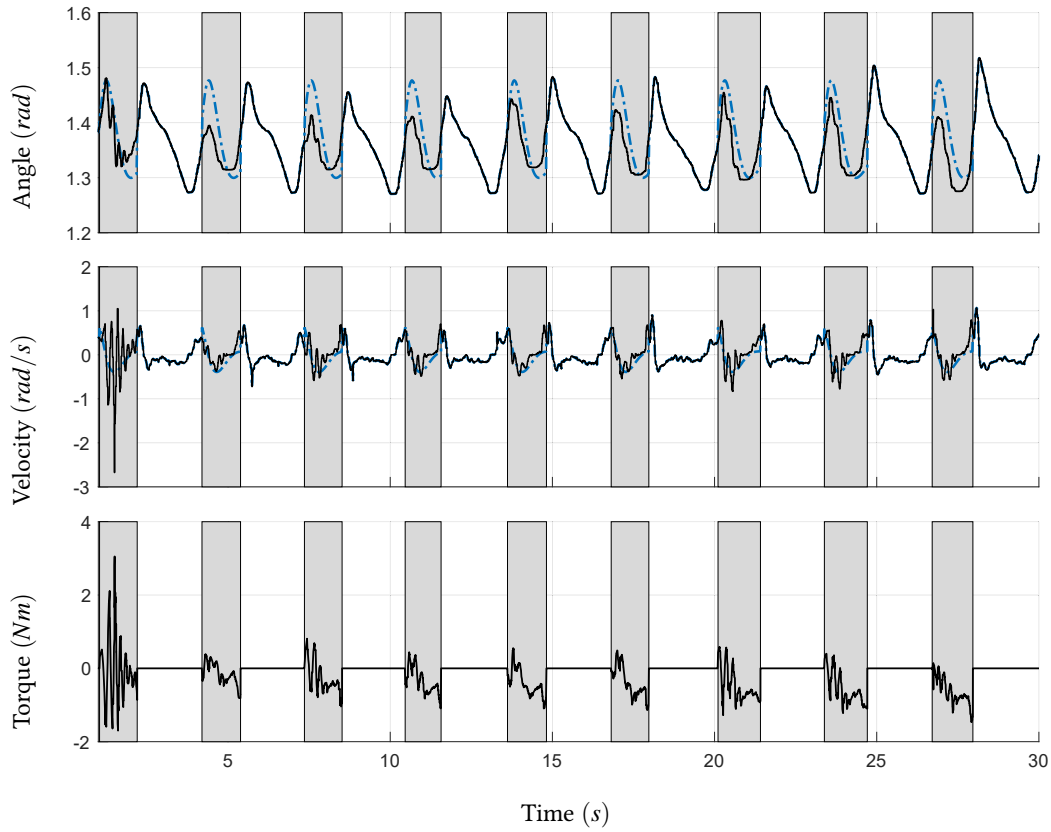

Figure 7.4 – System's performance tracking a healthy ankle profile during the swing phase. In the first two plots, the dash-dotted blue line represents the desired profile and the solid black line is the current profile. In the last plot (bottom), the control torque is represented. The grey areas represent the swing phases when the controller and the adaptation law were enabled and applied to the AAFO. The subject is walking on a treadmill at 1 Km/h, freely actuating his TA and GAS muscles.

a higher level of assistance is provided during the dorsiflexion with respect to plantar flexion. This comparison was done after processing the EMG signals per session for each muscle. The signal processing consists on a rectification and subtraction of the mean value, then application of a fourth order Butterworth lowpass filter with a cut-off frequency of 3 Hz. Notice that the TA muscle is activated during the swing phase (grey bars in Fig. 7.7) while the GAS muscle is activated during the stance phase (white bars in Fig. 7.7). According to ([174]), the push-off impulse power is provided by the energy stored in the ankle extensors, therefore the activation of the GAS muscle ensures such behaviour. This has been observed when analyzing the EMG signals during the gait cycle in Fig. 7.7.

The reduction of the TA and GAS muscular activities involvement proves the effectiveness of the proposed system to assist gait of foot-drop subjects. Furthermore, the assis-

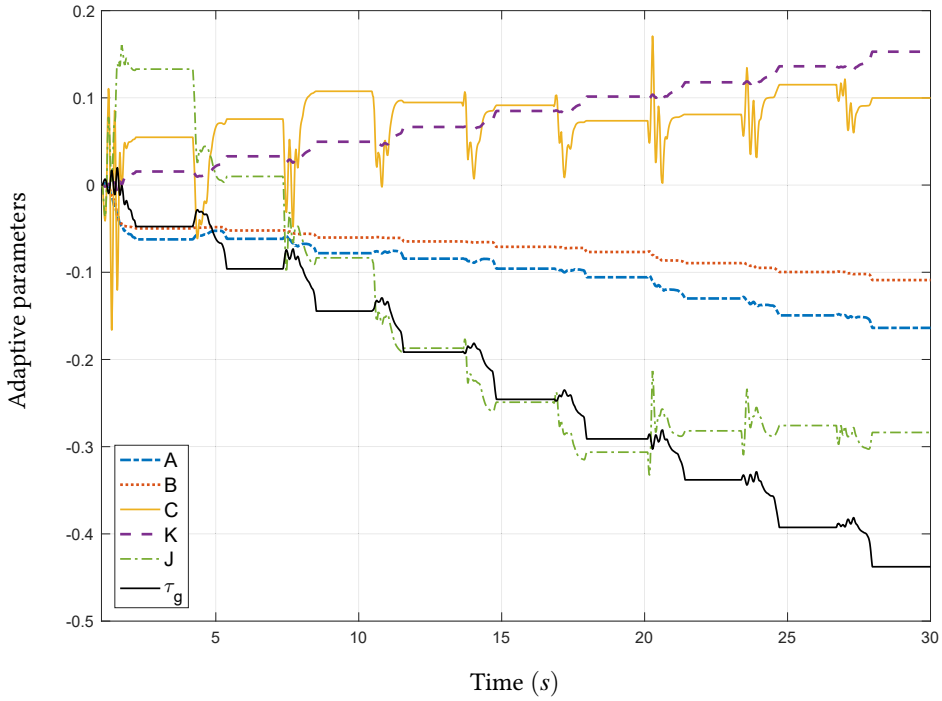

Figure 7.5 – System's adaptive parameters values during the active case study.

tance provided by the AAFO was able to reduce the tracking position error at the end of the swing phase, which effectively corrects foot-drop, as can be seen in Fig. 7.4 from the sixth step forward.

Due to the impact with the ground, the initial position of the ankle joint in the swing sub-phase is different for every step, and the resulting error could negatively affect the adaptive performance of the estimated parameters, preventing some parameters from a relatively fast convergence to a bounded range.

7.4.2. Full gait cycle assistance

The next step to assess the MRAC performance through the whole gait cycle. For this purpose, three healthy subjects (H1, H2 and H3 from table 7.1) wearing the AAFO and walking on a treadmill and one paretic patient (P1 from table 7.1) walking on level ground have participated to the study.

The experiments with the healthy subjects have been performed according to the following scenario. At first, each subject undertakes a series of sessions at a self-selected step duration with the AAFO assistance. A session, lasting 60 s, starts when the AARG algorithm (4.4) is stable, i.e. after 5 steps. The IC, TL, HO, TO, and MD gait event values are the same for every healthy subject and are shown in Table 7.2. Three sessions per

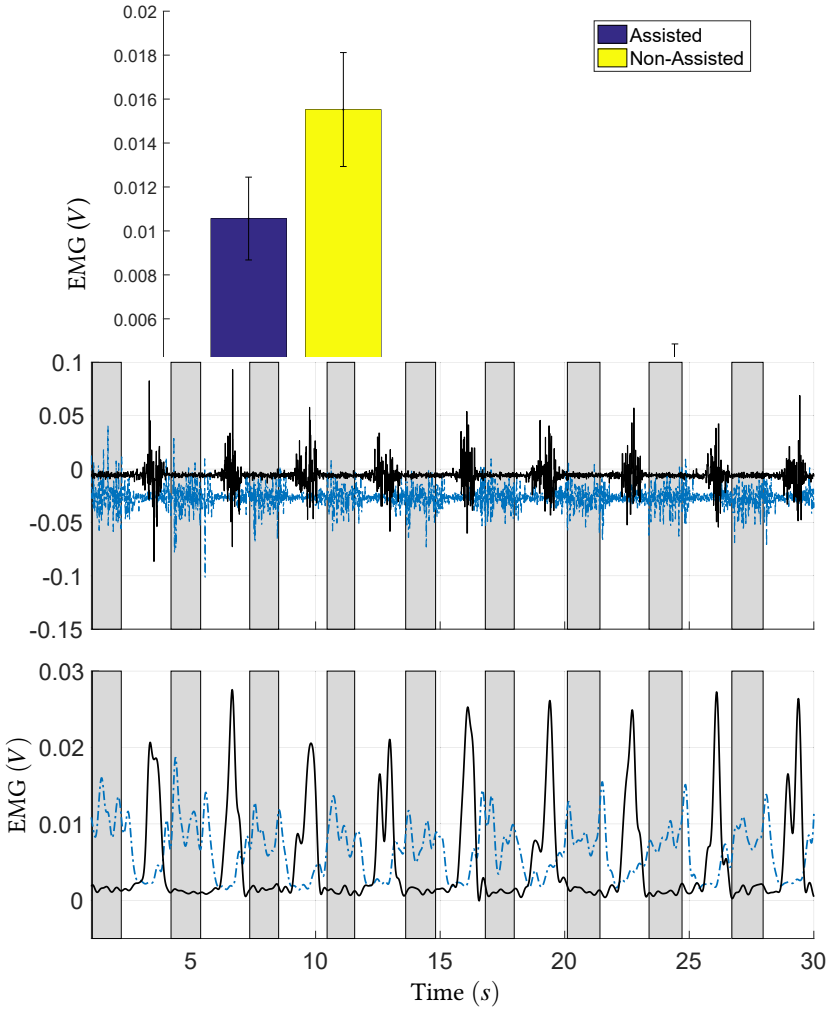

Figure 7 ıase for assisted

Figure 7.7 – Treated signals from EMGs on TA (dotted blue line) and GAS muscles (solid black line). The grey areas represent the periods of time when the controller and the adaptation law were enabled and applied to the AAFO.

subject are performed to evaluate the repeatability and the consistency of the results. A resting time of 60 s between the sessions is provided. Finally, three more sessions per subject are performed without the AAFO's assistance in order to compare the results with those recorded during the assistance sessions.

The scalar gains a_n of the adaptive law (5.8) have been set for the first subject, using trial and error (Remark 2): $a_1 = a_2 = 0.002$, $a_3 = 0.01$, $a_4 = 1$, $a_5 = 0.00001$, $a_6 = 3$, and $a_7 = 2$. The controller's gains (5.7) have been set to: $\kappa = 0.9$ and $\lambda = 7$ with all the adaptive parameters initialized to zero, and the ankle joint angle at the rest position $\theta_r = \frac{\pi}{2}$. These tuning gains values have been considered for all the subjects who participated in this study.

Table 7.2 – *Experimental ankle joint angle key points values in degrees* (°) *for the AARG.*

	IC	TL	HO	TO	MD
Healthy subjects	-1	-3	6	-8.5	0
Paretic patient	-8	-13	3	-16.5	1

Regarding the experiments with the paretic patient (P1 from table 7.1), three sessions without assistance and three sessions with assistance were conducted. All sessions were performed at a relatively slow self-selected walking speed for improved safety. One session consists of a 8 m walking on level ground with the first 5 steps used to intialize the AARG. A resting period of 1 minute is provided between sessions. The paretic patient suffered a stroke 6 years before the experiments and followed a classical clinical rehabilitation process at the Henri Mondor Hospital for 4 years. The patient had an absence of spasticity and no plantar flexors spasms were observed during the experiments. The scalar gains a_n of the adaptive law, equation (5.8), have been set for the patient (Remark 2): $a_1 = a_2 = 0.002$, $a_3 = 0.1$, $a_4 = 1$, $a_5 = 0.00001$, $a_6 = 2.5$, and $a_7 = 2$, the controller's gains (5.7) have been set by trial and error as follows: $\kappa = 0.5$ and $\lambda = 6$ with all the adaptive parameters initialized to zero, and the ankle joint angle at the rest position $\theta_r = \frac{\pi}{2}$. These tuning gains were defined in order to produce a relatively lower assistive torque with respect to the one developed with healthy subjects for improved safety. The ankle joint key point values used for defining the AARG are presented in Table 7.2. These key point values generate an ankle joint angle reference profile that aims to increase the plantar flexion during the terminal stance (TS) sub-phase and to increase the dorsiflexion of ankle joint at the end of the swing phase.

7.4.2.1. Experimental results - Healthy subjects

For the healthy subjects, the proposed controller was able to track the generated adaptive desired ankle trajectory profile within the first seconds and the error has decreased over time. The results for one assisted session for subject 1 is shown in Fig. 7.8. The first 20 s of the tracking performance of the ankle joint angle and angular velocity, as well as the assistive torque delivered by the AAFO are shown in Fig. 7.8a. The assistive torque presents an increasing peak value in the plantar flexion direction during the TS, which represents an increasing assistance for push-off at the end of the stance phase. However, the assistance does not continue to increase after the 8th step, which means the system has reached convergence of the adaptive parameters. In Fig. 7.8b, the performance of the adaptive parameters from equations (5.8) is shown for the complete session lasting

60 *s*. It can be seen that all parameters have converged to their final values, except for the stiffness parameter which is still updating.

Using the gait phase detection algorithm shown in section 4.4, the assistive torque, the reference and the current ankle joint angles have been normalized with respect to the gait cycle. The results of an experimental session for the three subjects are shown in Fig 7.9. In Fig. 7.9a, 7.9b, and 7.9c, the mean torques are shown for subject 1, 2, and 3, respectively; a positive torque represents a plantar-flexion assistance while a negative torque represents a dorsiflexion assistance. From Fig. 7.9a and 7.9c, a predominately plantar flexion assistance can be observed due to the fact that the reference trajectory is more plantar-flexed than the normal ankle angle profile performed by subjects 1 and 3. Nevertheless, all subjects present an increased plantar-flexion assistance during the PS sub-phase, which corresponds to the push-off assistance. Since the ankle joint reference has a relatively smaller range of motion compared to that of healthy subjects, this push-off assistance is quickly reduced, or even changed to a dorsiflexion assistance as in the case of subject H2 (Fig. 7.9b). During the swing phase, all the three healthy subjects have reported an assistance provided by the AAFO. This assistance is greater in the plantar-flexion direction, which is deliberate in order to assess the effectiveness of the system to modify the ankle joint angle even with healthy subjects. Hence, if the key-points in the AARG are adjusted, the assistance direction and magnitude can be manipulated. Furthermore, during the loading response (LR) sub-phase, the assistance provided for subjects H1 and H3 is provided in the dorsiflexion direction, as shown in Fig. 7.9a and 7.9c. The percentage of the gait sub-phase durations with respect to the whole gait cycle is different for each stride, and for each subject. This can be seen in Fig. 7.9, where the mean sub-phase duration percentage is represented by the vertical lines dividing the gait cycle into LR, MS, TS, PS, and swing sub-phases. Despite these different gait sub-phase and step durations for the different subjects participating in this study, the AARG was able to correctly update the generated trajectory and produce an ankle joint angle reference tailored for the subject profiles.

The assistive torque behavior is different from one subject to another but is consistent across all the sessions for each subject. This is shown in the left column of Fig. 7.10, where the mean assistive torque provided by the AAFO and its standard deviation, normalized with respect to the gait cycle, for each assisted session are presented. It is worth noting that the assistive torque provided during the swing phase is not as large as the one generated during the stance phase, even though the position error is larger in the later. This is mainly due to the fact that the torque generated from the ground reaction force is contributing to the total assistive torque.

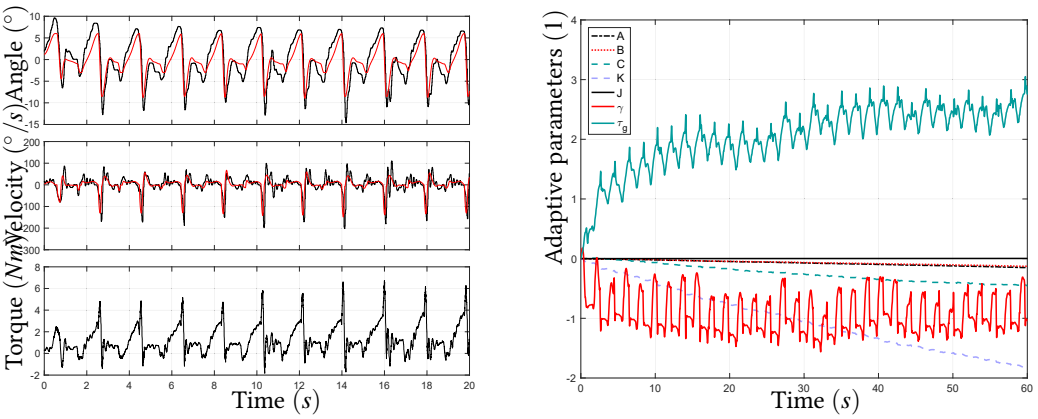

(a) (b)

Figure 7.8 – On the left, the system's performance tracking the desired ankle joint angle profile during one session for subject 1 zoomed in for the first 20s. In the top two plots, the light gray line represents the desired profile and the solid black line is the profile executed by the subject's ankle. In the bottom plot, the control torque delivered by the motor is presented. On the right, the system's adaptive parameters performance during the whole session.

Table 7.3 – *Position error in RMS for each session* $(error(^\circ) \pm std(^\circ))$. *A = assistance session, NA = no assistance session.*

Session	Subject H1	Subject H2	Subject H3
A 1	2.07±2.39	3.02±4.28	3.69±4.61
A 2	2.12±2.53	2.97±4.3	3.09±4.14
A 3	2.17±2.63	2.99±4.35	3.21±4.29
NA 1	5.22±3.45	4.49±3.94	4.43±3.92
NA 2	5.63±6.38	5.43±6.55	4.92±6.32
NA 3	6.88±6.65	6.44±6.07	6.33±6.57

The root-mean-square value of the position error is computed as well as its standard deviation. Table 7.3 shows the mean position error values for each subject and session, both with and without assistance. It can be observed that the tracking error is reduced by 55%, 44%, and 49% in average for subject H1, H2, and H3, respectively, when the assistive torque is provided. Furthermore, in the right column of Fig. 7.10, the comparison of the normalized ankle joint angle and its reference for the six sessions (three sessions with assistance and three without assistance) is shown for each subject.

7.4.2.2. Experimental results - Paretic patient

Fig. 7.11a shows, for one assisted session, the tracking performance for the ankle joint angle and angular velocity, as well as the assistive torque generated by the AAFO. Due to

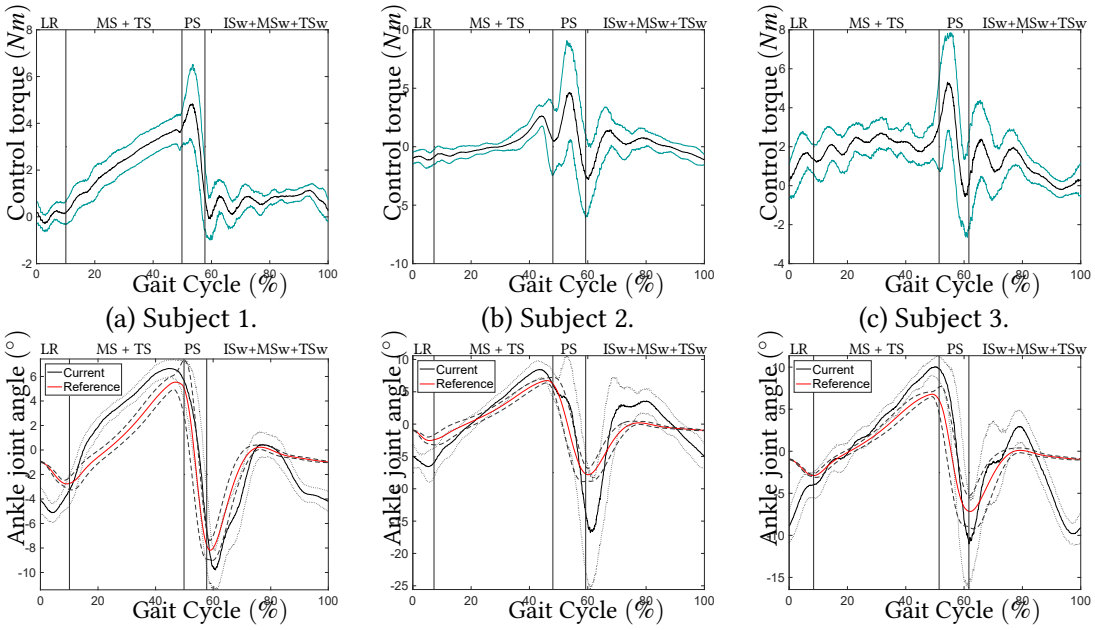

(a) Subject 1. (b) Subject 2. (c) Subject 3.

(d) Subject 1. (e) Subject 2. (f) Subject 3.

Figure 7.9 – On the top row, the system's normalized mean assistive torque for one assisted session of each subject. The black lines represents the mean value and the cyan lines represent the standard deviations about the mean value. On the bottom row, the black lines represent the current ankle joint angle, the red lines represent the ankle joint reference angle, and the dotted and dashed grey lines represent the standard deviation for the current and reference ankle joint profiles, respectively. In all figures the vertical lines represent the divisions between the gait sub-phases relevant to the ankle reference update.

the gait deficiencies of the patient compared to the healthy subjects, the assistive torque presents chattering at some moments during the session. However, the system remains stable and the ankle joint position error is reduced. In Fig. 7.11b, the performance of the adaptive parameters is shown, similarly to the healthy subject experiments; all the adaptive parameters from equations (5.8) converge to their final values, except for the stiffness parameter that keeps updating its value till the end of the session. Using the gait phase detection algorithm, the assistive torque, the reference and the current ankle joint angles have been normalized with respect to the gait cycle. The results of one assisted and one unassisted sessions are shown in Fig 7.12b and Fig 7.12a, respectively. From these figures, a comparison between the normalized ankle joint angle profiles during the assisted and unassisted sessions can be done. On the one hand, for the unassisted session, the patient shows a gait cycle with a predominate plantar flexion, specially at the end of the swing phase and during the loading response sub-phase where the foot plantar flexes excessively, probably due to co-contraction between the plantar flexion

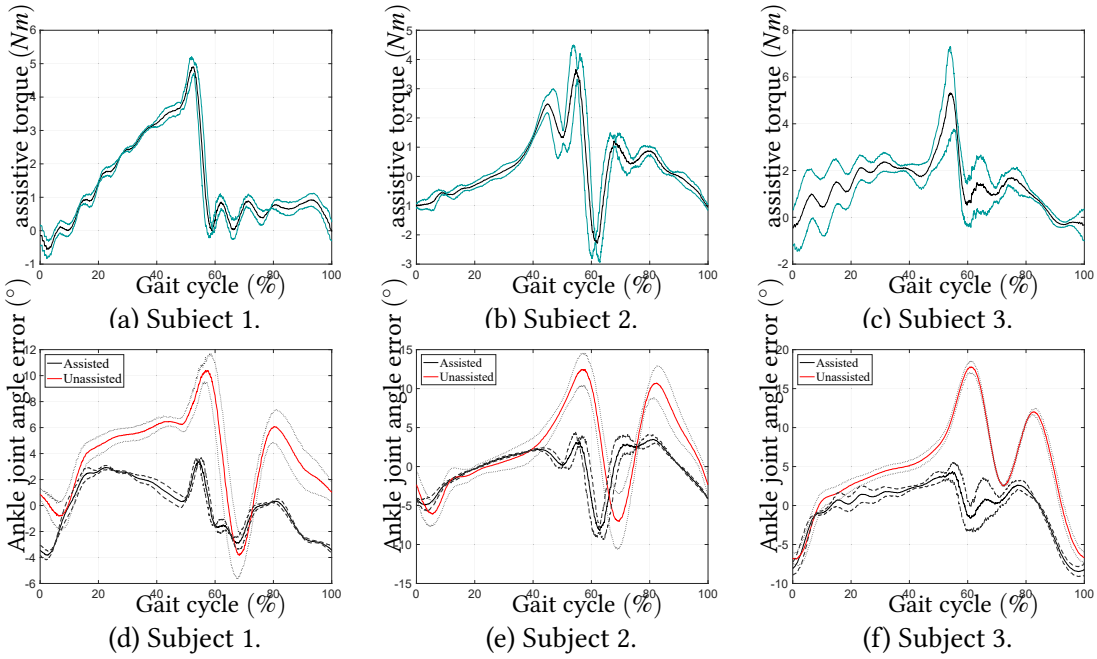

Figure 7.10 – On the top row, the mean normalized assistive torque for all the 3 sessions for each healthy subject. The black lines represent the mean value and the cyan lines represent the standard deviation from the mean. On the bottom row, the mean normalized ankle joint error for the 3 sessions with assistance and the 3 sessions without assistance, for each subject. The black lines represent the assisted scenario and the red lines represent the unassisted scenario. The dashed and dotted grey lines represent the standard deviations from the mean for the assisted and unassisted scenarios, respectively.

and the dorsiflexion muscle groups. However, due to the limited range of motion (ROM) of the ankle joint during TS and PS sub-phases, the patient does not show sufficient push-off movement. On the other hand, for the assisted session, the ankle joint angle profile shows an increased dorsiflexion during the whole gait cycle and the plantar flexion motion at the loading response sub-phase is reduced. Likewise, an increased ROM of the ankle joint during the TS and PS sub-phases (from 7.86±1.98° to 18.09±3.83°) results in an improved push-off motion while increasing the maximum dorsiflexion achieved during the swing phase (from -5.59±1.46° to 0.61±2.03°).

In Fig. 7.12c, the mean torque across all three assisted sessions is shown, as well as its standard deviation. It can be observed a relatively higher standard deviation value across the gait cycle with respect to the one observed with the healthy subjects, mainly due to the variations between each step of the paretic leg of the patient. In Fig. 7.12d, a comparison between the mean ankle joint angle profiles for the assisted and unassisted sessions is shown. It can be seen that the maximum plantar flexion angle prior to the swing phase increased, effectively contributing to push-off. Furthermore, the maximum

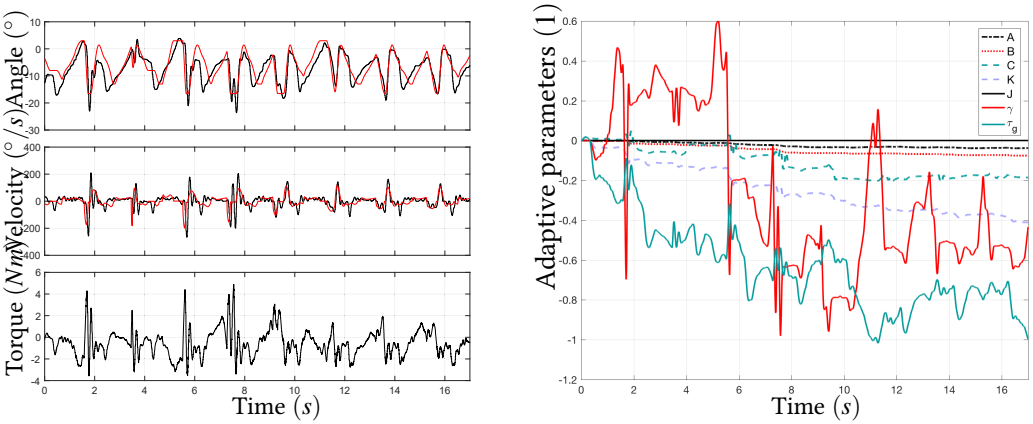

(a) System performance (b) Adaptive parameters

Figure 7.11 – On the left, the system's performance tracking the desired ankle joint angle profile during one session for the patient. In the top two plots, the light grey line represents the desired profile and the solid black line is the profile executed by the patient's ankle. In the bottom plot, the control torque delivered by the motor is presented. On the right, the system's adaptive parameters performance during the same session.

dorsiflexion angle during the swing phase increased, reducing the risk of foot-drop.

The root-mean-square value of the position error is computed as well as the standard deviation and classified in four gait groups relative to the sub-phases: loading response (LR), roll over (MS plus TS), push-off (PS), and swing (ISw plus MSw plus TSw). Fig. 7.13 shows the position error values for each session, both with and without assistance, classified by the aforementioned gait groups. It can be observed that the normalized tracking error is reduced by 51%, 77%, 74%, and 60% for the loading response, roll over, push-off, and swing gait groups, respectively, when the assistive torque is provided.

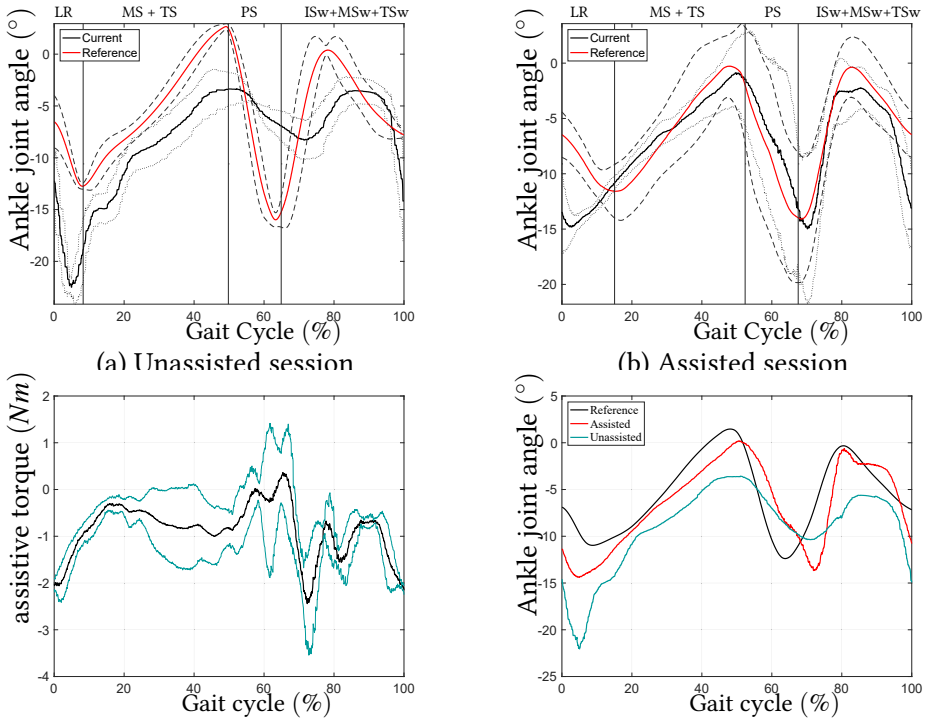

(a) Unassisted session

(b) Assisted session

(c) Mean assistive torque from each assisted session.

(d) Ankle joint reference, assisted and unassisted angles.

Figure 7.12 – On the top, the normalized ankle joint angles for one unassisted and one assisted session with the patient; in dotted and dashed grey lines the standard deviation for the current and reference ankle profiles, respectively. On the bottom left, the mean normalized assistive torque from the three assisted sessions; in cyan the standard deviation from the mean. On the bottom right, a comparison between the ankle joint reference, and real angles from the 3 assisted and the 3 unassisted sessions with the patient.

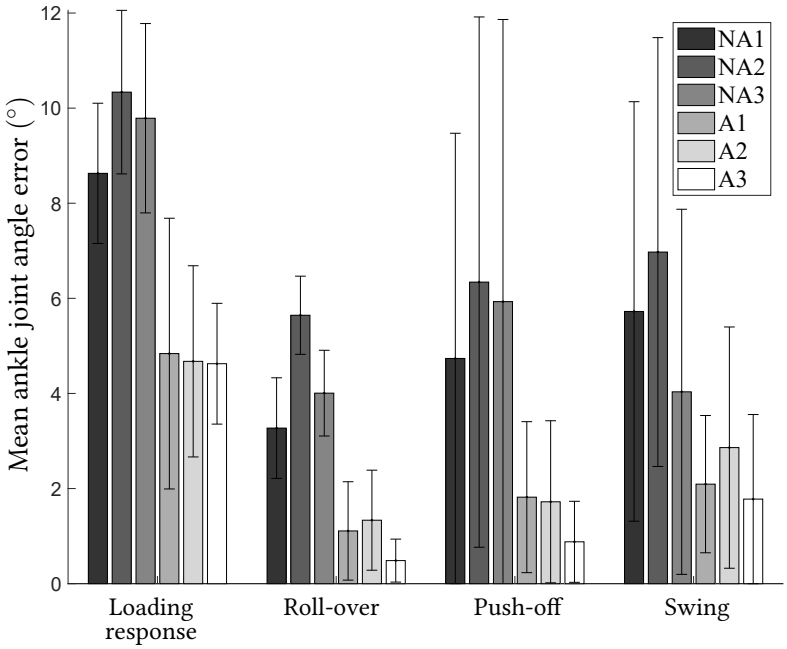

Figure 7.13 – Mean ankle joint angle position errors across the gait cycle for the assisted and unassisted sessions with patient.

7.5 Projection based adaptive control

In this section, the projection based MRAC is used. The system's effectiveness to assist the gait is assessed through experiments performed by one healthy subject (H1 from table 7.1) wearing the AAFO and walking on a treadmill at a self-selected walking speed. Experiments with paretic patients were not conducted due to schedule unavailability. The subject walks in synchronization with a reference ankle angle profile, described in section 4.4, in chapter 4.

A session, lasting 30 s, starts when the subject's gait pace is synchronized with the audible cue. Seven sessions have been performed to evaluate the repeatability and the consistency of the results. Also, three more sessions were recorded with no assistance provided by the AAFO's to compare the results with the ones recorded during the seven assistance sessions.

The controller's parameters in (5.8) and (5.17) were set to: $\kappa = 1$, $\lambda = 6$, $W_M = 6$, $\Gamma_1 = \Gamma_2 = \Gamma_3 = 0.1$, $\Gamma_4 = 20$, $\Gamma_5 = 0.001$, $\Gamma_6 = 0.1$, and $\Gamma_7 = 4$, using trial and error, with all the adaptive parameters initialized to zero, and $\theta_r = \frac{\pi}{2}$. During the assistance sessions, the ankle joint angle was able to track the desired profile within the first seconds and improve its performance over time, as seen in Fig. 7.14. Furthermore, all the adaptive parameters converged to a bounded range of values defined by W_M, as shown in Fig. 7.15. It is worthy to note that some parameters can have a greater value than W_M, e.g., the stiffness in this experiment, since only $||\hat{W}||$ is bounded, not each component of the vector $\hat{W}$.

During the loading response sub-phase, the weight of the wearer is rapidly shifting to the ipsilateral leg, which can generate an increased tracking error due to the relatively big ground reaction forces. For example, in Fig. 7.15, the oscilations of the stiffness and gravity adaptive parameters (k_s and k_g) correspond to the IC event of the gait. Nevertheless, the adaptive parameters remained bounded during the session.

In Fig. 7.16, the normalized torque data are presented in order to asses the assistance provided by the AAFO. During the LR phase and at the end of the TSw phase, the assistance is provided in the dorsiflexion direction, in order to prevent foot-slap. During the MS phase, the assistance is provided in the dorsiflexion direction, in order to assist the wearer's ability to move the leg forward. During the TS and PS phases, the assistance is mostly delivered in the plantar flexion direction, in order to assist the foot to push-off the ground and to start the swing phase. During the ISw and at the end of the

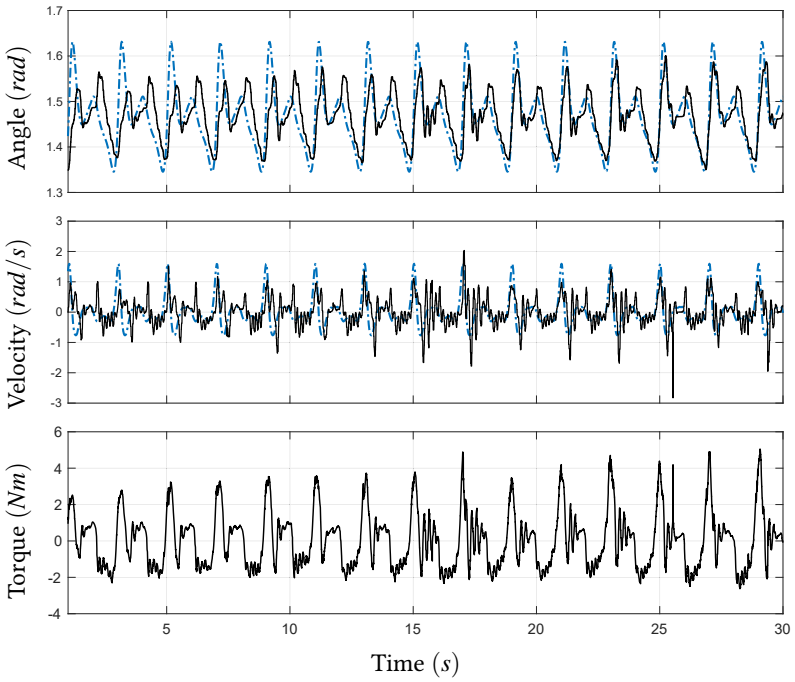

Figure 7.14 – System's performance tracking the desired ankle angle profile during the complete session. In the first two plots, the dash-dotted blue line represents the desired profile and the solid black line is the current profile. In the last plot (bottom), the control torque is represented.

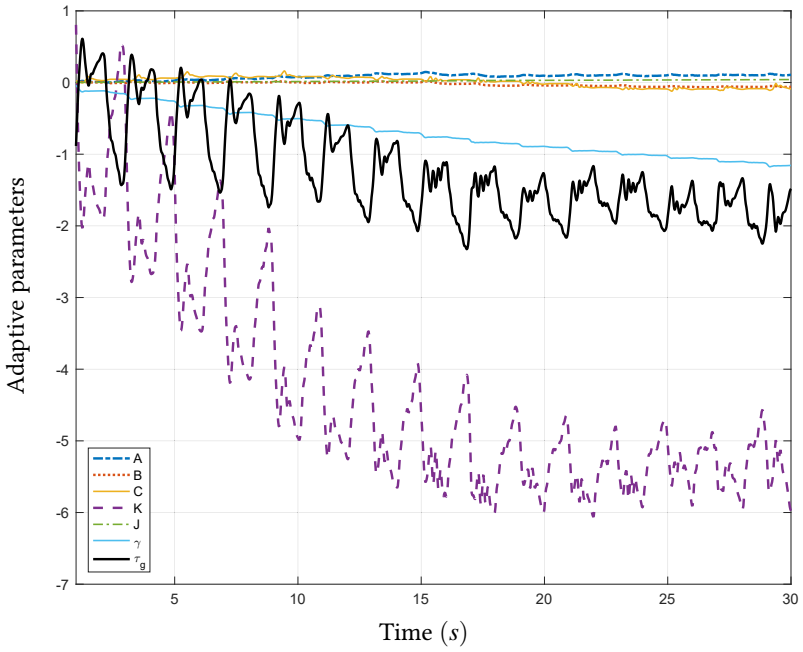

Figure 7.15 – System's adaptive parameters performance during the complete session.

PS phases, the assistance is provided in the dorsiflexion direction to assist the wearer to

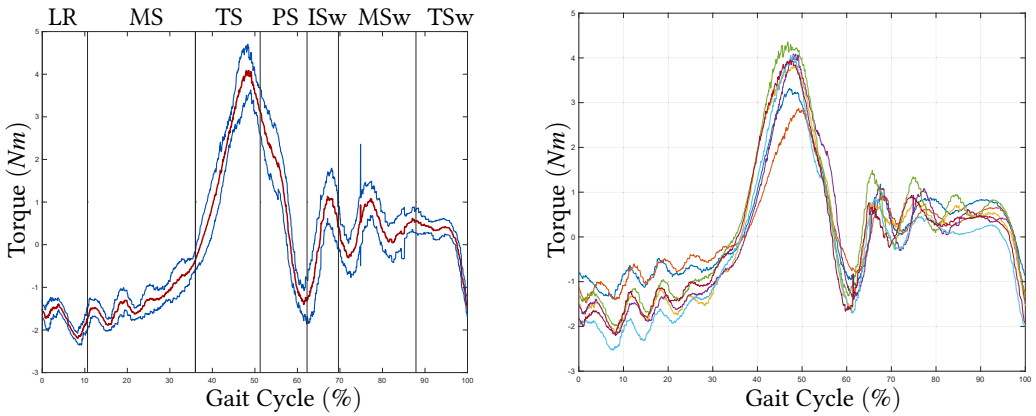

Figure 7.16 – On the left, the system's normalized mean assistive torque. The red line represents the mean value and the blue lines are the standard deviations, the vertical divisions represent the different gait phases. On the right, normalized mean assistance from multiple sessions with the AAFO providing torque to the ankle. Each line represents one of the seven assistance sessions.

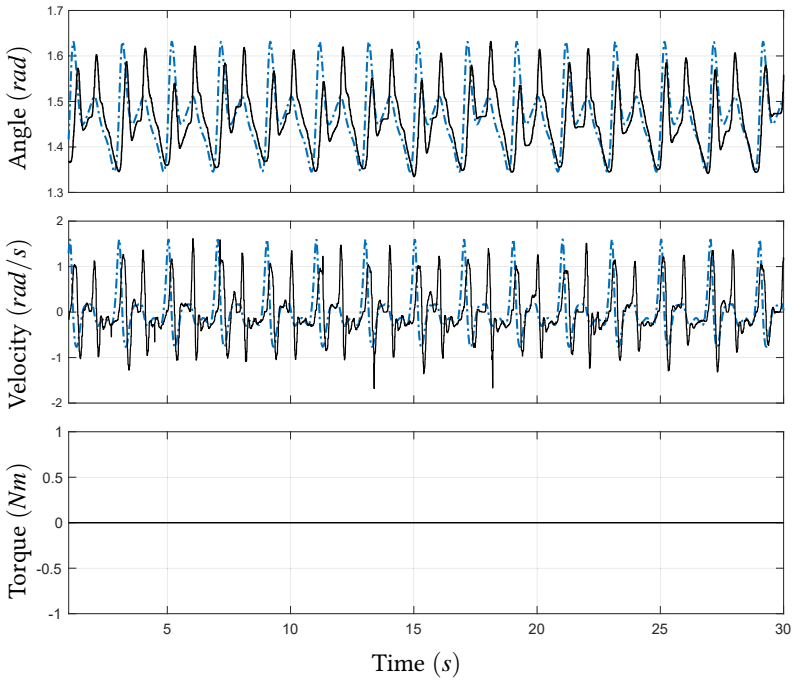

Figure 7.17 – Wearer's normal gait (no assistance). In the plots, the dash-dotted blue line represents the desired profile and the solid black line is the current profile.

prevent foot-drop during swing. Finally, during the MSw and most of the TSw phases, the assistance is provided in the plantar flexion direction, which is due to the fact that the subject has a natural gait with a greater dorsiflexion during the swing phase with respect to the reference trajectory, as shown in Fig. 7.17. These results were consistent

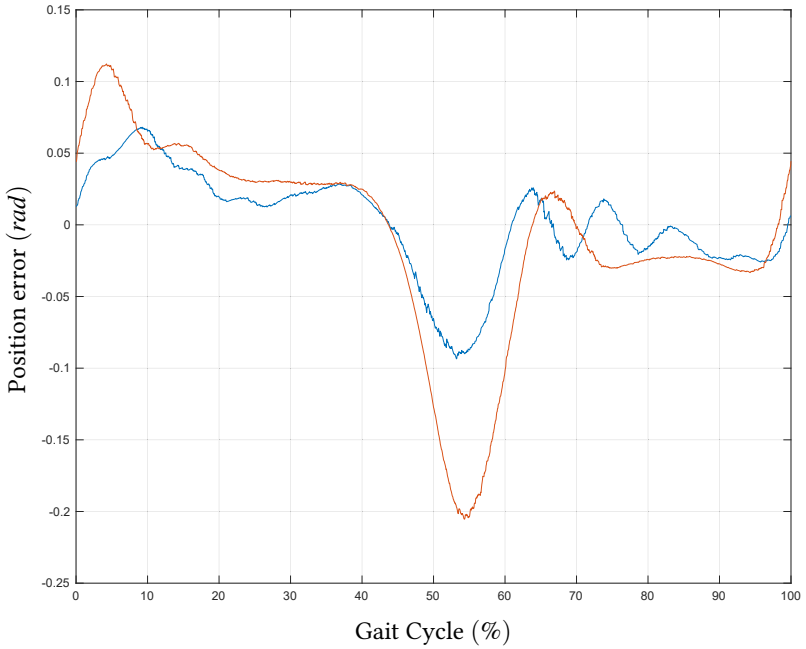

Figure 7.18 – Position error comparison. The error is normalized to the duration percentage of a gait cycle. The comparison is between a session with assistance (blue line) and a session with no assistance (red line).

through all the seven assistance sessions, as shown in Fig. 7.16b, proving the system's repeatability.

The mean tracking angle error for the whole seven sessions is 0.03953 *rad*, with a standard deviation of 0.05247. After approximately 15 *s*, the tracking performance has improved. The mean tracking angular error for the rest of the session became 0.02872 *rad*, with a standard deviation of 0.03653. Therefore the system has proved to be adapting and improving over time. The gait phases where the peaks of the angular error occur are the PS and LR phases. During these gait phases two events occur: the heel strike and the toe-off, making it difficult for the human-AAFO system to track correctly the desired ankle profile. Nonetheless, the system presents an improved tracking compared to the sessions where no assistance was provided by the AAFO, as shown in Fig. 7.18.

7.6 Saturation PD adaptive control

In this section, the effectiveness of the AAFO's controller (with a saturated PD control element) to assist the wearer during walking is assessed through real-time experiments.

Subject H1 walking on a treadmill and the paretic patient P2 (table 7.1) walking on level ground have participated in the experiments. The paretic patient has suffered from a stroke seven months before the experiments. An adaptive reference joint ankle profile was generated while the subjects were walking, as presented in section 4.4, in chapter 4.

The scenario of the experiments with the healthy subject is as follows: first, the subject walks on a treadmill at a speed of 2 Km/h at a self-selected step duration. The ankle joint reference profile is deliberately adjusted to be different from the subject's ankle joint angle profile to test the capability of the system to update the current ankle joint profile during the gait cycle. Then, three unassisted sessions and six assisted sessions, each lasting 30 s, are performed to evaluate the repeatability and the consistency of the results. A resting time of 30 s between the sessions is provided.

The scenario for the experiment with the patient is as follows: initially, the patient wears the AAFO and walks on level ground without any assistance from the orthosis. The ankle joint reference profile is adjusted in order to promote dorsiflexion assistance during the swing and loading response phases and plantar flexion assistance during push-off. Afterwards, three unassisted sessions and three assisted sessions are conducted. All sessions are performed at a self-selected walking speed. One session consists of a 8 m walking on level ground. A resting period of 60 s is provided between sessions.

7.6.1. Experimental results - Healthy subject

The tuning gains a_n of the adaptive law (5.8) have been set for the healthy subject, using trial and error: $a_1 = 0.001$, $a_2 = 0.0001$, $a_3 = 0.02$, $a_4 = 0.9$, $a_5 = 0.000001$, $a_6 = 1.4$, and $a_7 = 0.8$. The controller's gains (5.24) have been set to: $\alpha_p = \alpha_v = 1, N_1 = 8, N_2 = 1.3$ and $\lambda = 6$ with all the adaptive parameters initialized to zero, and the ankle joint angle at the rest position $\theta_r = \frac{\pi}{2}$. The proposed controller was able to track the generated ankle reference profile, as shown in Fig. 7.19. The ankle joint angle error was reduced from an average of 7.2° for the unassisted sessions to an average of 3.0° for the assisted sessions. The ankle joint angle profile of the subject is updated by the assistive torque during the whole gait cycle, as shown in Fig. 7.20. The ankle joint angle and reference profiles are normalized with respect to the gait cycle and then averaged for the three unassisted and the six assisted sessions. The assistive torque developed for each session is given a similar treatment as with the ankle joint angle profiles, and it is presented in Fig. 7.21. Given that the ankle joint reference profile is more plantar-flexed than the ankle joint profile of the subject without assistance, the mean assistive torque is predominantly positive (plantar-

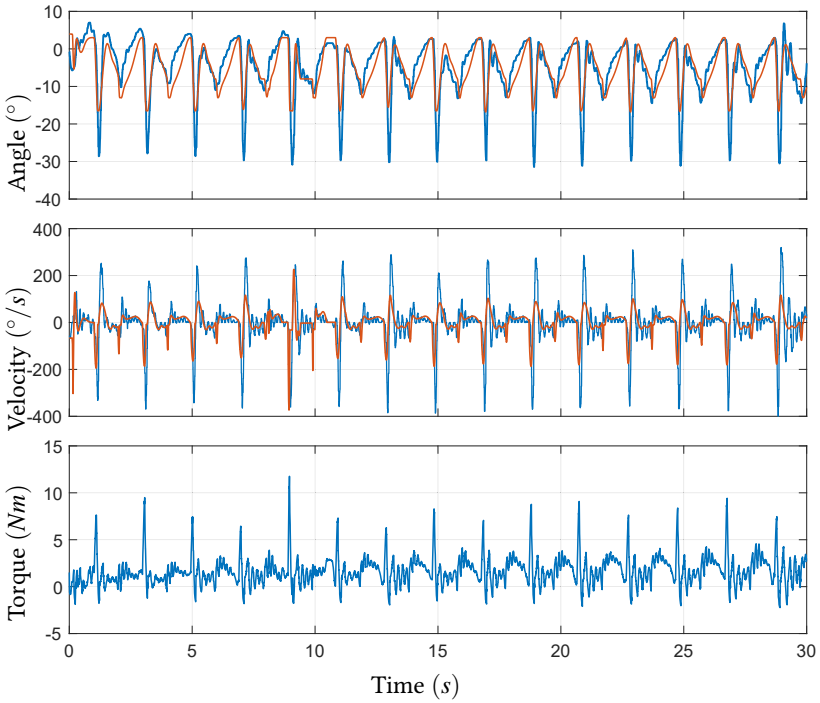

Figure 7.19 – Healthy subject. System's performance tracking the desired ankle angle profile during the complete session. In the first two plots, the red line represents the desired profile and the blue line is the current profile. In the last plot (bottom), the control torque is presented.

flexion). However, since the plantar flexion movement prior to the toe off is required, an increased assistive torque is developed during the late stance and pre-swing sub-phases to contribute to the push-off. Afterwards, a dorsiflexion assistive torque is generated at the beginning of the swing phase to compensate for the plantar-flexed ankle joint at toe off. It can be seen from the standard deviation in Fig. 7.21 that the control law has a high repeatability and it is able to update the ankle joint angle profile during the gait cycle (Fig. 7.20), which makes it suitable for gait assistance applications.

7.6.2. Experimental results - Paretic patient

The tuning gains a_n of the adaptive law (5.8) have been set for the patient, using trial and error: $a_1 = 0.001$, $a_2 = 0.0001$, $a_3 = 0.02$, $a_4 = 0.9$, $a_5 = 0.000001$, $a_6 = 0.8$, and $a_7 = 0.8$. The controller's gains (5.24) have been set to: $\alpha_p = \alpha_v = 1$, $N_1 = 10$, $N_2 = 0.9$ and $\lambda = 6$ with all the adaptive parameters initialized to zero, and the ankle joint angle at the rest position $\theta_r = \frac{\pi}{2}$. In Fig. 7.22, a comparison between the mean ankle joint angle profiles for the assisted and unassisted sessions is shown. The patient shows a predominantly dorsiflexed ankle joint angle profile, probably due to co-contraction. Therefore,

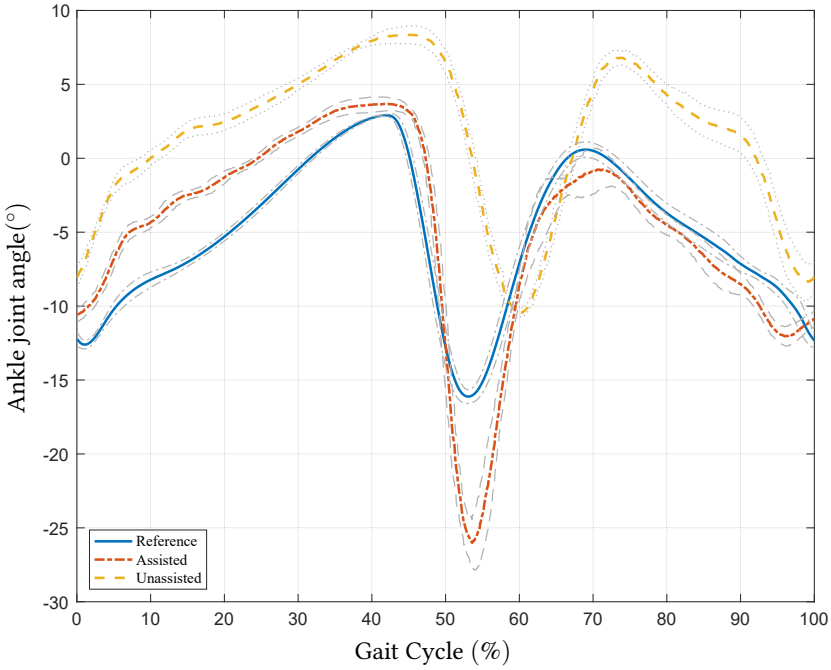

Figure 7.20 – Healthy subject. The mean ankle joint angle profile, normalized with respect to the gait cycle, for the assisted and unassisted sessions and the reference. The standard deviation is presented for each ankle joint angle profile.

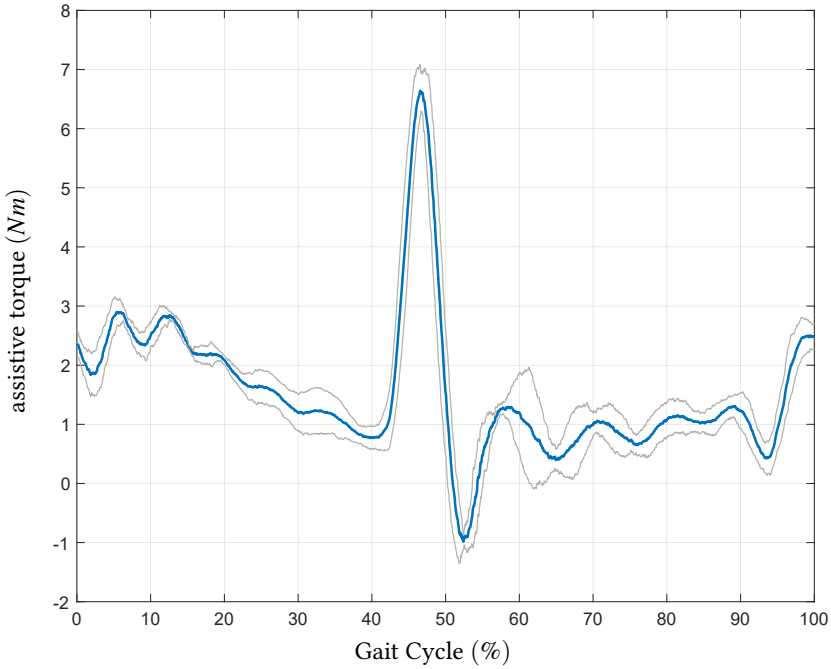

Figure 7.21 – Healthy subject. Mean assistive torque normalized with respect to the gait cycle for the six assisted sessions and the standard deviation. The negative values represent a dorsiflexion assistance while the positive values represent a plantar-flexion assistance.

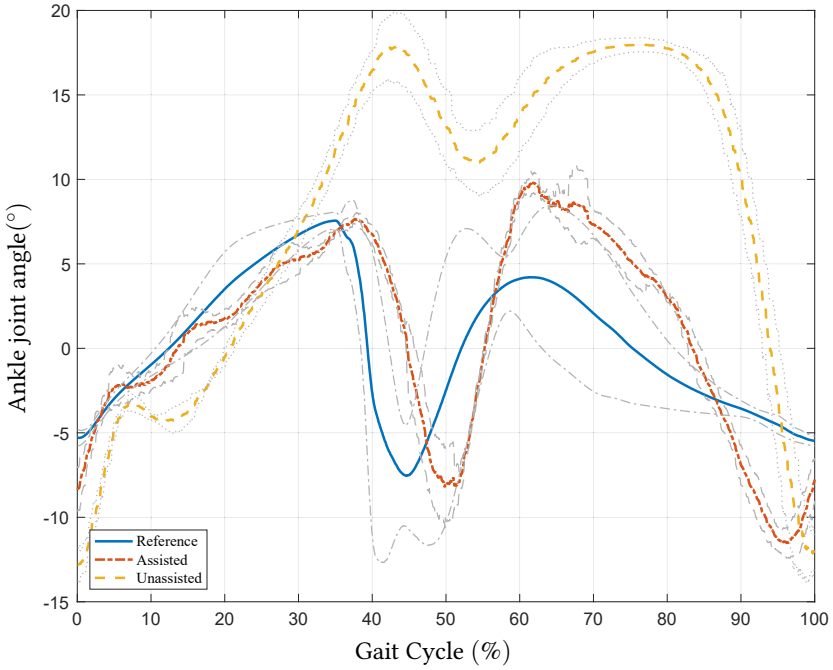

Figure 7.22 – Paretic patient. The mean ankle joint angle profile, normalized with respect to the gait cycle, for the assisted and unassisted sessions and the reference. The standard deviation is presented for each ankle joint angle profiles.

the ankle joint angle reference profile was selected to be more plantar-flexed with an increased range of motion of the ankle joint during the gait. Both the maximum plantar flexion angle prior to the swing phase and the maximum dorsiflexion angle at the end of the swing phase are increased. For the assisted ankle joint angle profile, it can be observed a relatively higher standard deviation value across the gait cycle with respect to the one observed with the healthy subject (Fig. 7.20), mainly due to the variations between each step of the paretic leg of the patient. Nevertheless, the ankle joint profile presents an increased range of motion, especially during the late stance, where an increased dorsiflexion of the ankle joint at heel strike, and a reduction of foot slap (visible during the first 10% of the gait cycle in the unassisted ankle joint profile) can be shown. In Fig. 7.23, the mean torque across all three assisted sessions is shown, as well as its standard deviation. During the loading response phase of the gait cycle, the AAFO system is providing dorsiflexion assistance to prevent foot slap, followed by a transition to plantar-flexion assistance to promote push-off before the swing phase. Finally providing dorsiflexion assistance at the end of the swing phase to promote heel strike and reduce foot drop.

The root-mean-square value of the position error is calculated as well as the standard deviation and classified in four gait groups relative to the sub-phases presented in Fig. 4.1:

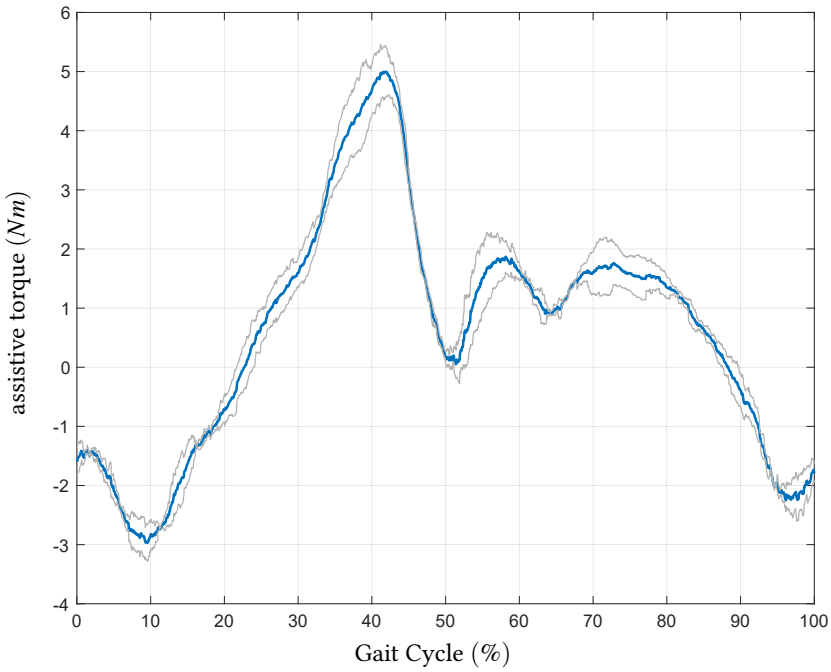

Figure 7.23 – Paretic patient. Mean assistive torque normalized with respect to the gait cycle for the six assisted sessions and the standard deviation. The negative values represent a dorsiflexion assistance while the positive values represent a plantar-flexion assistance.

loading response (LR), roll over (MS plus TS), push-off (PS), and swing (ISw plus MSw plus TSw). Fig. 7.24 shows the position error values for each session, both with and without assistance, classified by the aforementioned gait groups. It can be observed that the normalized tracking error is reduced by an average of 72.6%, 75.4%, 79.8%, and 74.9% for the loading response, roll over, push-off, and swing gait groups, respectively, when the assistive torque is provided.

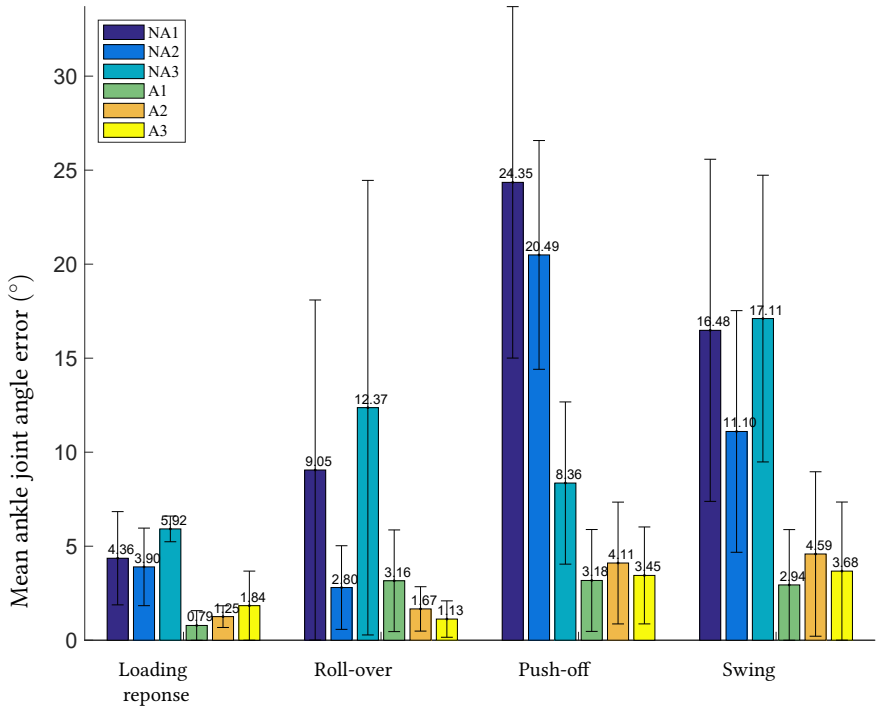

Figure 7.24 – Mean ankle joint angle position errors across the gait cycle for the assisted and unassisted sessions with the patient.

7.7 Adaptive proxy-based sliding mode control

To evaluate the performance of the proposed APSMC, three experiments were carried out. The first experiment is aimed to compare the tracking performance of the proposed APSMC compared to the one of the conventional proxy-based sliding mode control, and the second experiment is designed to show the effectiveness of the proposed method in assisting the paretic patients during walking. Finally, the compliance of the APSMC was evaluated.

Two healthy subjects (H1 and H4 from table 7.1) participated in the first experiments and were asked to simulate abnormal gaits (i.e., fix the knee joint) during walking on a treadmill with the AAFO under three states: 1) without assistance, 2) with PSMC control, and 3) with APSMC. During each state, the subjects were asked to walk for 80s with a low walking speed ($\approx 0.39m/s$). The parameters for PSMC are set as $K_P = 7, K_I = 1, K_D = 0.5$, while the H is set based on the gait phases, i.e., $H = 0.01$ during swing phase and $H = 0.1$ during stance phase. The same PID control gains are also used as the initial values of the adaptive PID control gains in the APSMC, and the adaptive gain is set to $\gamma = 20$.

During the second experiment, two paretic patients (P2 and P3 from Table 7.1) were

asked to perform the overground walking while wearing the AAFO on their affected legs (left legs for both patients) under two conditions: *without assistance, and with APSMC control*. The same parameter values of the APSMC used during the first experiment were also used.

In order to evaluate the compliance of the foot-AAFO system by using the proposed APSMC controller, experiments of tracking a step input of joint angle with an amplitude of 1.8 *rad* was carried out when a healthy subject sat on a chair while wearing the AAFO. The step input was used to simulate a large tracking error.

7.7.0.1. Experimental results - Simulated abnormal gaits

Fig. 7.27 (a) and (b) show the average ankle joint angles without assistance for the two healthy subjects. It can be observed that the simulated ankle joint ankles of the two subjects were both significantly different from the references which are close to the one of the healthy gaits as shown in [119]. Using the conventional PSMC, the subjects' ankle angles are assisted to be close to the reference trajectory, as seen in Fig. 7.27 (c) and (d). Furthermore, the errors between the subjects' ankle angles and the reference trajectory can be reduced using the proposed APSMC control method. Fig. 7.25 shows the root-mean-square-errors (RMSE) between the two subjects' ankle angles and the references during the three states (without assistance: Subject 1, 4.3 ± 5.6, Subject 2, 4.1 ± 5.2; with PSMC: Subject 1, 2.8 ± 4.4, Subject 2, 3.1 ± 4.0; with APSMC: Subject 1, 2.0 ± 2.9, Subject 2, 2.1 ± 2.9, unit: deg). The tracking errors using the APSMC can be reduced by $\approx 28.6\%$ and $\approx 32.3\%$ for two subjects compared to the ones using PSMC, respectively.

It should be noted that the references shown in Fig. 7.27 were separately generated based on the measured group reaction forces during each state for two subjects. Fig. 7.26a presents the experimental results measured with Subject 1 using the proposed APSMC, such as the ankle angles, ankle velocities, tracking error, detected gait phases and changes of the PID gains. All phases mentioned in section 4.3 can be clearly detected and the gait-phase based reference angles show the similar profile among different gait cycles. Regarding the performance of adaptive algorithm of the PID gains, one can observe that the tracking error during the last 30 s (RMSE: 2.01 deg) are much lower than the ones during the first 20s (RMSE: 4.01 deg), as seen in Fig. 7.26a. Correspondingly, significant changes can be observed in the three PID gains in the first 20s. As analyzed in Section 5.6.1, the proportional gain K_P always increase unless the tracking error converge to zero, which is difficult to be guaranteed in practice. Hence, an upper limitation is used as shown in Fig. 7.26b. Here, the upper limitation was selected using a trial-and-error

method to ensure the stability of the closed-loop system as well as a sufficient tracking accuracy.

7.7.0.2. Experimental results - Paretic patient

Fig. 7.28 shows the average ankle angles measured with the paretic patients during two conditions: without assistance and with APSMC. It is shown that patient 1 presents an over-dorsiflexed ankle joint profile while patient 2 shows an insufficient dorsiflexion throughout the gait cycle. The ankle joint trajectory, velocity, and detected gait phases when the patients were assisted using APSMC method are presented in Fig. 7.29 (a) and (c), and the changes of the PID gains' values in Fig. 7.29 (b) and (d). Although some abnormal gait-phase sequences were performed by the patient during some steps (see Fig. 7.29a), the generated ankle references are not affected.

For the first patient, a limited ankle joint ROM during push-off was performed during the unassisted session, which leads to an insufficient plantar flexion angle at the end of the push-off motion, as seen in Fig. 7.28. Note that the peak dorsiflexion angle at the end of the stance phase without assistance is similar to that with assistance, but a higher plantar flexion angle at the end of push-off motion can be observed when the assistance is provided. Hence, the patient's ankle joint push-off ROM can be significantly increased by 96.3% with assistance. Similarly, there exists a significant increase (by 130.1%) of the ankle joint ROM during the swing phase.

The second patient presented an insufficiently dorsiflexed ankle joint profile, as seen in Fig. 7.28. The ankle joint ROM during push-off was increased by 13% when the assistance was provided. Moreover, the dorsiflexion angle was increased by 11.9° during swing phase (from $-2.8°$ to 9.1°), which effectively compensates for the foot drop deficiency (with a 32.5% increase in the ankle joint ROM during the swing phase).

Some important kinematic features, such as the average ROM during push off and swing phase, the average peak planterflexion and dorsiflexion angle during push off, and the average peak dorsiflexion ankle angle during swing phase (see Fig. 7.28), were analyzed and shown in Fig. 7.30. Without power assistance, the patient could perform a limited ankle ROM during the push-off, which also leads to a high peak planterflexion angle at the end of push-off motion. Note that the peak doriflexion angle before the end of push-off motion without assistance is similar to the one with assistance, but a lower peak planterflexion angle at the end of push-off motion can be observed with assistance. Hence, the patient's ankle joint push-off ROM can be significantly increased by 96.3%

with assistance. Similarly, there exists a significant increase (by 130.1%) of the ankle joint swing phase ROM.

To compare the performances of the propose method with those of a PID control, a trial-and-error method for PID parameters tuning was adopted. The parameters were set to: $K_p = 9, K_i = 2, K_d = 1$. To guarantee similar experimental conditions, the same values of these gains in PID control were set as the initial values of the adaptive proportional, integral and derivative gains in APSMC. The adaptive gain γ is set to 20. Three trials were performed with different values of H: $H = 0.5, 0.2, 0.1$. The ankle angle and angular velocity are shown in Fig. 7.31. The results show that with a reasonable high value of H, the system using APSMC achieves a smooth, slow and safe tracking towards desired value. The smaller the H, the faster the tracking speed is. With a very small H, APSMC behaves closer to the PID controller. Thus, with an appropriate value of H, the APSMC insures the compliance of the system, while PID has a relative abrupt response to a high tracking error. Although small PID gains or large K_d can also increase the damping of the close-loop system, however, cannot ensure the accurate tracking performance when the tracking error are relatively small.

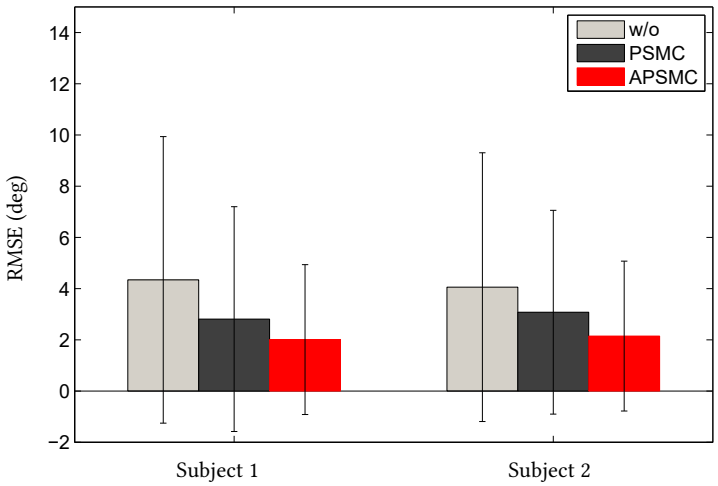

Figure 7.25 – The measured RMSE during three states: without assistance (w/o), with PSMC, and with APSMC

The tracking experiments with the online generated reference ankle joint trajectory have been carried out to prove the efficiency of the proposed method compared to the PSMC. The safety aspects of APSMC have been also evaluated by tracking experimentally a step signal input, which simulates a relative high tracking error. Experimental results show that APSMC provides better tracking performances with repsect to the standard PSMC

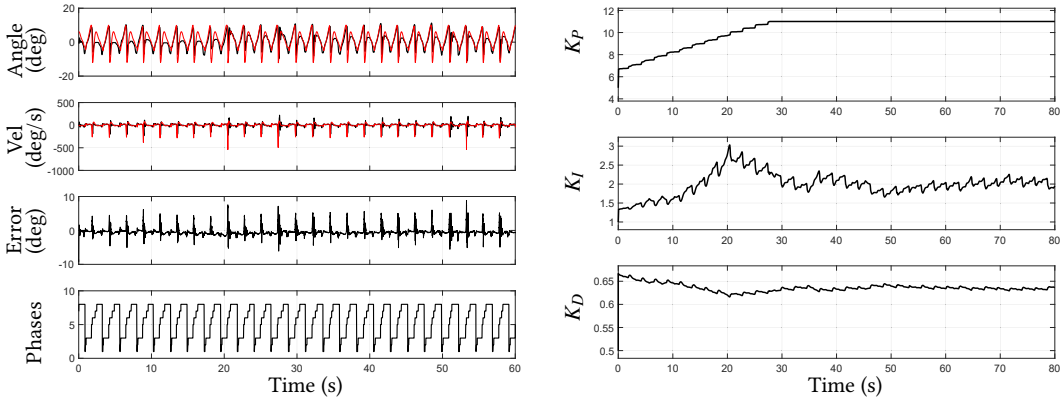

Figure 7.26 – Experimental results with subject H1.

and at the same time is safer than the PID controller.

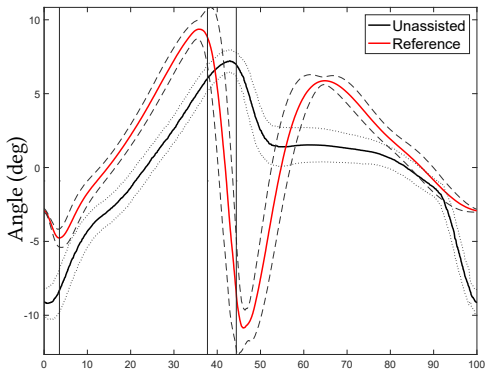

(a) Subject 1: without assistance

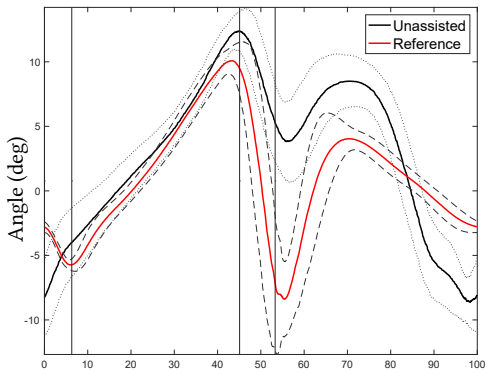

(b) Subject 2: without assistance

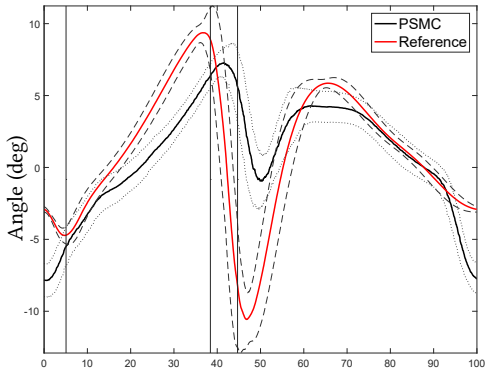

(c) Subject 1: PSMC

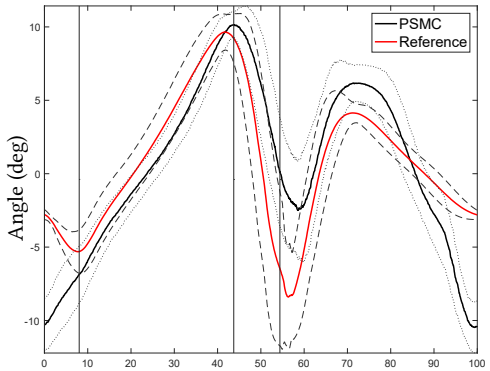

(d) Subject 2: PSMC

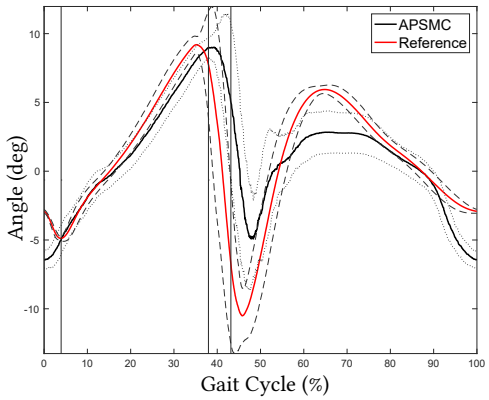

(e) Subject 1: APSMC

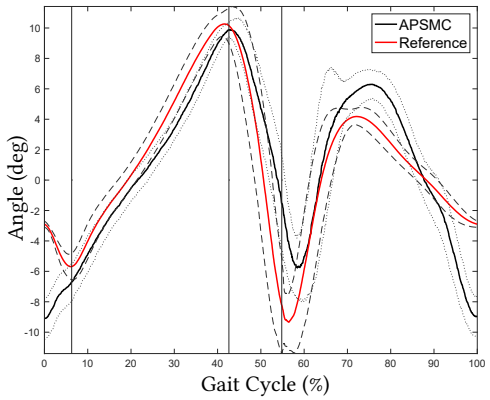

(f) Subject 2: APSMC

Figure 7.27 – Healthy subjects - Average ankle joint trajectories measured under three conditions: without assistance, with PSMC control, and with APSMC control.

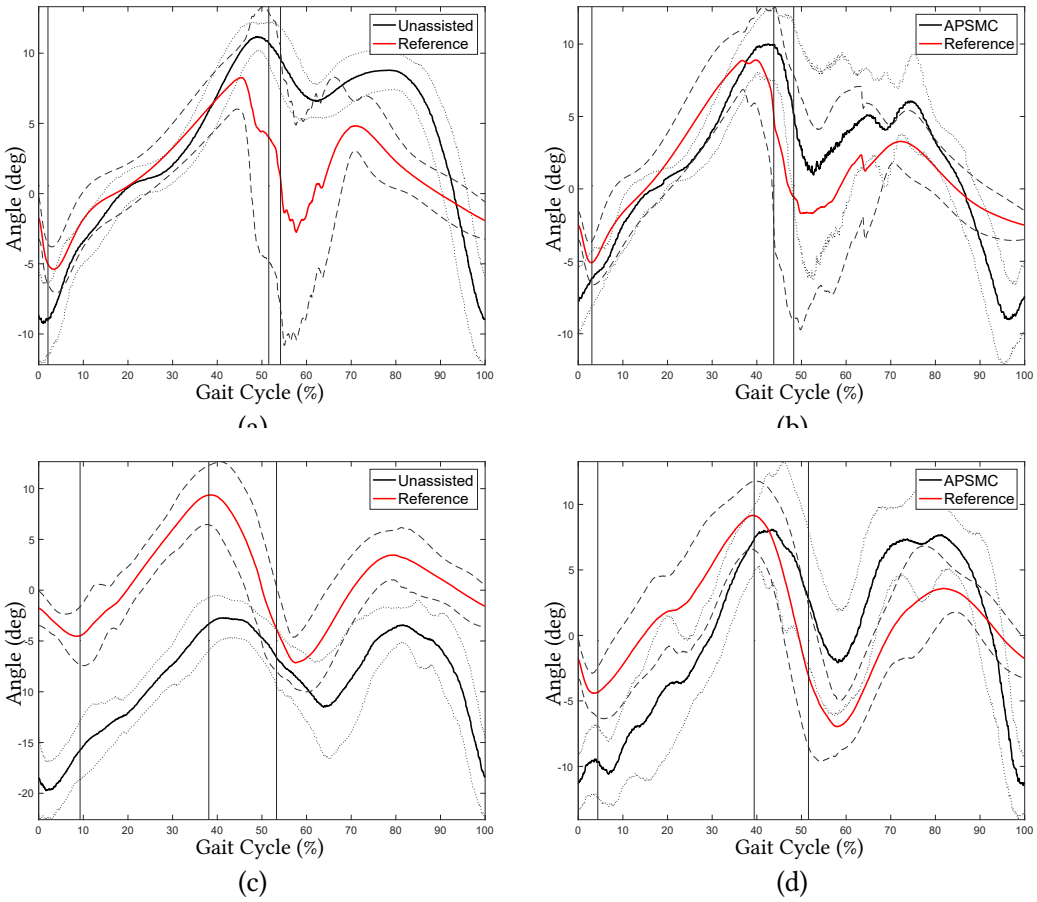

Figure 7.28 – The patients' average ankle joint trajectories measured under two conditions: without assistance and with APSMC control. The red lines represent the reference trajectory and black lines are the ankle joint angles produced by the patient. The grey dotted and slashed lines show the standard deviation for the unassisted and assisted sessions, respectively. All figures are normalized with respect to the gait cycle.

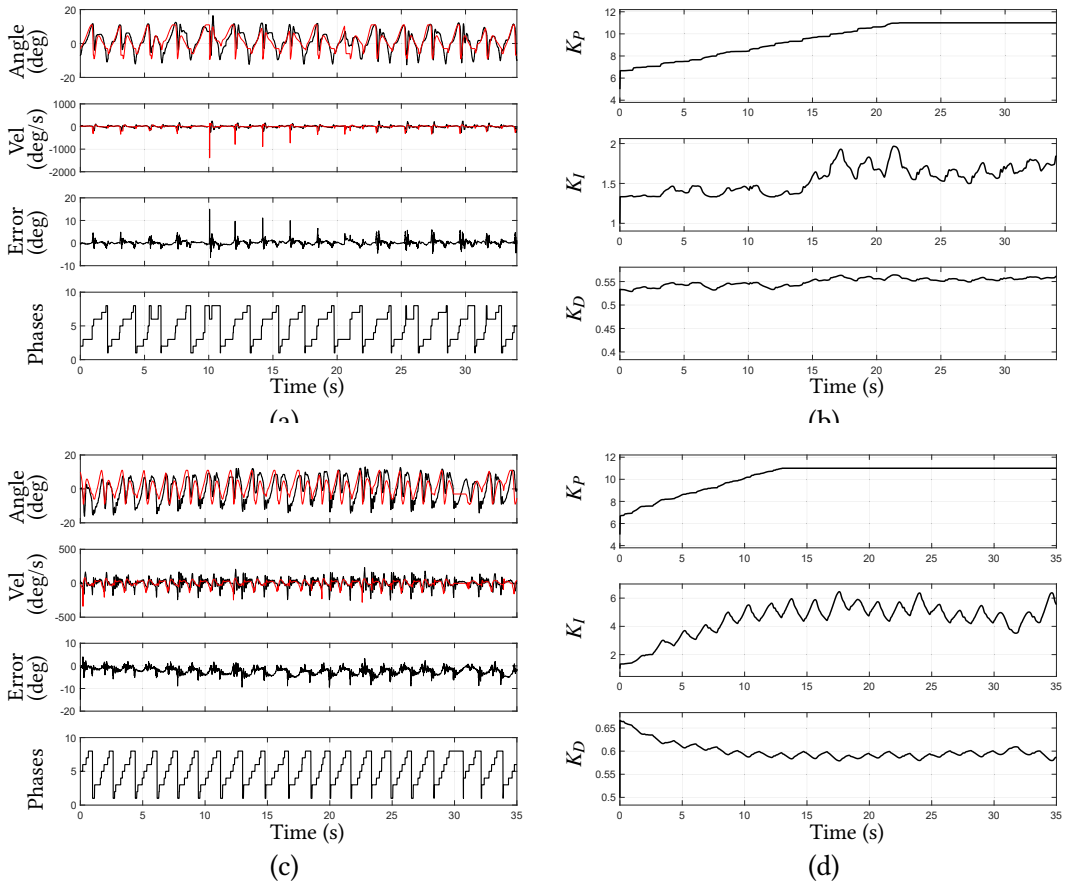

Figure 7.29 – Experimental results with the paretic patients. In (a) and (b), the ankle angles (red line: reference; black line: measured), ankle velocities (red line: reference; black line: measured), tracking error, and detected gait phases (1:LR; 2:EMS; 3:LMS; 4:TS; 5:PS; 6:ISw; 7:MSw; 8:LSw)

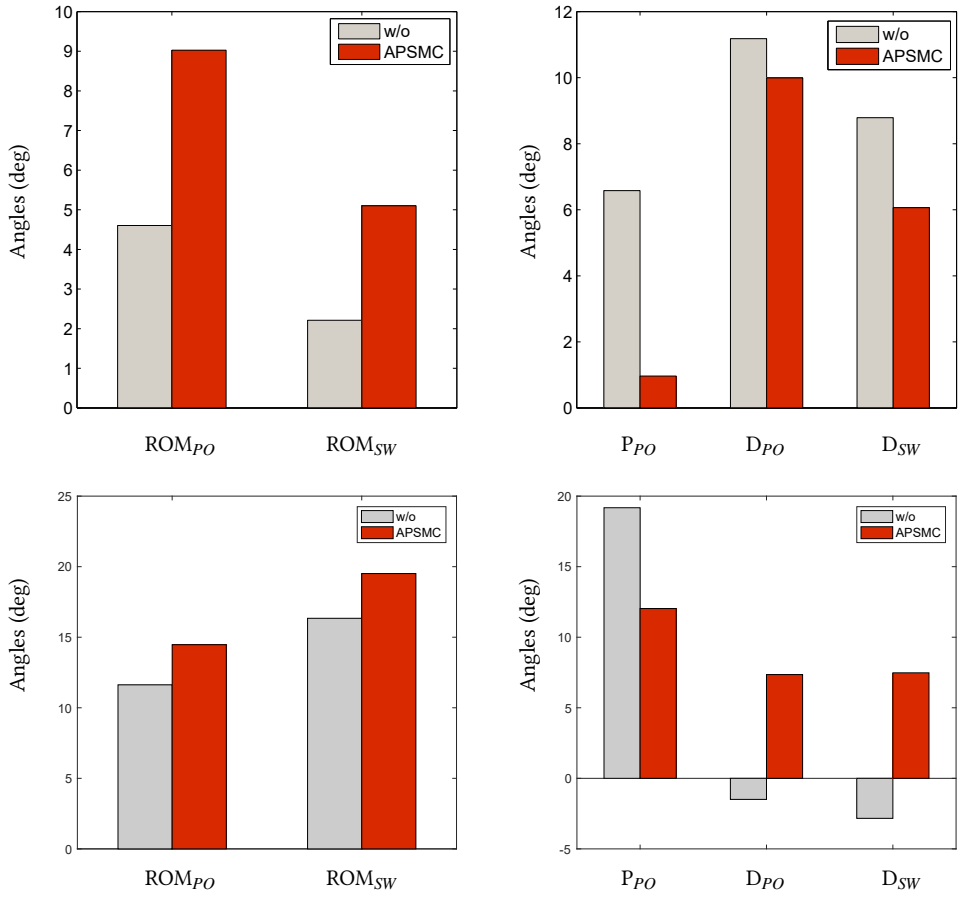

Figure 7.30 – The changes of the main walking kinematic features of the paretic patients from the condition "without assistance (w/o)" to the condition "with assistance (APSMC)". ($_{PO}$: Push off moment; $_{SW}$: Swing phase, ROM: Range of Motion, P: Planter flexion, D: Dorsiflexion)

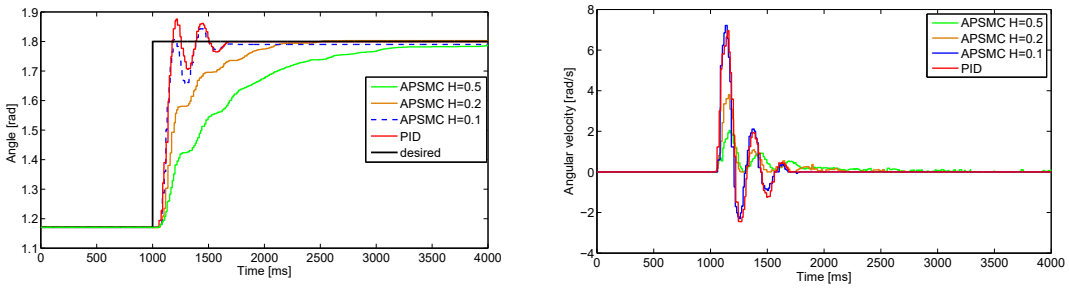

(a) (b)

Figure 7.31 – Safety tests using PID and APSMC. (a)Step wave tracking which simulates the big error occurs. (b)Angular velocity during the tracking process.

7.8 Active disturbance rejection control

In this section, the effectiveness of the AAFO's active disturbance rejection control (ADRC) to assist the wearer during walking is assessed through real-time experiments. The objective is to prove the feasibility and safety of the system, i.e., the ankle joint needs to track the reference even in the presence of the endogenous and exogenous disturbances (which are considered bounded and unpredictable), with a high level of repeatability and stability. To evaluate the feasibility of the system, the ankle position and velocity errors are measured and compared between unassisted and assisted sessions. Furthermore, the profiles of both errors are normalized with respect to the gait cycle and analyzed in order to evaluate the repeatability of the assistance even in the presence of the wearer's voluntary action.

Subject H1 (see table 7.1) walking on a treadmill has participated in the experiments. Since it is understood that the healthy subjects produce healthy ankle joint profiles, the reference profile is deliberately different from the wearer's normal ankle joint trajectory. When the paretic patient is wearing the AAFO, the reference trajectory would be adjusted to better represent a healthy ankle joint profile. The algorithm to generate the ankle joint reference trajectory is presented in chapter 4, section 4.4.

The scenario of the experiment with the healthy subject is as follows: first, the subject walks on a treadmill at a speed of 2 Km/h at a self-selected step duration. The ankle joint reference profile is deliberately adjusted to be different from the proper ankle joint angle profile to test the ability of the system to update the current ankle joint profile during the gait cycle. Then, three unassisted sessions and ten assisted sessions, each lasting 60 s, are performed to evaluate the repeatability and the consistency of the results. A resting time of 30 s between the sessions is provided.

To tune the controller gains, several calibration sessions were done prior to the experiments on the treadmill. The subject was seated on a chair with the leg hanging over the ground (no GRF) and was asked to not produce any muscular activity ($\tau_h = 0$). The system then tracks a healthy ankle joint walking profile (see section 4.4 for further details). After each session, the tracking performance is evaluated and the subject is asked about the comfort of the provided assistance. With this tests, the solution of the Ricatti equation (6.21) was adjusted until the tracking error was considered sufficiently small while remaining comfortable to the subject. The values of the observer gains were selected from a simulation in Matlab, Simulink, and further refined in the calibration sessions.

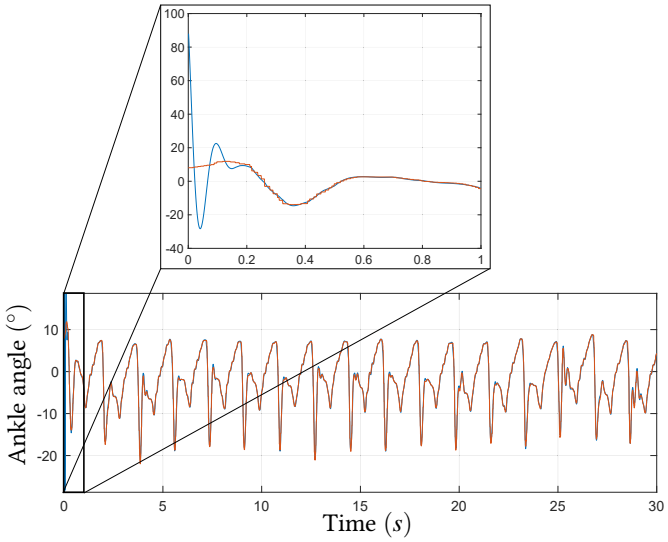

Figure 7.32 – The performance of the estimation of the angular position of the ankle joint for the first 30s (R_1 vs θ). The first second of the session is rescaled in order to observe the transient of the estimation convergence.

The exact value of J cannot be measured but it can be estimated using biomechanical regression equations from Winter et al. [105] to estimate the mass and the center of mass of the foot. Afterwards, the moment of inertia J is calculated.

$$J = (m_{foot} + m_{shoe}) d_G^2 \tag{7.1}$$

where m_{foot} and m_{shoe} are the mass of the foot and the shoe, respectively, and d_G is the distance between the ankle joint to the center of mass of the foot.

First of all, the performance of the ESO (6.7) is evaluated with the design parameters: $l_0 = 17160$, $l_1 = 6026$, $l_2 = 791$, $l_3 = 46$, and the nominal value $J = 0.03$. The controller 6.22 uses the CLF 6.17 with P set to:

$$P = \begin{pmatrix} 58.8087 & 1.7321 \\ 1.7321 & 0.1698 \end{pmatrix}$$

which corresponds to $\varepsilon = 106.3$, $q_1 = 637$ and $q_2 = 2$. Besides, $\kappa = 20$. Note that these parameters allow tunning the controller and they were selected, first in simulation, and finely adjusted in practice, in order to provide better control impact in the position and velocity errors. All the observer's states are initialized to zero.

The measured angular position and velocity, as well as the redundant estimate of the

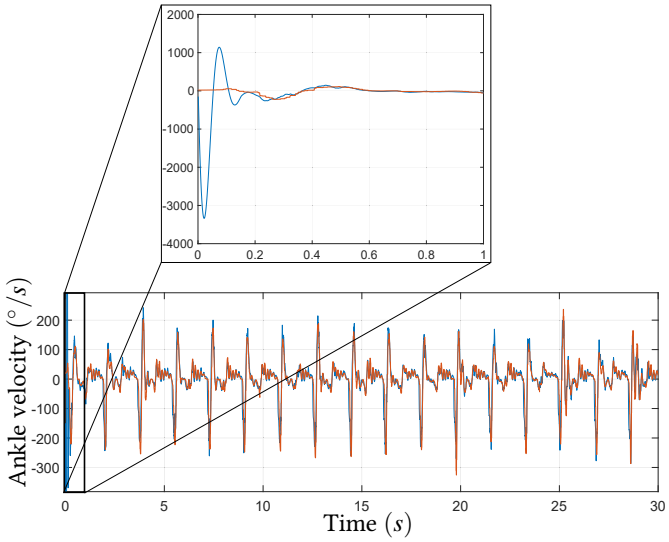

Figure 7.33 – The performance of the estimation of the angular velocity of the ankle joint for the first 30s (R_2 vs $\dot{\theta}$). The first second of the session is rescaled in order to observe the transient of the estimation convergence.

angular position (Fig. 7.32) and velocity (Fig. 7.33) are presented. Note that there is a small transient of approximately 0.2 s (showed in a zoom for the first second of the session); when the estimations of the angular position and velocity, F_1 and F_2, overshoot the current value of the ankle joint angle and velocity, θ and $\dot{\theta}$. After this transient phase, the estimated angular position and angular velocity converge to the measured ones. The average error of the estimation of the angular position of the ankle joint across all ten assisted sessions is 1.41° with a standard deviation of $\pm$ 0.07°, and for the estimation of the angular velocity is 86.77°/s with a standard deviation of $\pm$ 3.66°/s. The average error in the estimation of the angular position and velocity for each session is presented in Table 7.4.

The proposed controller was able to track the generated adaptive desired ankle trajectory profile with an average root-mean-square (RMS) angular position error of 5.42° and a standard deviation of 2.52 ° across all ten assisted sessions. This represents a reduction in the angular position error of 53.37% compared to the average RMS angular position error of the three unassisted sessions. The RMS angular position error is classified in four gait groups relative to the sub-phases: loading response (LR), roll over (MS plus TS), push-off (PS), and swing (ISw plus MSw plus TSw). Fig. 7.34 shows the position error values for each session, both with and without assistance, classified by the aforementioned gait groups. It can be observed that the normalized tracking error is reduced in average

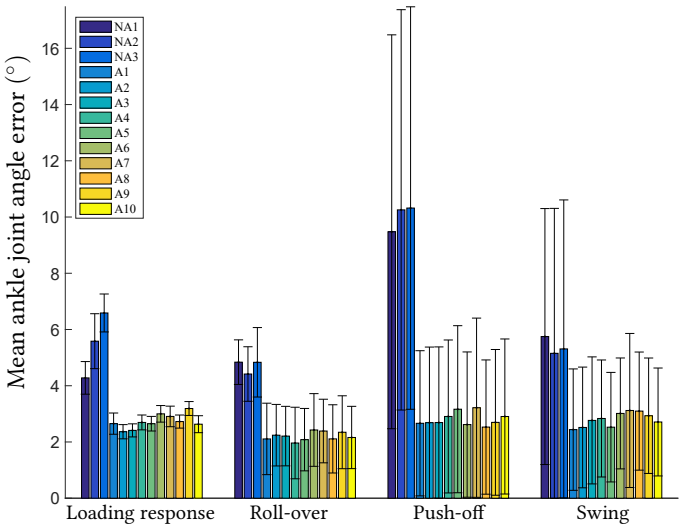

Figure 7.34 – Mean ankle joint angle position errors across the gait cycle for the assisted and unassisted sessions with one healthy subject.

by 50.34%, 53.08%, 71.96%, and 48.26% for the loading response, roll over, push-off, and swing gait groups, respectively, when the assistive torque is provided. The values of the RMS angular position error for each gait group of every session is presented in Table 7.5.

The angular position and velocity ankle joint profiles have been normalized with respect to the gait cycle to compare the reference trajectory with the assisted and unassisted mean ankle joint profiles. The results are presented in Fig. 7.35 and Fig. 7.36, where it can be seen that the controller is able to track the ankle joint reference profiles, especially during push-off (this can also be seen in Fig. 7.34)

In Fig. 7.37, the assistive torque presents a plantar flexion assistance during the stance phase, with a peak value during the TS, which represents an increasing assistance for push-off at the end of the stance phase. Immediately after this moment, the torque changes direction to provide dorsiflexion assistance to begin the swing phase. It can be seen from the standard deviation that the control law has a high repeatability.

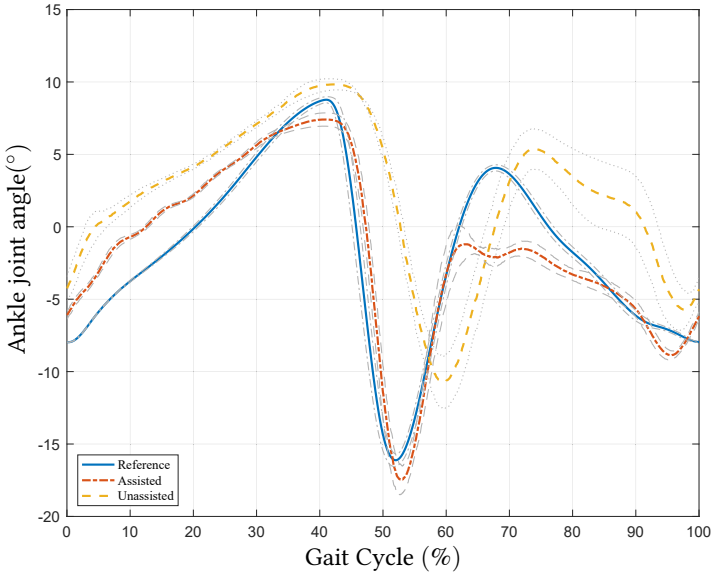

Figure 7.35 – The mean ankle joint angle profile, normalized with respect to the gait cycle, for the assisted and unassisted sessions and the reference. The standard deviation is presented for each ankle joint angle profile.

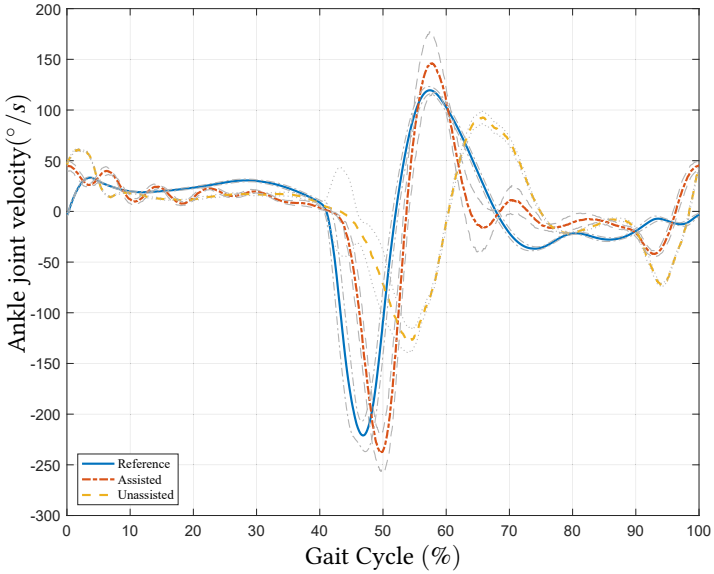

Figure 7.36 – The mean ankle joint velocity profile, normalized with respect to the gait cycle, for the assisted and unassisted sessions and the reference. The standard deviation is presented for each ankle joint velocity profile.

Table 7.4 – *Estimation error of the angular position and velocity in RMS for each session (error±std)*

Assisted session	$F - F_1(^\circ)$	$\dot{F} - F_2(^\circ/s)$
1	1.3382±1.3382	82.4550±82.4455
2	1.4302±1.4302	87.9357±87.9236
3	1.4276±1.4276	87.5018±87.4862
4	1.4016±1.4016	86.2706±86.2625
5	1.4104±1.4104	86.7709±86.7609
6	1.2993±1.2993	80.3256±80.3139
7	1.5318±1.5318	92.4811±92.4718
8	1.5002±1.5002	91.7413±91.7260
9	1.3910±1.3910	86.4614±86.4458
10	1.3940±1.3940	85.7532±85.7419

Table 7.5 – *RMS error of the angular position for each gait group for each session (error$^\circ$±std$^\circ/s$). A = assistance session, NA = no assistance session.*

Session	Loading Response	Roll-over	Push off	Swing
NA1	4.2793±0.5803	4.8386±0.7933	9.4753±7.0040	5.7494±4.5516
NA2	5.5842±0.9772	4.4168±0.9698	10.2550±7.1190	5.1530±5.1546
NA3	6.5880±0.6745	4.8336±1.2353	10.3196±7.1570	5.3097±5.2984
A1	2.6521±0.3778	2.1085±1.2706	2.6645±2.5814	2.4389±2.1589
A2	2.3647±0.2528	2.2412±1.0942	2.6866±2.6885	2.5164±2.1465
A3	2.4122±0.2325	2.2089±1.0579	2.6906±2.6902	2.7672±2.2588
A4	2.6950±0.2642	1.9628±1.2724	2.9073±2.7199	2.8354±2.0806
A5	2.6496±0.2596	2.0826±1.1097	3.1649±2.9709	2.5263±1.9478
A6	3.0005±0.2949	2.4264±1.2929	2.6185±2.5833	3.0150±1.9721
A7	2.9084±0.3658	2.3892±1.1309	3.2182±3.1869	3.1200±2.7394
A8	2.7258±0.2328	2.1099±1.2132	2.5300±2.3874	3.0981±2.1004
A9	3.1901±0.2471	2.3458±1.2967	2.6972±2.5914	2.9332±2.0527
A10	2.6322±0.3016	2.1597±1.1076	2.9059±2.7573	2.7109±1.9190

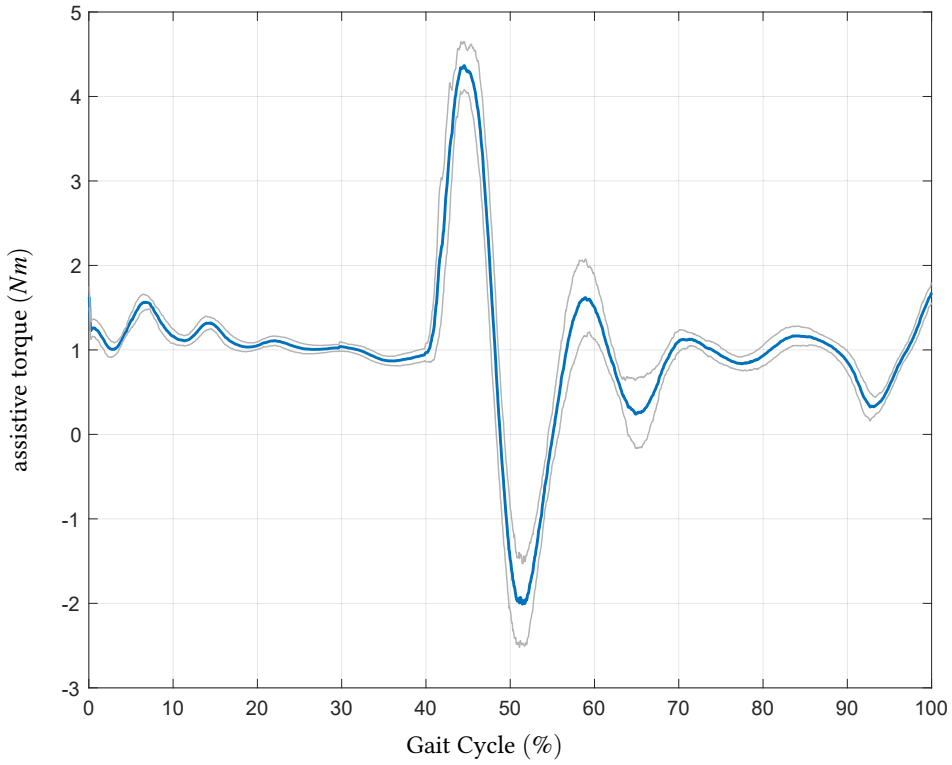

Figure 7.37 – Mean assistive torque normalized with respect to the gait cycle for ten assisted sessions and the standard deviation. The negative values represent a dorsiflexion assistance while the positive values represent a plantar-flexion assistance.

7.9 Conclusion and discussion

The purpose of the experiments is to evaluate the feasibility of the different control approaches proposed in chapters 5 and 6 to estimate the assistance provided by the AAFO to the ankle joint. For this reason, the desired ankle joint angle profile was selected based on one of two objectives: 1) with healthy subjects, an assistive torque is promoted by forcing the natural ankle joint profile to follow a different trajectory, 2) with paretic patients (or healthy subjects that emulate a gait pathology), the reference is the same as a healthy ankle joint profile to promote an assistive torque that can reduce the effects of gait deficiencies.

In the literature, one can note several ankle assessment techniques [45]. For example, the ROM of the ankle joint is one important criterion as it reflects the efficiency of the gait, and the ability to generate movement. Therefore, the ROM is used for this study for evaluating the effectiveness of the AAFO system to assist the ankle joint.

First, the basic MRAC was assessed first during the swing phase with a healthy subject and then the system was providing assistive torque during the whole gait cycle. The results show an improvement of the convergence of the adaptive parameters in the control law compared to the first set of experiments. Furthermore, the normalized assistive torque profile relative to the gait cycle is consistent across all steps for each healthy subject. Therefore, the MRAC implemented in the AAFO was deemed safe for tests on a clinical environment. The results with one paretic patient show that the ankle joint ROM through the gait cycle was improved from $7.86 \pm 1.98^{\circ}$ to $18.09 \pm 3.83^{\circ}$ when the assistive torque was provided. Also, the dorsiflexion was increased during the swing phase from $-5.59 \pm 1.46^{\circ}$ to $0.61 \pm 2.03^{\circ}$, limiting the effects of the foot drop. Finally, during the loading response sub-phase, the plantar flexion movement of the ankle joint was reduced, which means that the foot slap was compensated.

The aforementioned results could be attributed to the capacity of the control strategy to individually estimate and compensate for the gait deficiencies with the adaptive law. For this reason, it is important to ensure that the adaptive parameters remain bounded in order to ensure the stability of the system. Therefore, the projection based MRAC approach was tested with one healthy subject. The results show that the adaptive parameters converge to a final value faster than the basic MRAC approach. However, the gait pace had to be synchronized with an audible cue in order to provide an appropriate assistance. Further experiments with paretic patients are needed in order to compare

the MRAC and the projection based approaches in assisting a deficient gait of paretic subjects.

With the use of the PD saturated action of the MRAC, during the late stance of the gait cycle, the AAFO's torque show an improvement in the assistance of the push-off power of the ankle joint. Furthermore, the oscillations produced by the assistive torque during the swing phase is one of the main limitations of this control approach. In the experiment using the PD saturation MRAC with a paretic subject, the patient showed an over-dorsiflexed ankle joint profile through the whole gait cycle, which limits the plantar flexion movement at the late stance phase. However, the PD saturated MRAC is able to compensate for this effect by assisting the push-off power during the late stance and pre-swing sub-phases, and by assisting in dorsiflexion at the beginning of the swing phase, effectively increasing the ankle joint ROM.

Regarding the APSMC approach, fewer sensors are required for the system to provide assistive torque compared to the MRAC based approaches. It was shown that this controller is able to compensate for the difference in disturbance magnitudes between the stance and swing phases. Moreover, the controller is able to adapt the derivative and integral parameters to improve performance and to possibly compensate for the wearer's fatigue.

All controllers were able to assist the gait during the loading response sub-phase; the adaptive controllers show an oscilation of the adaptive parameters at the intial contact of the gait but remain bounded, and the ADRC is able to compensate for the external disturbance and remain stable.

The linear ESO was able to estimate the ankle position and velocity after the first 200 *ms* of the session. The ADRC with the Lyapunov function selected was able to track the adaptive ankle reference with high repeatability even in the presence of unpredictable endogenous and exogenous disturbances. As with the APSMC approach, the advantage of the ADRC is the reduced number of sensors compared to the MRAC implementations. Indeed, the system is able to track the trajectory using the ankle joint angle as the only input, while the FSR embedded in the insoles were used to generate the desired trajectory.

Comparing the results from this study with the literature is dificult as there is no consensed evaluation protocol for AAFOs in rehabilitation, and quantitative data are unavailable or represents a different criteria from the one used in this study. Nevertheless, some works in the literature are referenced in this discussion.

For example, it is reported in [29] an elimination of foot slap occurrences with two drop

foot patients at slow and self-selected walking speed. During the swing phase, a variable impedance controller was able to increase the ROM amount, as compared to the constant impedance controller, by 200% and 37% for slow and self-selected gait speeds, respectively. However, no quantitative information is given when comparing to a unassisted scenario. These results can be compared to those obtained in this thesis. For instance, the adaptive controller proposed in this study was able to increase the ROM during the swing phase by 98%, as compared to the unassisted scenario fro the basic MRAC approach. The difference between results could be attributed to the difference in strategy during the swing phase; i.e., in [29], the controller was tuned to promote the dorsiflexion velocity of the ankle joint in the early swing phase matching the unaffected side, without a prior knowledge of the maximum dorsiflexion angle during the swing phase.

Roy et al. [79], used an AAFO with a gait-deficit adjusted controller to assist the gait of a stroke survivor, specifically during the loading response and the swing phase. The controller was tracking an ankle desired trajectory only during the swing phase, but no quantitative data were reported of the tracking performance. Nevertheless, the gains in ankle dorsiflexion retained by the patient after six weeks suggest that appropriate assistance during the gait cycle can promote rehabilitation. This remark is important for this thesis, as it suggest that a trajectory tracking control approach could be efficient for rehabilitation process.

In [85], an AAFO with a proportional controller following a dynamic trajectory [75] was tested with three able bodied subjects and two stroke survivors. However, no quantitative data are provided to assess the controller performance on tracking the desired trajectory.

8 — Summary

8.1 Conclusions

In this thesis, three joint-reference tracking controllers that are robust to variations in the dynamics of the system and do not require prior identification of the model parameters were developed and tested in experiments with healthy and paretic patients in a clinical environment. Also, an algorithm that generates an adaptive desired trajectory based on the step duration of the wearer was developed. The major contributions of this work are listed in the following:

- An algorithm that generates an ankle reference profile in real time was developed. The following is a summary of the conclusion for this algorithm:

    1. By measuring the ground reaction forces with insoles embedded with force sensitive resistors, a method to detect the gait sub-phases using a fuzzy based approach was proposed. This method can detect eight gait sub-phases in the correct order with healthy subjects. When tested with paretic patients, the algorithm detected irregularities in the gait cycle, possibly due to pathologies.
    2. Using the gait sub-phase detection algorithm, the step and sub-phase durations are calculated in real time. This is important in order to determine the ankle joint velocity and acceleration profiles to be used as a reference for the control approaches.
    3. The adaptive ankle reference generator (AARG) algorithm proposed is able to generate an angle, velocity and acceleration ankle joint profiles in real time by using the walking parameters calculated with the gait sub-phase detection algorithm. Further, the ankle angle profile can be adjusted to promote

dorsiflexion or plantar flexion at specific events of the gait cycle in order to compensate for gait pathologies.

4. The proposed method was evaluated with healthy and paretic subjects and the obtained results showed that an ankle reference profile generated in real time based on the current state of the wearer's gait could potentially assist the ankle joint of paretic subjects.

- An adaptive controller based on the system dynamic model was developed. The conclusions can be summarized as follows:

1. A model reference adaptive controller (MRAC) was proposed to assist the ankle joint on a healthy subject to track a desired trajectory. The proposed method uses the tracking error to estimate the system model parameters, except for the human muscular torque. Then, these estimations are use to adapt the assistive torque to the ankle joint in order to improve the tracking performance.
2. The MRAC approach was improved by bounding the adaptive law of the controller using a projection function. This approach improves the stability of the system, compared to the MRAC approach, by ensuring convergence of the adaptive parameters.
3. The MRAC approach was improved by bounding the PD gain of the controller using a saturation operator. This method improved the safety of the system, compared to the previous MRAC approaches.
4. The control approaches were tested with paretic patients. The results show satisfactory tracking and a relatively fast convergence of the adaptive parameters without any prior system identification, making the proposed approach suitable for rehabilitation purposes. The system proved to be stable for its use in a clinical environment. The assistive torque provided by the AAFO increased the ROM of the ankle during push-off and swing phase.
5. The stability of the controllers was analyzed with Lyapunov functions for two cases: passive and active wearer. The former case is asymptotically stable while the latter is input-to-state stable with respect to the muscular torque.

- An adaptive proxy-based sliding mode controller (APSMC) was developed. The conclusions are summarized as follows:

1. The proposed APSMC can select the damping magnitude of the system at different gait phases. This increases the stability of the system, especially during the transitions from stance to swing phase, in viceversa.
2. APSMC is achieved by introducing a suitable adaptation of the PID parameter values of the conventional PSMC. Thus APSMC is able to improve the tracking performance of the PSMC and guarantee the compliance, i.e., safety.
3. The controller was tested in a clinical environment with two paretic patients to assist their gaits. The results show that the ankle joint profile for both patients was modified by the assistive torque of the AAFO and the effects of the pathologies presented prior to the experiments were reduced.

- An active disturbance rejection control (ADRC) was developed. This approach uses an extended state observer (ESO) to estimate the state variables of the system and compensates for the endogenous and exogenous disturbances. Further, a control Lyapunov function (CLF) was incorporated to this approach. The main conclusions are summarized as follows:

  1. The ESO was able to estimate the state variables in the first second of the experimental sessions. Which is important for the overall stability of the system and the correct compensation for the disturbances.
  2. The system was tested with one healthy subject walking on a treadmill. The tracking error of the ankle joint angle was reduced when compared between the assisted and unassisted scenarios.
  3. The stability of the system was analyzed using the flatness property of the system and the CLF. It was found to be input-to-state stable with respect to the exogenous and endogenous disturbances.

8.2 Perspectives

Based on the promising results in this thesis, the study can be extended in different perspectives. First, the proposed control strategies can be applied for other joints to assist the lower limbs during gait, e.g., knee and hip. This would allow to use the system with patients with more acute symptoms of gait deficienies, and not only to those patients with deficiencies at the ankle level. This will require to define the profile trajectories for

each joint and implement an adaptive joint reference generator that synchronizes the joint to the walking speed of the wearer. Furthermore, an upper body application can also be considered for a grasping and reaching tasks.

Since providing too much assistance may have negative consequences for learning, if the wearer is able to initiate movement, a common paradigm is to provide assistance as needed. Example strategies of this paradigm is to include some error variability around the desired movement using a deadband (an area around the trajectory in which no assistance is provided) triggering assistance only when the participant joint position is outside of this error band, or including a forgetting factor in the robotic assistance [46]. Therefore, another perpective of this thesis is to include a deadband to the reference profile and study the level of engagement of the wearer when being assisted by the AAFO.

To more effectively engage user interaction with the exoskeleton, another potential approach may be to integrate real-time biofeedback. In the controllers presented in this thesis, no formal instructions are given to the users to interact with the AAFO, e.g., produce more dorsiflexion at specific moements of the gait, more plantar flexion at push-off, an other instructions. This may undermine the potential benefits of the device as the muscular activity of the ankle muscles might be reduced when receiving external assistance from the exoskeleton. Thus, complementary systems that can help in increasing the engagement of the wearer by stimultating the ankle muscles or by providing a bio-feedback could prove to be effective to accentuate the viability of exoskeleton interventions in rehabilitation.

As such, a hybrid approach including functional electrical stimulation (FES) and the AAFO will be studied. The effectiveness of FES has been proved to produce positive orthotic effects on many gait parameters, such as increasing walking speed and improving symmetry index [175]. FES offers many advantages compared to AAFOs, such as active muscle contraction, muscle strength improvement [176, 177], muscle tone reduction and efficient energy use of proximal lower limb [178]. However, there are some challenges facing the development of such systems for long-term daily use such as the rapid muscular fatigue, the great physical effort required, the need to extensive training programs. While previous works have highlighted mechanisms of dropped foot impairments and positive effects of AAFO and FES devices independently, few studies have addressed the effect of a hybrid approach applied to patients suffering from foot drop and a lack of foot propulsion during the push-off phase. A better understanding of how AAFO/FES devices could affect the gait performance of individuals with different underlying gait

pathologies will advance the success of such hybrid design.

Also, since the assistive torque can be considered as a kinematic haptic feedback, a vibrotactile feedback will be studied in conjunction with the AAFO to be used as a biofeedback signal to the wearer. The purpose of this additional feedback is to give formal instructions to the wearer about the required ankle movement to follow the desired trajectory. This hybrid haptic approach could be used to promote a higher level of engagement from the wearer, therefore, a higher activation of the muscles spanning at the ankle joint.

Finally, it would be interesting to compare the performance of the proposed controllers with several patients in a clinical study. Furthermore, the benefits of using the AAFO system with a reference tracking control approach should be studied in a rehabilitation environment.

List of Figures

List of Tables

Glossary

AAFO	Actuated Ankle Foot Orthosis
AARG	Adaptive Ankle Reference Generator
MRAC	Model Reference Adaptive Controller
PSMC	Proxy-based Sliding Mode Controller
APSMC	Adaptive Proxy-based Sliding Mode Controller
ADRC	Active Disturbance Rejection Control
CLF	Control Lyapunov Function
ESO	Extended State Observer
FSR	Force Sensitive Resistor
FES	Functional Electrical Stimulation
CNS	Central Nervous System
ROM	Range Of Motion
PMA	Pneumatic Muscle Actuators
EMG	Electromyography
DOF	Degrees Of Freedom
SEA	Series Elastic Actuator
DCO	Dynamically Controlled ankle-foot-Orthosis
TA	Tibialis Anterior
GAS	Gastrocnemius
SOL	Soleus
IMU	Inertia Measurement Units
GRF	Ground Reaction Force

IC	Initial Contact
TL	Toe Landing
HO	Heel Off
TO	Toe Off
LR	Loading Response
EMS	Early Mid-Stance
LMS	Late Mid-Stance
TS	Terminal Stance
PS	Pre-Swing
ISw	Initial Swing
MSw	Mid-Swing
TSw	Terminal Swing
MD	Maximum Dorsiflexion
FMV	Fuzzy Membership Value
MSD	Mean Step Duration
PD	Proportional Derivative
PID	Proportional Integral Derivative
AC	Adaptive Control
SMC	Sliding Mode Control
ISS	Input-to-State Stability
ISO	Input to Output Stability
AG	Asymptotic Gain
RMSE	Root-Mean-Square-Errors
RMS	Root-Mean-Square

A — List of publications

Journals:

[1] **V. Arnez-Paniagua**, H. Rifaï, Y. Amirat, S. Mohammed. Adaptive Control of an Actuated Ankle Foot Orthosis for Paretic Patients. *Control Engineering Practice*, p. 16. Elsevier, 2018. *(In revision)*

[2] J.F. Guerrero-Castellanos, H. Rifai, **V. Arnez-Paniagua**, J. Linares-Flores, L. Saynes-Torres, S. Mohammed. Robust Active Disturbance Rejection Control via Control Lyapunov Functions: application to Actuated-Ankle-Foot-Orthosis. *Control Engineering Practice*, p. 32. Elsevier, 2018.

[3] Weiguang Huo, **Victor Arnez-Paniagua**, Guangzheng Ding, Yacine Amirat and Samer Mohammed. Adaptive Proxy-Based Controller of an Active Ankle Foot Orthosis to Assist Lower Limb Movements of Paretic Patients. *Robotica*, p. 27. Cambridge University Press, 2018. *(Minor revision)*

[4] Weiguang Huo, Mouna Ghedira, Samer Mohammed, **Victor Arnez-Paniagua**, Emilie Hutin, Jean-Michel Gracies. Effect of knee joint angle-based adaptive Functional Electrical Stimulation of the Peroneal Nerve in Spastic Paresis - A case report. *Annals of Physical and Rehabilitation Medicine*. Elsevier, 2018.

Peer-reviewed conferences:

[5] **Arnez-Paniagua, Victor** and Huo, Weiguang and Colorado-Cervantes, Ivan and Mohammed, Samer and Amirat, Yacine. A hybrid approach towards assisting ankle joint of paretic patients. In *IFES Hybrid Approaches to FES*, p. 4. IEEE, 2016.

[6] **Arnez-Paniagua, V** and Rifai, H and Mohammed, S and Amirat, Y. Adaptive control of an actuated ankle foot orthosis for foot-drop correction. In *International Federation of Automatic Control (IFAC)*, pages 1420–1425. 2017.

[7] **Arnez-Paniagua, Victor** and Rifa, Hala and Amirat, Yacine and Mohammed, Samer. Adaptive control of an actuated-ankle-foot-orthosis. In *International Conference on Rehabilitation Robotics (ICORR)*, pages 1584–1589. IEEE, 2017.

[8] **V. Arnez-Paniagua**, H. Rifaï, Y. Amirat, M. Ghedira, J. M. Gracies, S. Mohammed. Modified Adaptive Control of an Actuated Ankle Foot Orthosis to assist Paretic Patients. In *International Conference on Intelligent Robots and Systems (IROS)*, p. 7. IEEE, 2018.

[9] Weiguang Huo, **Victor Arnez-Paniagua**, Ghedira Mouna, Yacine Amirat, Jean-Michel Gracies, Samer Mohammed. Adaptive FES Assistance using a Novel Gait Phase Detection Approach. In *International Conference on Intelligent Robots and Systems (IROS)*, p. 8. IEEE, 2018.

Bibliography

[1] Antonio Carolei, Simona Sacco, Federica De Santis, and Carmine Marini. Epidemiology of stroke. *Clinical and Experimental hypertension*, 24(7-8):479–483, 2002.

[2] John D Stewart. Foot drop: where, why and what to do? *Practical neurology*, 8(3):158–169, 2008.

[3] Kenneth Lo, Matthew Stephenson, and Craig Lockwood. Effectiveness of robotic assisted rehabilitation for mobility and functional ability in adult stroke patients: a systematic review. *JBI database of systematic reviews and implementation reports*, 15(12):3049–3091, 2017.

[4] Jill Whitall. Stroke rehabilitation research: time to answer more specific questions?, 2004.

[5] Joseph R Dettori and Carl J Basmania. Early ankle mobilization, part ii: A one-year follow-up of acute, lateral ankle sprains (a randomized clinical trial). *Military medicine*, 159(1):20–24, 1994.

[6] Saul G Trevino, Pamela Davis, and Paul J Hecht. Management of acute and chronic lateral ligament injuries of the ankle. *The Orthopedic clinics of North America*, 25(1):1–16, 1994.

[7] Barbara L Braun. Effects of ankle sprain in a general clinic population 6 to 18 months after medical evaluation. *Archives of family medicine*, 8(2):143, 1999.

[8] Dora YL Chan, Chetwyn CH Chan, and Derrick KS Au. Motor relearning programme for stroke patients: a randomized controlled trial. *Clinical rehabilitation*, 20(3):191–200, 2006.

[9] R PS Van Peppen, Gert Kwakkel, Sharon Wood-Dauphinee, H JM Hendriks, Ph J Van der Wees, and Joost Dekker. The impact of physical therapy on functional outcomes after stroke: what's the evidence? *Clinical rehabilitation*, 18(8):833–862, 2004.

[10] Beverley French, Lois H Thomas, Michael J Leathley, Christopher J Sutton, Joanna McAdam, Anne Forster, Peter Langhorne, CI Price, Andrew Walker, Caroline L Watkins, et al. Repetitive task training for improving functional ability after stroke. *Cochrane Database Syst Rev*, 4(4), 2007.

[11] Naoyuki Takeuchi and Shin-Ichi Izumi. Rehabilitation with poststroke motor recovery: a review with a focus on neural plasticity. *Stroke research and treatment*, 2013, 2013.

[12] Mingming Zhang, T Claire Davies, and Shane Xie. Effectiveness of robot-assisted therapy on ankle rehabilitation–a systematic review. *Journal of Neuroengineering and Rehabilitation*, 10(1):1, 2013.

[13] Divya Shakti, Lini Mathew, Neelesh Kumar, and Chitra Kataria. Effectiveness of robo-assisted lower limb rehabilitation for spastic patients: A systematic review. *Biosensors and Bioelectronics*, 117:403–415, 2018.

[14] Wayne L Anderson, Brian S Armour, Eric A Finkelstein, and Joshua M Wiener. Estimates of state-level health-care expenditures associated with disability. *Public Health Reports*, 125(1):44–51, 2010.

[15] Fitri Yakub, Ahmad Zahran Md Khudzari, and Yasuchika Mori. Recent trends for practical rehabilitation robotics, current challenges and the future. *International Journal of Rehabilitation Research*, 37(1):9–21, 2014.

[16] Weiguang Huo, Samer Mohammed, Juan C Moreno, and Yacine Amirat. Lower limb wearable robots for assistance and rehabilitation: A state of the art. *Systems Journal*, 10(3):1068–1081, 2016.

[17] Pei-Chun Kao and Daniel P Ferris. Motor adaptation during dorsiflexion-assisted walking with a powered orthosis. *Gait and Posture*, 29(2):230–236, 2009.

[18] Larry W Forrester, Anindo Roy, Charlene Hafer-Macko, Hermano I Krebs, and Richard F Macko. Task-specific ankle robotics gait training after stroke: a randomized pilot study. *Journal of neuroengineering and rehabilitation*, 13(1):1, 2016.

[19] Stefano Masiero, Patrizia Poli, Giulio Rosati, Damiano Zanotto, Marco Iosa, Sefano Paolucci, and Giovanni Morone. The value of robotic systems in stroke rehabilitation. *Expert review of medical devices*, 11(2):187–198, 2014.

[20] René Jimenez-Fabian and Olivier Verlinden. Review of control algorithms for robotic ankle systems in lower-limb orthoses, prostheses, and exoskeletons. *Medical Engineering & Physics*, 34(4):397–408, 2011.

[21] Saartje Duerinck, Eva Swinnen, Pieter Beyl, Friso Hagman, Ilse Jonkers, Peter Vaes, and Peter Van Roy. The added value of an actuated ankle-foot orthosis to restore normal gait function in patients with spinal cord injury: a systematic review. *Journal of rehabilitation medicine*, 44(4):299–309, 2012.

[22] Disa K Sommerfeld, Elsy U-B Eek, Anna-Karin Svensson, Lotta Widén Holmqvist, and Magnus H von Arbin. Spasticity after stroke: its occurrence and association with motor impairments and activity limitations. *Stroke*, 35(1):134–139, 2004.

[23] Maria Vinti, Annabelle Couillandre, Jérôme Hausselle, Nicolas Bayle, Aldo Primerano, Andrea Merlo, Emilie Hutin, and Jean-Michel Gracies. Influence of effort intensity and gastrocnemius stretch on co-contraction and torque production in the healthy and paretic ankle. *Clinical Neurophysiology*, 124(3):528–535, 2013.

[24] Anne Moseley, Amanda Wales, Rob Herbert, Karl Schurr, and Sally Moore. Observation and analysis of hemiplegic gait: stance phase. *Australian journal of physiotherapy*, 39(4):259–267, 1993.

[25] Sally Moore, Karl Schurr, Amanda Wales, Anne Moseley, and Rob Herbert. Observation and analysis of hemiplegic gait: swing phase. *Australian journal of physiotherapy*, 39(4):271–278, 1993.

[26] Kenneth Alex Shorter, Jicheng Xia, Elizabeth T Hsiao-Wecksler, William K Durfee, and Géza F Kogler. Technologies for powered ankle-foot orthotic systems: Possibilities and challenges. *IEEE/ASME Transactions on mechatronics*, 18(1):337–347, 2013.

[27] P Hunter Peckham and Jayme S Knutson. Functional electrical stimulation for neuromuscular applications. *Annu. Rev. Biomed. Eng.*, 7:327–360, 2005.

[28] Christine Azevedo Coste, Jovana Jovic, Roger Pissard-Gibollet, and Jérôme Froger. Continuous gait cycle index estimation for electrical stimulation assisted foot drop correction. *Journal of neuroengineering and rehabilitation*, 11(1):118, 2014.

[29] Joaquin A Blaya and Hugh Herr. Adaptive control of a variable-impedance ankle-foot orthosis to assist drop-foot gait. *IEEE Transactions on neural systems and rehabilitation engineering*, 12(1):24–31, 2004.

[30] Sungjae Hwang, Jungyoon Kim, Jinbock Yi, Kisik Tae, Kihong Ryu, and Youngho Kim. Development of an active ankle foot orthosis for the prevention of foot drop and toe drag. In *International Conference on Biomedical and Pharmaceutical Engineering (ICBPE)*, pages 418–423, 2006.

[31] Vijaya Krishnamoorthy, Wei-Li Hsu, Trisha M Kesar, Daniel L. Benoit, Sai K. Banala, Ramu Perumal, Vivek Sangwan, Stuart A. Binder-Macleod, Sunil K. Agrawal, and John P Scholz. Gait training after stroke: a pilot study combining a gravity-balanced orthosis, functional electrical stimulation, and visual feedback. *Journal of Neurologic Physical Therapy*, 32(4):192–202, 2008.

[32] DPM Nicholas Romansky, MD Kelly Scollon-Grieve, and CPO James G. McGinness. Current concepts in diagnosing and treating drop foot. *Podiatry Today*, 25(6):68–75, 2012.

[33] Elizabeth B Brokaw, Diane Nichols, Rahsaan J Holley, and Peter S Lum. Robotic therapy provides a stimulus for upper limb motor recovery after stroke that is complementary to and distinct from conventional therapy. *Neurorehabilitation and Neural Repair*, 28(4):367–376, 2014.

[34] Verena Klamroth-Marganska, Javier Blanco, Katrin Campen, Armin Curt, Volker Dietz, Thierry Ettlin, Morena Felder, Bernd Fellinghauer, Marco Guidali, Anja Kollmar, et al. Three-dimensional, task-specific robot therapy of the arm after stroke: a multicentre, parallel-group randomised trial. *The Lancet Neurology*, 13(2):159–166, 2014.

[35] Peter S Lum, Charles G Burgar, Peggy C Shor, Matra Majmundar, and Machiel Van der Loos. Robot-assisted movement training compared with conventional therapy techniques for the rehabilitation of upper-limb motor function after stroke. *Archives of Physical Medicine and Rehabilitation*, 83(7):952–959, 2002.

[36] Won Hyuk Chang and Yun-Hee Kim. Robot-assisted therapy in stroke rehabilitation. *Journal of Stroke*, 15(3):174, 2013.

[37] Xiao Xie, Hao Sun, Qing Zeng, Pengcheng Lu, Yijin Zhao, Tao Fan, and Guozhi Huang. Do patients with multiple sclerosis derive more benefit from robot-assisted gait training compared with conventional walking therapy on motor function? a meta-analysis. *Frontiers in Neurology*, 8(260):9, 2017.

[38] Stefano Masiero, Mario Armani, Gregorio Ferlini, Giulio Rosati, and Aldo Rossi. Randomized trial of a robotic assistive device for the upper extremity during early inpatient stroke rehabilitation. *Neurorehabilitation and Neural Repair*, 28(4):377–386, 2014.

[39] D CM De Wit, JH Buurke, J MM Nijlant, MJ Ijzerman, and HJ Hermens. The effect of an ankle-foot orthosis on walking ability in chronic stroke patients: a randomized controlled trial. *Clinical Rehabilitation*, 18(5):550–557, 2004.

[40] Sai K Banala, Suni K Agrawal, and John P Scholz. Active leg exoskeleton (ALEX) for gait rehabilitation of motor-impaired patients. *International Conference on Rehabilitation Robotics (ICORR)*, pages 401–407, 2007.

[41] Markus Wirz, David H Zemon, Ruediger Rupp, Anke Scheel, Gery Colombo, Volker Dietz, and T George Hornby. Effectiveness of automated locomotor training in patients with chronic incomplete spinal cord injury: a multicenter trial. *Archives of physical medicine and rehabilitation*, 86(4):672–680, 2005.

[42] Andrés Martínez, Brian Lawson, and Michael Goldfarb. A controller for guiding leg movement during overground walking with a lower limb exoskeleton. *Transactions on Robotics*, 34(1):183–193, 2018.

[43] Susan E Fasoli, Hermano I Krebs, Joel Stein, Walter R Frontera, Richard Hughes, and Neville Hogan. Robotic therapy for chronic motor impairments after stroke: Follow-up results. *Archives of Physical Medicine and Rehabilitation*, 85(7):1106–1111, 2004.

[44] Zhihao Zhou, Yao Sun, Ninghua Wang, Fan Gao, Kunlin Wei, and Qining Wang. Robot-assisted rehabilitation of ankle plantar flexors spasticity: A three-month study with proprioceptive neuromuscular facilitation. *Frontiers in neurorobotics*, 10:14, 2016.

[45] Mingming Zhang, T Claire Davies, Yanxin Zhang, and Shane Xie. Reviewing effectiveness of ankle assessment techniques for use in robot-assisted therapy. *Journal of rehabilitation research and development*, 51(4):517–534, 2014.

[46] Laura Marchal-Crespo and David J Reinkensmeyer. Review of control strategies for robotic movement training after neurologic injury. *Journal of Neuroengineering and Rehabilitation*, 6(1):15, 2009.

[47] Samer Mohammed, Yacine Amirat, and Hala Rifai. Lower-limb movement assistance through wearable robots: State of the art and challenges. *Advanced Robotics*, 26(1-2):1–22, 2012.

[48] Stephen M Cain, Keith E Gordon, and Daniel P Ferris. Locomotor adaptation to a powered ankle-foot orthosis depends on control method. *Journal of neuroengineering and rehabilitation*, 4(1):1, 2007.

[49] Joseph Hidler, Diane Nichols, Marlena Pelliccio, Kathy Brady, Donielle D Campbell, Jennifer H Kahn, and T George Hornby. Multicenter randomized clinical trial evaluating the effectiveness of the lokomat in subacute stroke. *Neurorehabilitation and neural repair*, 23(1):5–13, 2009.

[50] Slavka Viteckova, Patrik Kutilek, and Marcel Jirina. Wearable lower limb robotics: A review. *Biocybernetics and Biomedical Engineering*, 33(2):96–105, 2013.

[51] Mohd Azuwan Mat Dzahir and Shin-ichiroh Yamamoto. Recent trends in lower-limb robotic rehabilitation orthosis: Control scheme and strategy for pneumatic muscle actuated gait trainers. *Robotics*, 3(2):120–148, 2014.

[52] Baltej Singh Rupal, Sajid Rafique, Ashish Singla, Ekta Singla, Magnus Isaksson, and Gurvinder Singh Virk. Lower-limb exoskeletons: Research trends and regulatory guidelines in medical and non-medical applications. *International Journal of Advanced Robotic Systems*, 14(6):27, 2017.

[53] Aaron M Dollar and Hugh Herr. Lower extremity exoskeletons and active orthoses: challenges and state-of-the-art. *Transactions on robotics*, 24(1):144–158, 2008.

[54] Hugh Herr. Exoskeletons and orthoses: classification, design, challenges and future directions. *Journal of Neuroengineering and Rehabilitation*, 6(1):9, 2009.

[55] B Katherine Salter, B Mark Hartley, and B Norine Foley. Impact of early vs delayed admission to rehabilitation on functional outcomes in persons with stroke. *J Rehabil Med*, 38(113Á/117), 2006.

[56] Sarah A Maulden, Julie Gassaway, Susan D Horn, Randall J Smout, and Gerben DeJong. Timing of initiation of rehabilitation after stroke. *Archives of physical medicine and rehabilitation*, 86(12):34–40, 2005.

[57] Yupeng Ren, Yi-Ning Wu, Chung-Yong Yang, Tao Xu, Richard Harvey, and Li-Qun Zhang. Developing a wearable ankle rehabilitation robotic device for in-bed acute stroke rehabilitation. *Transactions on neural systems and rehabilitation engineering*, 25(6):589–596, 2016.

[58] Prashant K Jamwal, Sheng Q Xie, Shahid Hussain, and John G Parsons. An adaptive wearable parallel robot for the treatment of ankle injuries. *Transactions on mechatronics*, 19(1):64–75, 2014.

[59] Guoli Zhu, Xiangfeng Zeng, Mingming Zhang, Shane Xie, Wei Meng, Xiaolin Huang, and Qun Xu. Robot-assisted ankle rehabilitation for the treatment of drop foot: a case study. In *Mechatronic and Embedded Systems and Applications (MESA)*, pages 1–5. IEEE, 2016.

[60] Mingming Zhang, Jinghui Cao, Sheng Q Xie, Guoli Zhu, Xiangfeng Zeng, Xiaolin Huang, and Qun Xu. A preliminary study on robot-assisted ankle rehabilitation for the treatment of drop foot. *Journal of Intelligent & Robotic Systems*, pages 1–9, 2017.

[61] Wei Meng, Quan Liu, Mingming Zhang, Qingsong Ai, and Sheng Quan Xie. Compliance adaptation of an intrinsically soft ankle rehabilitation robot driven by pneumatic muscles. In *Advanced Intelligent Mechatronics (AIM), 2017 IEEE International Conference on*, pages 82–87. IEEE, 2017.

[62] Daniel Ferris, Gregory Sawicki, and Antoinette Domingo. Powered lower limb orthoses for gait rehabilitation. *Topics in spinal cord injury rehabilitation*, 11(2):34–49, 2005.

[63] RR Neptune, SA Kautz, and FE Zajac. Contributions of the individual ankle plantar flexors to support, forward progression and swing initiation during walking. *Journal of biomechanics*, 34(11):1387–1398, 2001.

[64] Martin Noël, Benoit Cantin, Sébastien Lambert, Clément M Gosselin, and Laurent J Bouyer. An electrohydraulic actuated ankle foot orthosis to generate force fields and to test proprioceptive reflexes during human walking. *IEEE Transactions on Neural Systems and Rehabilitation Engineering*, 16(4):390–399, 2008.

[65] Martin Noel, Karine Fortin, and Laurent J Bouyer. Using an electrohydraulic ankle foot orthosis to study modifications in feedforward control during locomotor adaptation to force fields applied in stance. *Journal of neuroengineering and rehabilitation*, 6(1):16, 2009.

[66] K Alex Shorter, Géza F Kogler, Eric Loth, William K Durfee, and Elizabeth T Hsiao-Wecksler. A portable powered ankle-foot orthosis for rehabilitation. *Journal of rehabilitation research and development*, 48(4):459–472, 2011.

[67] Steve Davis, N Tsagarakis, J Canderle, and Darwin G Caldwell. Enhanced modelling and performance in braided pneumatic muscle actuators. *The International Journal of Robotics Research*, 22(3-4):213–227, 2003.

[68] Daniel P Ferris, Keith E Gordon, Gregory S Sawicki, and Ammanath Peethambaran. An improved powered ankle–foot orthosis using proportional myoelectric control. *Gait & posture*, 23(4):425–428, 2006.

[69] Keith E Gordon, Gregory S Sawicki, and Daniel P Ferris. Mechanical performance of artificial pneumatic muscles to power an ankle–foot orthosis. *Journal of biomechanics*, 39(10):1832–1841, 2006.

[70] Keith E Gordon and Daniel P Ferris. Learning to walk with a robotic ankle exoskeleton. *Journal of biomechanics*, 40(12):2636–2644, 2007.

[71] Catherine R Kinnaird and Daniel P Ferris. Medial gastrocnemius myoelectric control of a robotic ankle exoskeleton. *IEEE Transactions on Neural Systems and Rehabilitation Engineering*, 17(1):31–37, 2009.

[72] Kota Z Takahashi, Michael D Lewek, and Gregory S Sawicki. A neuromechanics-based powered ankle exoskeleton to assist walking post-stroke: a feasibility study. *Journal of neuroengineering and rehabilitation*, 12(1):23, 2015.

[73] Yong-Lae Park, Bor-rong Chen, Diana Young, Leia Stirling, Robert J Wood, Eugene Goldfield, and Radhika Nagpal. Bio-inspired active soft orthotic device for ankle foot pathologies. In *International Conference on Intelligent Robots and Systems (IROS)*, pages 4488–4495. IEEE, 2011.

[74] Yong-Lae Park, Bor-rong Chen, Néstor O Pérez-Arancibia, Diana Young, Leia Stirling, Robert J Wood, Eugene C Goldfield, and Radhika Nagpal. Design and control of a bio-inspired soft wearable robotic device for ankle–foot rehabilitation. *Bioinspiration & biomimetics*, 9(1):016007, 2014.

[75] Jeffrey A Ward, Joseph Hitt, Thomas Sugar, and Kartik Bharadwaj. Dynamic pace controller for the robotic gait trainer. *International Design Engineering Technical Conferences and Computers and Information in Engineering Conference*, pages 575–581, 2006.

[76] Adam Zoss and Hami Kazerooni. Design of an electrically actuated lower extremity exoskeleton. *Advanced Robotics*, 20(9):967–988, 2006.

[77] Hanqi Zhu, Jack Doan, Calvin Stence, Ge Lv, Toby Elery, and Robert Gregg. Design and validation of a torque dense, highly backdrivable powered knee-ankle orthosis. *International Conference Robotic Automation (ICRA)*, page 7, 2017.

[78] Anindo Roy, Hermano Igo Krebs, Dustin J Williams, Christopher T Bever, Larry W Forrester, Richard M Macko, and Neville Hogan. Robot-aided neurorehabilitation: a novel robot for ankle rehabilitation. *Transactions on Robotics*, 25(3):569–582, 2009.

[79] Anindo Roy, Hermano I Krebs, Joseph E Barton, Richard F Macko, and Larry W Forrester. Anklebot-assisted locomotor training after stroke: A novel deficit-adjusted control approach. In *International Conference on Robotics and Automation (ICRA)*, pages 2175–2182. IEEE, 2013.

[80] Anindo Roy, Hermano I Krebs, Kamran Iqbal, Nathan R Macko, Richard F Macko, and Larry W Forrester. Facilitating push-off propulsion: A biomechanical model of ankle robotics assistance for plantarflexion gait training in stroke. In *International Conference on Biomedical Robotics and Biomechatronics*, pages 656–663. IEEE, 2014.

[81] Mohd Nor Azmi Bin Ab Patar, Mohamad Mali, Mohd Hanif Mohd Ramli, Ahmad Khushairy Makhtar, and Jamaluddin Mahmud. Simulation and performance evaluation of a new type of powered dynamic ankle foot orthosis. In *Humanities, Science and Engineering (CHUSER), 2011 IEEE Colloquium on*, pages 167–171. IEEE, 2011.

[82] Mohd Nor Azmi Ab Patar, Ahmad Fahmi Said, Jamaluddin Mahmud, Anwar PP Abdul Majeed, and Mohd Azraai Razman. System integration and control of

dynamic ankle foot orthosis for lower limb rehabilitation. In *International Symposium on Technology Management and Emerging Technologies (ISTMET)*, pages 82–85. IEEE, 2014.

[83] Ivanka Veneva and Nuno Ferreira. Adaptive system for control of active ankle-foot orthosis and gait analysis. In *Mathematical Methods in Engineering*, pages 153–163. Springer, 2014.

[84] Alexander W Boehler, Kevin W Hollander, Thomas G Sugar, and Dosun Shin. Design, implementation and test results of a robust control method for a powered ankle foot orthosis (afo). *International conference on Robotics and automation (ICRA)*, pages 2025–2030, 2008.

[85] Joseph Hitt, A Mehmet Oymagil, Thomas Sugar, Kevin Hollander, Alex Boehler, and Jennifer Fleeger. Dynamically controlled ankle-foot orthosis (DCO) with regenerative kinetics: incrementally attaining user portability. *International Conference on Robotics and Automation (ICRA)*, pages 1541–1546, 2007.

[86] Marta Moltedo, Tomislav Baček, Kevin Langlois, Karen Junius, Bram Vanderborght, and Dirk Lefeber. Design and experimental evaluation of a lightweight, high-torque and compliant actuator for an active ankle foot orthosis. *International Conference on Rehabilitation Robotics (ICORR)*, pages 283–288, 2017.

[87] Juanjuan Zhang, Chien Chern Cheah, and Steven H Collins. Experimental comparison of torque control methods on an ankle exoskeleton during human walking. In *Robotics and Automation (ICRA), 2015 IEEE International Conference on*, pages 5584–5589. IEEE, 2015.

[88] Kevin W Hollander, Robert Ilg, Thomas G Sugar, and Donald Herring. An efficient robotic tendon for gait assistance. *Journal of biomechanical engineering*, 128(5):788–791, 2006.

[89] Jeffrey Ward, Thomas Sugar, John Standeven, and Jack R Engsberg. Stroke survivor gait adaptation and performance after training on a powered ankle foot orthosis. In *International Conference on Robotics and Automation (ICRA)*, pages 211–216. IEEE, 2010.

[90] Wietse van Dijk, Cory Meijneke, and Herman Van Der Kooij. Evaluation of the achilles ankle exoskeleton. *IEEE transactions on neural systems and rehabilitation engineering*, 25(2):151–160, 2017.

[91] Shahid Hussain, Sheng Quan Xie, and Guangyu Liu. Robot assisted treadmill training: Mechanisms and training strategies. *Medical engineering & physics*, 33(5):527–533, 2011.

[92] Neville Hogan. Impedance control: An approach to manipulation. In *American Control Conference, 1984*, pages 304–313. IEEE, 1984.

[93] Justin Ghan, Ryan Steger, and Hami Kazerooni. Control and system identification for the berkeley lower extremity exoskeleton (BLEEX). *Advanced Robotics*, 20(9):989–1014, 2006.

[94] Juan C Pérez Ibarra, Wilian M dos Santos, Hermano I Krebs, and Adriano AG Siqueira. Adaptive impedance control for robot-aided rehabilitation of ankle movements. In *Biomedical Robotics and Biomechatronics (2014 5th IEEE RAS & EMBS International Conference on*, pages 664–669. IEEE, 2014.

[95] Juan C Pérez-Ibarra, Adriano AG Siqueira, and Hermano I Krebs. Assist-as-needed ankle rehabilitation based on adaptive impedance control. In *Rehabilitation Robotics (ICORR), 2015 IEEE International Conference on*, pages 723–728. IEEE, 2015.

[96] Juan C Pérez-Ibarra and Adriano AG Siqueira. Comparison of kinematic and EMG parameters between unassisted, fixed-and adaptive-stiffness robotic-assisted ankle movements in post-stroke subjects. *International Conference on Rehabilitation Robotics (ICORR)*, pages 461–466, 2017.

[97] Daniel P Ferris, Joseph M Czerniecki, and Blake Hannaford. An ankle-foot orthosis powered by artificial pneumatic muscles. *Journal of applied biomechanics*, 21(2):189–197, 2005.

[98] Keith E Gordon, Catherine R Kinnaird, and Daniel P Ferris. Locomotor adaptation to a soleus emg-controlled antagonistic exoskeleton. *Journal of Neurophysiology*, 109(7):1804–1814, 2013.

[99] Matthew A Holgate, Alexander W Bohler, and Thomas G Suga. Control algorithms for ankle robots: A reflection on the state-of-the-art and presentation of two novel algorithms. *International Conference on Biomedical Robotics and Biomechatronics*, pages 97–102, 2008.

[100] Takahiro Kagawa, Hironori Ishikawa, Takayuki Kato, ChangHyun Sung, and Yoji Uno. Optimization-based motion planning in joint space for walking assistance with wearable robot. *Transactions on Robotics*, 31(2):415–424, 2015.

[101] Jun-ichiro Furukawa, Tomoyuki Noda, Tatsuya Teramae, and Jun Morimoto. Human movement modeling to detect biosignal sensor failures for myoelectric assistive robot control. *Transactions on Robotics*, 33(4):846–857, 2017.

[102] Bryan L Riemann, Richard G DeMont, Keeho Ryu, and Scott M Lephart. The effects of sex, joint angle, and the gastrocnemius muscle on passive ankle joint complex stiffness. *Journal of athletic training*, 36(4):369, 2001.

[103] M Mirbagheri, H Barbeau, M Ladouceur, and R Kearney. Intrinsic and reflex stiffness in normal and spastic, spinal cord injured subjects. *Experimental brain research*, 141(4):446–459, 2001.

[104] Claire L Brockett and Graham J Chapman. Biomechanics of the ankle. *Orthopaedics and trauma*, 30(3):232–238, 2016.

[105] David A Winter. *Biomechanics and motor control of human movement*. John Wiley & Sons, 2009.

[106] DH Sutherland, L Cooper, and D Daniel. The role of the ankle plantar flexors in normal walking. *JBJS*, 62(3):354–363, 1980.

[107] Jacquelin Perry, Jon R Davids, et al. Gait analysis: normal and pathological function. *Journal of Pediatric Orthopaedics*, 12(6):815, 1992.

[108] DAVID A Winter. Energy generation and absorption at the ankle and knee during fast, natural, and slow cadences. *Clinical orthopaedics and related research*, (175):147–154, 1983.

[109] Thomas M Kepple, Karen Lohmann Siegel, and Steven J Stanhope. Relative contributions of the lower extremity joint moments to forward progression and support during gait. *Gait & Posture*, 6(1):1–8, 1997.

[110] At L Hof, Jelle Nauta, Erik R van der Knaap, Michiel AA Schallig, and D Peter Struwe. Calf muscle work and segment energy changes in human treadmill walking. *Journal of electromyography and kinesiology*, 2(4):203–216, 1992.

[111] Marjan Meinders, Andrew Gitter, and Joseph M Czerniecki. The role of ankle plantar flexor muscle work during walking. *Scandinavian journal of rehabilitation medicine*, 30(1):39–46, 1998.

[112] Jongsang Son, Sungjae Hwang, and Youngho Kim. An emg-based muscle force monitoring system. *Journal of mechanical science and technology*, 24(10):2099–2105, 2010.

[113] Victor Arnez-Paniagua, Hala Rifaï, Yacine Amirat, and Samer Mohammed. Adaptive control of an actuated-ankle-foot-orthosis. *International Conference on Rehabilitation Robotics (ICORR)*, pages 1584–1589, 2017.

[114] Ion PI Pappas, Milos R Popovic, Thierry Keller, Volker Dietz, and Manfred Morari. A reliable gait phase detection system. *IEEE Transactions on neural systems and rehabilitation engineering*, 9(2):113–125, 2001.

[115] Kyoungchul Kong and Masayoshi Tomizuka. A gait monitoring system based on air pressure sensors embedded in a shoe. *Transactions on mechatronics*, 14(3):358–370, 2009.

[116] Pyeong-Gook Jung, Sehoon Oh, Gukchan Lim, and Kyoungchul Kong. A mobile motion capture system based on inertial sensors and smart shoes. *Journal of Dynamic Systems, Measurement, and Control*, 136(1):011002, 2014.

[117] Samer Mohammed, Allou Same, Latifa Oukhellou, Kyoungchul Kong, Weiguang Huo, and Yacine Amirat. Recognition of gait cycle phases using wearable sensors. *Robotics and Autonomous Systems*, 75:50–59, 2016.

[118] Victor Arnez-Paniagua, Weiguang Huo, Ivan Colorado-Cervantes, Samer Mohammed, and Yacine Amirat. A hybrid approach towards assisting ankle joint of paretic patients. In *International Functional Electrical Stimulation Society conference (IFESS)*, 2016.

[119] Emilie Hutin, Didier Pradon, Franck Barbier, Bernard Bussel, Jean-Michel Gracies, and Nicolas Roche. Walking velocity and lower limb coordination in hemiparesis. *Gait & posture*, 36(2):205–211, 2012.

[120] Weiguang Huo, Samer Mohammed, Yacine Amirat, and Kyoungchul Kong. Fast gait mode detection and assistive torque control of an exoskeletal robotic orthosis for walking assistance (e-rowa). *IEEE Transactions on Robotics*, 2017.

[121] Prashant Jamwal. *Design analysis and control of wearable ankle rehabilitation robot.* PhD thesis, The university of Auckland, New Zealand, 2011.

[122] Fatima el Zahraa Wehbi, Weiguang Huo, Yacine Amirat, Maher El Rafei, Mohamad Khalil, and Samer Mohammed. Active impedance control of a knee-joint orthosis during swing phase. *International Conference on Rehabilitation Robotics (ICORR)*, pages 435–440, 2017.

[123] Murray J Lawn, Makoto Takashima, Makoto Ninomiya, Jiangli Yu, Kayano Soma, and Takakazu Ishimatsu. Development of an actuation system for a rotary hydraulic brake on a low cost light weight knee-ankle-foot orthosis. *Sensors*, pages 1–4, 2015.

[124] Eric T Wolbrecht, Vicky Chan, Vu Le, Steven C Cramer, David J Reinkensmeyer, and James E Bobrow. Real-time computer modeling of weakness following stroke optimizes robotic assistance for movement therapy. *International Conference on Neural Engineering*, pages 152–158, 2007.

[125] Hala Rifaï, Samer Mohammed, Walid Hassani, and Yacine Amirat. Nested saturation based control of an actuated knee joint orthosis. *Mechatronics*, 23(8):1141–1149, 2013.

[126] Brahim Brahmi, Maarouf Saad, Cristobal Ochoa-Luna, and Mohammad H Rahman. Adaptive control of an exoskeleton robot with uncertainties on kinematics and dynamics. *International Conference on Rehabilitation Robotics (ICORR)*, pages 1369–1374, 2017.

[127] Kartik Bharadwaj, Thomas G Sugar, James B Koeneman, and Edward J Koeneman. Design of a robotic gait trainer using spring over muscle actuators for ankle stroke rehabilitation. *Journal of biomechanical engineering*, 127(6):1009–1013, 2005.

[128] Tarek Madani, Boubaker Daachi, and Karim Djouani. Finite-time control of an actuated orthosis using fast terminal sliding mode. *International Federation of Automatic Control (IFAC)*, 47(3):4607–4612, 2014.

[129] Michäel Van Damme, Bram Vanderborght, Bjorn Verrelst, Ronald Van Ham, Frank Daerden, and Dirk Lefeber. Proxy-based sliding mode control of a planar pneumatic manipulator. *The International Journal of Robotics Research*, 28(2):266–284, 2009.

[130] Miroslav Krstic, Ioannis Kanellakopoulos, and Petar V. Kokotovic. *Nonlinear and Adaptive Control Design*. Jhon Wiley & Sons, Inc., New York, 1995.

[131] J. C. P. Ibarra, W. M. dos Santos, H. I. Krebs, and A. A. G. Siqueira. Adaptive impedance control for robot-aided rehabilitation of ankle movements. In *5th IEEE RAS/EMBS International Conference on Biomedical Robotics and Biomechatronics*, pages 664–669, Aug 2014.

[132] Jian Huang, Zhi-Hong Guan, Takayuki Matsuno, Toshio Fukuda, and Kosuke Sekiyama. Sliding-mode velocity control of mobile-wheeled inverted-pendulum systems. *IEEE Transactions on robotics*, 26(4):750–758, 2010.

[133] Ryo Kikuuwe and Hideo Fujimoto. Proxy-based sliding mode control for accurate and safe position control. In *IEEE International Conference on Robotics and Automation (ICRA)*, pages 25–30, 2006.

[134] Bader Badreddine, Alex Zaremba, Jing Sun, and Feng Lin. Active damping of engine idle speed oscillation by applying adaptive pid control. Technical report, SAE Technical Paper, 2001.

[135] E. D. Sontag. *Mathematical control theory, deterministic finite dimensional systems*. Springler Verlag, New York Berlin Heidelberg, second edition, 1998.

[136] Eduardo D. Sontag. *Input to State Stability: Basic Concepts and Results*, pages 163–220. Springer Berlin Heidelberg, Berlin, Heidelberg, 2008.

[137] E.D. Sontag and Y. Wang. On characterizations of the input-to-state stability property. *Systems and Control Letters*, 24:351–359, 1995.

[138] J-JE Slotine and Li Weiping. Adaptive manipulator control: A case study. *Transactions on Automatic Control*, 33(11):995–1003, 1988.

[139] H.K. Khalil. *Nonlinear systems*. Prentice Hall, 2002.

[140] F. Pazos and L. Hsu. Controle de robos manipuladores em modo dual adaptativo/robusto. *Sba controle & automacao*, 14(1):30–40, 2003.

[141] G. Satori-Natal, A. Chemori, and F. Pierrot. Nonlinear control of parallel manipulators for very high accelerations without velocity measurement: stability analysis and experiments on par2 parallel manipulator. *Robotica*, pages 1–28, 2014.

[142] Ryo Kikuuwe, Satoshi Yasukouchi, Hideo Fujimoto, and Motoji Yamamoto. Proxy-based sliding mode control: a safer extension of pid position control. *IEEE Transactions on Robotics*, 26(4):670–683, 2010.

[143] Ming Huang, Xinhan Huang, Xikai Tu, Zefang Li, and Yue Wen. An online gain tuning proxy-based sliding mode control using neural network for a gait training robotic orthosis. *Cluster Computing*, 19(4):1987–2000, 2016.

[144] Robert D Brandt and Feng Lin. Adaptive interaction and its application to neural networks. *Information Sciences*, 121(3-4):201–215, 1999.

[145] Corina Barbalata, Valerio De Carolis, Matthew W Dunnigan, Yvan Petillot, and David Lane. An adaptive controller for autonomous underwater vehicles. In *IEEE/RSJ International Conference on Intelligent Robots and Systems (IROS)*, 2015.

[146] Zhen-Yu Zhao, Masayoshi Tomizuka, and Satoru Isaka. Fuzzy gain scheduling of pid controllers. *IEEE transactions on systems, man, and cybernetics*, 23(5):1392–1398, 1993.

[147] Bader M Badreddine and Feng Lin. Adaptive pid controller for stable/unstable linear and non-linear systems. In *Proceedings of the 2001 IEEE International Conference on Control Applications (CCA)*, pages 1031–1036, 2001.

[148] R. Sepulchre, M. Jankovic, and P. V. Kokotović. *Constructive Nonlinear Control*. Springler, London, 1997.

[149] J.A. Primbs, V. Nevistic, and J.C. Doyle. Nonlinear optimal control: A control lyapunov function and receding horizon perspective. *Asian Journal of Control*, 1(1):14–24, 1999.

[150] Ricardo G. Sanfelice. On the existence of control lyapunov functions and state-feedback laws for hybrid systems. *Transactions on Automatic Control, (2013)*, 58, 2013.

[151] N. Marchand, S. Durand, and J. F. Guerrero-Castellanos. A general formula for event-based stabilization of nonlinear systems. *Transactions on Automatic Control, (2013)*, 58(5), 2013.

[152] A. D. Ames, K. Galloway, K. Sreenath, and J. W. Grizzle. Rapidly exponentially stabilizing control lyapunov functions and hybrid zero dynamics. *Transactions on Automatic Control*, 59(4):876–891, April 2014.

[153] K. Galloway, K. Sreenath, A. D. Ames, and J. W. Grizzle. Torque saturation in bipedal robotic walking through control lyapunov function-based quadratic programs. *Access*, 3:323–332, 2015.

[154] M. Jankovic, R. Sepulchre, and P. V. Kokotović. Clf based designs with robustness to dynamic input uncertainties. *Systems Control Letters*, 37(5):45–54, 1999.

[155] J. Han. From pid to active disturbance rejection control. *Transactions on Industry Electronics*, 56(3):900–906, 2009.

[156] Hebertt Sira-Ramírez, Alberto Luviano-Juárez, Mario Ramírez-Neria, and Eric William Zurita-Bustamante. *Active Disturbance Rejection Control of Dynamic Systems: A Flatness-Based Approach*. Butterworth-Heinemann, 2017.

[157] Linping Chan, Fazel Naghdy, and David Stirling. Extended active observer for force estimation and disturbance rejection of robotic manipulators. *Robotics and Autonomous Systems*, 61(12):1277 – 1287, 2013.

[158] Wenchao Xue, Yi Huang, and Zhiqiang Gao. On adrc for non-minimum phase systems: canonical form selection and stability conditions. *Control Theory and Technology*, 14(3):199–208, Aug 2016.

[159] Haifa Mehdi and Olfa Boubaker. Robust impedance control-based lyapunov-hamiltonian approach for constrained robots. *International Journal of Advanced Robotic Systems*, 12(12):190, 2015.

[160] Disturbance-observer based control for magnetically suspended wheel with synchronous noise. *Control Engineering Practice*, 72:83 – 89, 2018.

[161] S. M. Orozco-Soto and J. M. Ibarra-Zannatha. Motion control of humanoid robots using sliding mode observer-based active disturbance rejection control. In *Colombian Conference on Automatic Control (CCAC)*, pages 1–8. IEEE, Oct 2017.

[162] Germán A Ramos Fuentes, John A Cortés-Romero, ZhiXiang Zou, Ramon Costa-Castelló, and Keliang Zhou. Power active filter control based on a resonant disturbance observer. *IET Power Electronics*, 8(4):554–564, 2015.

[163] Xiaoyong Chang, Yongli Li, Weiya Zhang, Nan Wang, and Wei Xue. Active disturbance rejection control for a flywheel energy storage system. *IEEE Transactions on Industrial Electronics*, 62(2):991–1001, 2015.

[164] Huanpao Huang, Liqiang Wu, Jingqing Han, Gao Feng, and Yongjun Lin. A new synthesis method for unit coordinated control system in thermal power plant-adrc control scheme. In *Power System Technology. International Conference on*, volume 1, pages 133–138. IEEE, 2004.

[165] H. Sira-Ramírez, A. Hernández-Méndez, J. Linares-Flores, and A. Luviano-Juarez. Robust flat filtering dsp based control of the boost converter. *Control Theory and Technology*, 14(3):224–236, 2016.

[166] H. Sira-Ramírez, J. Linares-Flores, C. García-Rodríguez, and M.A. Contreras-Ordaz. On the control of the permanent magnet synchronous motor: An active disturbance rejection control approach. *Transactions on Control Systems Technology*, 22(5):2056–2066, 2014.

[167] J. Linares-Flores, C. García-Rodríguez, H. Sira-Ramírez, and O.D. Ramírez-Cárdenas. Robust backstepping tracking controller for low-speed pmsm positioning system: Design, analysis, and implementation. *Transactions on Industrial Informatics*, 11(5):1130–1141, 2015.

[168] J. Linares-Flores, H. Sira-Ramírez, J. L. Barahona-Avalos, and M.A. Contreras-Ordaz. Robust passivity-based control of a buck–boost-converter/dc-motor system: An active disturbance rejection approach. *Transactions on Industry Applications*, 48(6):2362–2371, 2012.

[169] A. Hernandez-Méndez, J. Linares-Flores, H. Sira-Ramírez, J.F. Guerrero-Castellanos, and G. Mino-Aguilar. A backstepping approach to decentralized active disturbance rejection control of interacting boost converters. *Transactions on Industry Applications*, 53(4):4063–4072, 2017.

[170] Nadhynee Martínez-Fonseca, Luis Ángel Castañeda, Agustín Uranga, Alberto Luviano-Juárez, and Isaac Chairez. Robust disturbance rejection control of a biped robotic system using high-order extended state observer. *ISA Transactions*, 62:276 – 286, 2016.

[171] Hongjiu Yang, Yang Yu, and Jinhui Zhang. Angle tracking of a pneumatic muscle actuator mechanism under varying load conditions. *Control Engineering Practice*, 61:1 – 10, 2017.

[172] Yi Long, Zhijiang Du, Lin Cong, Weidong Wang, Zhiming Zhang, and Wei Dong. Active disturbance rejection control based human gait tracking for lower extremity rehabilitation exoskeleton. *ISA Transactions*, 67:389 – 397, 2017.

[173] Hebertt Sira-Ramírez and Suni K. Agrawal. *Differentially Flat Systems*. Marcel Dekker, Inc., 2004.

[174] Susanne W Lipfert, Michael Günther, Daniel Renjewski, and Andre Seyfarth. Impulsive ankle push-off powers leg swing in human walking. *Journal of experimental biology*, 217(8):1218–1228, 2014.

[175] Richard B Stein, Dirk G Everaert, Aiko K Thompson, Su Ling Chong, Maura Whittaker, Jenny Robertson, and Gerald Kuether. Long-term therapeutic and orthotic effects of a foot drop stimulator on walking performance in progressive and nonprogressive neurological disorders. *Neurorehabilitation and neural repair*, 24(2):152–167, 2010.

[176] David G Embrey, Sandra L Holtz, Gad Alon, Brenna A Brandsma, and Sarah Westcott McCoy. Functional electrical stimulation to dorsiflexors and plantar flexors during gait to improve walking in adults with chronic hemiplegia. *Archives of physical medicine and rehabilitation*, 91(5):687–696, 2010.

[177] Samer Mohammed, Philippe Fraisse, David Guiraud, Philippe Poignet, and HE Makssoud. Towards a co-contraction muscle control strategy for paraplegics. In *Decision and Control, 2005 and 2005 European Control Conference. CDC-ECC'05. 44th IEEE Conference on*, pages 7428–7433. IEEE, 2005.

[178] P Winchester, JJ Carollo, and R Habasevich. Physiologic costs of reciprocal gait in FES assisted walking. *Spinal Cord*, 32(10):680, 1994.